

# **Research & Development**

**2012**

# **Mechanical Engineering Letters, Szent István University**

Annual Technical-Scientific Journal of the Mechanical Engineering Faculty,  
Szent István University, Gödöllő, Hungary

Editor-in-Chief:  
Dr. István SZABÓ

Editor:  
Dr. Gábor KALÁCSKA

## Executive Editorial Board:

Dr. István BARÓTFI	Dr. István HUSTI
Dr. János BEKE	Dr. Sándor MOLNÁR
Dr. István FARKAS	Dr. Péter SZENDRŐ
Dr. László FENYVESI	Dr. Zoltán VARGA

## International Advisory Board:

Dr. Patrick DE BAETS (B)  
Dr. Radu COTETIU (Ro)  
Dr. Manuel GÁMEZ (Es)  
Dr. Klaus GOTTSCHALK (D)  
Dr. Yurii F. LACHUGA (Ru)  
Dr. Elmar SCHLICH (D)

Cover design:  
Dr. László ZSIDAI

HU ISSN 2060-3789

All Rights Reserved. No part of this publication may be reproduced, stored in a retrieval system or transmitted in any form or by any means, electronic, mechanical, photocopying, recording, scanning or otherwise without the written permission of Faculty.

Páter K. u. 1., Gödöllő, H-2103 Hungary  
dekan@gek.szie.hu, www.gek.szie.hu,

Volume 8 (2012)

**Selected Papers from the  
Doctoral School of Mechanical Engineering  
at the Szent István University**



## Contents

Zoltán BLAHUNKA, Zoltán BÁRTFAI, Rajmund LEFÁNTI: Soil surface monitoring with gyroscope	10
Róbert VARGA: Examination of Rigid Wall Biodegradable Packaging Materials	18
Anikó FÖLDI, Csaba MÉSZÁROS: Basic symmetry properties of thermodynamic cross-effects at coupled diffusion processes through porous media	26
István FEKETE, István FARKAS: Factorial experiment method for determining the efficiency of solar collectors	38
Ivett KOCSÁNY, István SERES: Performance of solar collectors by reflected spectral measurements	53
Attila SZILÁGYI, István SERES: Solar energy utilization in solar air conditioning systems	61
István Ervin HÁBER, Tamás BOTKOS, István FARKAS: Modelling of meteorological parameters for city Pécs in photovoltaic energy simulations	68
Dani RUSIRAWAN, István FARKAS: Spectral irradiance effects on exergetic performances of photovoltaic module: initial study	76
Zoltán KAPROS Predictive modeling for low power photovoltaic systems	84
Tamás MOLNÁR: Landfill gas quality and quantity parameter changes depending on precipitation intensity	90
László GURMAI, Péter KISS: Comparative analysis of destructive forces acting on the structure of off-road towed vehicles	98

Attila SZEGEDI, Antal LENGYEL: Analysis of Governing Process of the Underload Gear Shifting	107
Adrienn GODA, Viktor MEDINA, László ZSIDAI: Examination of the cob cracker adapter manufacturers' performance in Hungary	113
Imre KOVÁCS, István HUSTI: IT Development Trends in the Mechanization of Crop Production	123

## **Mechanical Engineering Doctoral School**



Prof. Dr. István FARKAS  
Head of the School

Dear Reader,

The Doctoral School of Mechanical Engineering at the Szent István University was established in 1993 with two specific orientations of which one is the "Basics of Agricultural Engineering" and the other one is the "Agricultural Energetics and Environmental Technique". The last accreditation of the Doctoral School took place in 2012.

During establishing of the School the following principles were taken into consideration: The predictable requirement based on developing tendency in the agriculture and food industry is that the production and application of the machines and tools should be environment-friendly, material- and energy-save. On the other hand it is important to organize the existing equipment to logistical system and arrange ecological operation and recycling. In the strategy of the research some promoted new topics should be emphasized, which ones serve same up-to-date production technologies.

The global increase of agricultural production has to be realized in an ecological balance having decreased volume of the applied chemicals and energies. For sustainable development it has a basic interest to decrease the polluting materials getting into the environment and to economize with the resources.

The typical research topics of the orientations are as follows:

### **Basics of agricultural engineering**

- Mechanizations of animal husbandry and plant growing
- Vehicle and tractor techniques, the off road running theory
- Mechanics of structural and agricultural materials
- Safety of machines
- Tribology and techniques of lubrication
- System of quality control, technical innovation and development
- Technologies and tools of primer crop processing
- Material-, and energy-save production technology
- Operations of machines and systems
- Maintenance machinery and recycling
- Materials rheology and structure of agricultural material sets
- Physiology effect of the electricity field

- Computer Aided Engineering techniques
- Separation techniques and equipment in crop processing
- Building structure.

### **Agricultural energetics and environmental technique**

- Energetic and physics of buildings
- Energy and mass transport processes
- Research of the energy sources in agriculture and in forestry
- Alternative and reusable energy sources
- High frequency and microwave energy used in food processing
- Technical and technological questions of environment protection
- Ecological correlation of settlement and development of area
- Protection of water-base
- Principle of environmental industry
- Engineering economics

The duration of the PhD education is 6 semesters, while the students have to collect 180 ECTS credits. The credits can be got in four educational units i.e. learning, research, teaching and publication activities.

After fulfilment the educational and the research requirements the student can get an „Absolutorium” certificate giving a prove for finishing a stage of their PhD activities.

After that they can apply for starting the degree process. As a prerequisite they should show an appropriate publishing achievement. During this period the students have to get through on a comprehensive exam, and prepare their Thesis work. In order to submit the Thesis work for final evaluation a good level of internationally recognized publication is needed. In this term the journal publications and the foreign language publications have got higher value. To defend the Thesis work a public meeting is organized with two official reviewers.

The recent special issue of Mechanical Engineering Letters serves also a possibility for the PhD students to publish the results of their research activities. The following topic groups were selected out to publish:

#### *Soil and environmental topics:*

- In this section soil surface monitoring, biodegradable packaging materials, and basic symmetry properties of thermodynamic cross-effects have been discussed.

#### *Solar energy, and landfill gas topics:*

- In this section solar collector efficiencies and performance, solar air conditioning systems, meteorological parameters for photovoltaic energy simulations, spectral irradiance effects, and predictive modelling of photovoltaic systems and landfill gas quality issues have been discussed.

*Mechanical development topics:*

- In this section a comparative analysis for off-road towed vehicles and a governing process analysis of an underload gear shifting have been performed.

*Engineering management topics:*

- In the final section two papers have been presented on an examination of a cob cracker adapter manufacturers' performance and on an IT development trends in the mechanization of crop production.

## **Soil surface monitoring with gyroscope**

Zoltán BLAHUNKA, Zoltán BÁRTFAI,

Rajmund LEFÁNTI

Mechanical Engineering Faculty,

Szent István University

### **Abstract**

One of the most important resources for agricultural production is the soil. The soil has many types of parameters. We can analyze it by chemical components or by physical parameters. Topographic maps present the landscape on a large scale: planes, hills, mountains have different agricultural advantages. Surface has its own importance as part of short scale geography. Every plant has an optimal surface. Moisture, dehydration also depends on surface and roughness. In our institute we are elaborating a new method to monitor soil surface roughness. In our method, a mobile robot is cruising through a field. While it is cruising, the chassis rolls over the clods of soil. By measuring the rolls we are able to estimate the roughness of the field. Using some statistical methods we can deduct the number of clods. Finally we calculate the entropy of the surface. Observing the entropy we are able to determine the end point of the measurement.

### **Keywords**

Mobile robot, IMU, soil surface monitoring

### **1. Introduction**

Soil surface roughness, terrain classification, terrain estimation are very interesting research areas nowadays. Agriculture is not its only end user. Autonomous vehicles [Sadhukhan, 2004] [Manduchi, Castano, Talukder, & Matthies, 2005], planet explorers [Iagnemma, Shibly, & Dubowsky, 2002] are also potential users of the information about current and future road surfaces. There are many technologies to obtain these information: optical or mechanical, fixed or moving.

The traditional way of measuring soil surface is the use of profilograph. This tool takes measurements along a few meters long line creating from these samples its vertical surface profile. To improve this technology the mechanical part can be changed for an optical laser sensor. Laser profilographs have bigger resolution and accuracy.

After we have the detailed profile information we are able to calculate the roughness parameters. There are some standards of tribology which define the calculations for parameters (ISO 25178).

Another way to get information about soil surface is to use cameras [Taconet & Ciarletti, 2007] [Halatci, Iagnemma, & others, 2008]. Images must be processed in order to obtain the roughness parameters. This technology has a big advantage: it can be used for forecasting as well. This method instead of measuring the detailed surface profile estimates terrain classification. This is useful for autonomous vehicles to be able to drive through less resistant surface (grass, stones, asphalt, etc.)

Another method to get information about surface is to use inertial sensors. Sensing the vehicle accelerations, vibrations [Brooks, Iagnemma, & Dubowsky, 2005] [Weiss, Frohlich, & Zell, 2006] and angular velocities is a new technology and method of soil surface topology. In this article we also use inertial measurement unit (IMU) [Sadhukhan, Moore, & Collins, 2004] to get classification information about surface. We generate a histogram from obstacle height and distance between obstacles. We are able to calculate the entropy of this histogram.

Unlike our development many researches use methods that calculate the RMS of vibration as for example [Brooks, Iagnemma, & Dubowsky, 2005].

## 2. Method

### *Equipment*

The main hardware are a Pioneer 3-MX3 mobile robot and an Analog Devices AD16365 6 degree of freedom IMU. To manage this computation we are using many software components: UltraVNC for remote access of moving robot platform, AriaDemo for driving the robot, iSensor to log the measured values, National Instruments LabVIEW for engineering calculations.

The Pioneer 3-MX3 mobile robot is suitable for outdoor use. Also it has good off-road capabilities which make it a good choice to hold the IMU sensor and cruise over soil surface. The axle distance of the mobile robot is 270 mm. This short distance is very practical at height calculation accuracy. The 3-MX3 mobile robot has two onboard computers. One is responsible for controlling peripherals like motors, encoders, sonar sensors. The other computer is a desktop PC running. A special software communicates with the controller computer to drive the robot or sense the environment. 3-MX3 has WLAN adapter. Using remote access we are able to control the robot from an external PC/laptop.

The Analog Devices 16365 IMU sensor consists of 3 acceleration sensors positioned in 3 directions (x-y-z axis) and 3 angular velocity sensors in 3 directions (x-y-z axis). It is also able to measure the temperature. In our method we don't use this sensor. The sampling frequency is 819,2 samples/seconds while in vehicle dynamics measurement standard is 100 samples/seconds. It is also fit to Shannon theory which tells that the measuring frequency should be at least two times bigger than the examined phenomenon.



*Figure 1. Pioneer P3AT on a field*

The software components are separated into two parts: one running on mobile robot and the other one on remote PC. The bridge between the two systems is a remote control software, in our case UltraVNC. Onboard softwares are AriaDemo and iSensor. Post process runs on external computer using National Instruments LabVIEW application.

#### *The process*

After installing all equipment (mobile robot fully charged, operating WLAN router, laptop connected to mobile robot) we are able to start recording the IMU values. We start the logger application first and only afterwards the mobile robot. When the mobile robot has cruised over the surface the robot is stopped. The logger application runs on a predefined time. Before the measurement we have to estimate the total cruising time. The log file should be copied to the external PC for future processing.

The first step of processing is to select the working range of measured values. As earlier said we estimated the total time, so in the beginning and in the end there are unnecessary values. After the trimming we use filtering. We tried more methods of filtering: Kalman filter, low pass filter and moving average. Based on validation we decided to use Kalman filter [Gelb, 1974]. After the filtering we got a smooth graph of angular velocity, removing high frequency components of measurement.

Using the IMU we faced some issues. **The inertial sensor measures the total acceleration which equals to the sum of gravity and kinetic acceleration.** In static situation it represents the components of gravity. This is used in modern mobile devices to show screens always in readable position. In dynamic situations the two components cannot be separated hence we don't have exact information about the position of the mobile robot (pitch, roll) and the kinetically acceleration. Because of this issue we concentrated only on angular velocity. When angle speed is not zero the platform turns around the current

axis. Integrating these values we get the current turning in angles. Knowing the physical parameters of the mobile robot platform (axis distance, distance of wheels) we are able to calculate the vertical difference (height) of the position of the wheels [Blahunka & Dr. Faust, 2009]. Turning around the z axis is the traditional way of turning left or right. Driving the mobile robot straight on it should be zero. Collision with obstacle can turn the robot. When the robot reaches the obstacle with only one wheel (asymmetric collision) the obstacle turns the mobile robot. This way the values from angle speed around z axis are not always zero. Turning around x axis is tilt by asymmetric surface. This could be an interesting research area to measure the profiles of the wheels on the two sides of the vehicle during one ride. We use turning around y axis which means the vertical difference of front and rear axis. Knowing the height of clouds and the distance between them (distance can be calculated by the elapsed time between cloud since the mobile robot cruises at constant speed), we can draw a histogram for height, distance and number of occurrence.

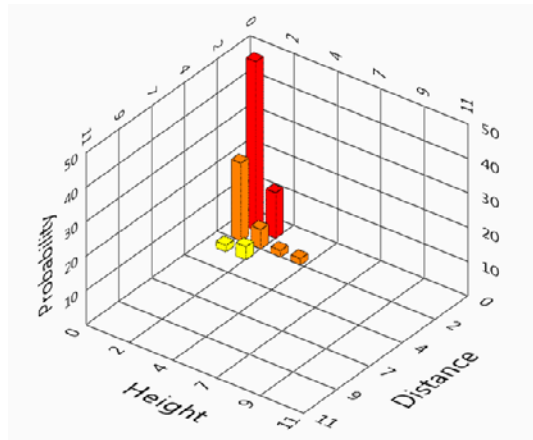


Figure 2. Histogram of height and distance

To make the histogram comparable we convert it to probability. We can calculate the probability ( $p$ ): the number of occurrences ( $n$ ) is divided by the total

number of occurrences as showed in equation  $p_{x,y} = \frac{n_{x,y}}{\sum_x \sum_y n_{x,y}}$  (1). This

way the integral of the total area of the histogram is 1. It does not depend on the length of the profile and the roughness of the surface. Also the values give us information about surface classification.

$$p_{x,y} = \frac{n_{x,y}}{\sum_x \sum_y n_{x,y}} \quad (1)$$

Using the probability we can calculate the entropy ( $H$ ) of the histogram (equation 2). The entropy [Shannon & Weaver, 1949] shows us the diversity of the surface.

$$H = -\sum_i p_i \log p_i \quad (2)$$

As the robot is cruising at constant speed both time and distance can be calculated from each other by a constant multiplication. Observing the entropy depending on time or distance, we can recognize this is a saturated function. When this function reaches the saturated value we get all information about the surface roughness. Continuing the measurement doesn't give more detail (assuming it is a homogeneous surface like a field).

### 3. Results

#### Test 1.

First test was in our university building corridor. We put shelves on the floor. The shelf height is 2 cm. Using 1-2-3 pieces of shelves we build 2-4-6 cm height obstacles. In this case the heights 2-4-6 cm and a distance between obstacles 10-50 cm.

#### Test 2.

Built outdoor environments are the walking ways next to university building. The stones average size is 1-2 cm. In this case the heights and distances are 1-2 cm.

#### Test 3.

There is a test field for agricultural vehicles. This is a flat surface. There are small spaces between concrete tables. In this case the heights are small distances are 3-4 m.

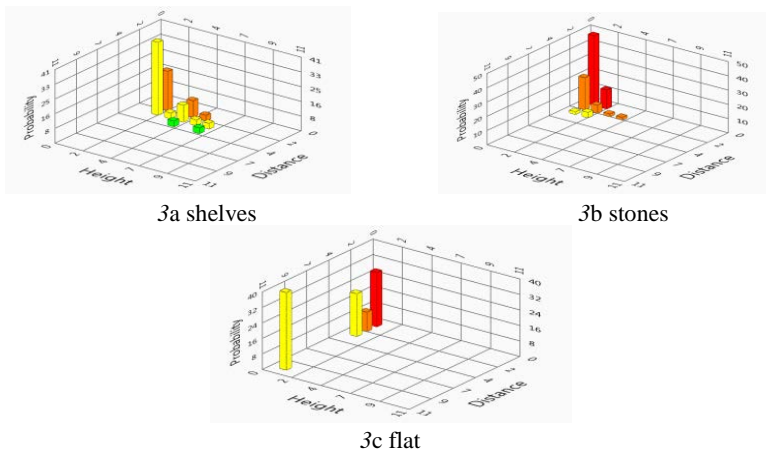


Figure 3. Histograms of different surfaces

Figure 3 shows three histograms of different test fields. At the first test field the maximum is in middle height. The distance maximum is at axle distance. Because of relative big distances between the obstacles, the axle distance makes the half of the occurrence.

The second test runs over small stones. The maximum occurrence is near to the origo, small distance, small height. There are some occurrences next to the origo, the concentration is the origo.

The last test runs on a flat concrete. Small obstacles make a concentration next to the origo, but there is a strong value in a big distance little height position.

The three histograms look different. Using the method we are able to classify the surface. This method is also suitable to compare different agricultural tools (the surface effect of applying the tool).

#### **4. Future possibilities**

There are many open questions. There are many automated calculations but the control of measurement is still human. One big development direction would be the total automation of the process.

Developing the mathematical method, it should calculate the detailed profile values. Using the profile values we can calculate the standard parameters of soil surface roughness.

#### **Conclusion**

Soil surface roughness is very complex. There are many technologies to measure the detailed profile. There are standard parameters to describe profile. On the other hand there are applications that need information about surface classification but do not need detailed profile values.

The method that we developed collects information about surface and classification of the surface. Processing IMU signals according to our method we are able to obtain terrain classification.

By observing the entropy we can detect the optimal measurement distance.

#### **Acknowledgement**

The research was supported/subsidized by the TÁMOP-4.2.2.B-10/1-2010-0011 „Development of a complex educational assistance/support system for talented students and prospective researchers at the Szent István University” project.

#### **References**

Blahunka, Z., & Dr. Faust, D. [2009]. Mobil robot platformra szerelt vezeték nélküli mérőhálózat alkalmazása talajfelszín egyenletlenség mérésére és értékelésére. *GÉP*, 2009(8), 32–38.

- Brooks, C., Iagnemma, K., & Dubowsky, S. [2005]. Vibration-based terrain analysis for mobile robots. *Robotics and Automation, 2005. ICRA 2005. Proceedings of the 2005 IEEE International Conference on* [pp. 3415–3420]. Retrieved from [http://ieeexplore.ieee.org/xpls/abs\\_all.jsp?arnumber=1570638](http://ieeexplore.ieee.org/xpls/abs_all.jsp?arnumber=1570638)
- Gelb, A. [1974]. *Applied Optimal Estimation*. MIT Press. Retrieved from [http://mseas.mit.edu/download/pierrel/jing/Applied%20Optimal%20Estimation%20-%20Gelb%20\(1974\).pdf](http://mseas.mit.edu/download/pierrel/jing/Applied%20Optimal%20Estimation%20-%20Gelb%20(1974).pdf)
- Halatci, I., Iagnemma, K., & others. [2008]. A study of visual and tactile terrain classification and classifier fusion for planetary exploration rovers. *Robotica, 26*[6], 767–779. Retrieved from <http://dl.acm.org/citation.cfm?id=1520079>
- Iagnemma, K., Shibly, H., & Dubowsky, S. [2002]. On-line terrain parameter estimation for planetary rovers. *Robotics and Automation, 2002. Proceedings. ICRA'02. IEEE International Conference on* [Vol. 3, pp. 3142–3147]. Retrieved from [http://ieeexplore.ieee.org/xpls/abs\\_all.jsp?arnumber=1013710](http://ieeexplore.ieee.org/xpls/abs_all.jsp?arnumber=1013710)
- Manduchi, R., Castano, A., Talukder, A., & Matthies, L. [2005]. Obstacle detection and terrain classification for autonomous off-road navigation. *Autonomous Robots, 18*[1], 81–102. Retrieved from <http://www.springerlink.com/index/RH4QRV5461300541.pdf>
- Sadhukhan, D. [2004]. Autonomous ground vehicle terrain classification using internal sensors. Retrieved from <http://diginole.lib.fsu.edu/etd/2115/>
- Sadhukhan, D., Moore, C., & Collins, E. [2004]. Terrain estimation using internal sensors. *Proceedings of the 10th IASTED International Conference on Robotics and Applications (RA)*. Retrieved from [https://www.eng.fsu.edu/ciscor/pdf/publications/Sadhukhan\\_TERRAIN\\_ESTIMATION\\_USING\\_INTERNAL\\_SENSORS\\_Aug\\_04.pdf](https://www.eng.fsu.edu/ciscor/pdf/publications/Sadhukhan_TERRAIN_ESTIMATION_USING_INTERNAL_SENSORS_Aug_04.pdf)
- Shannon, C. E., & Weaver, W. [1949]. *The mathematical theory of communication*. University of Illinois Press.
- Taconet, O., & Ciarletti, V. [2007]. Estimating soil roughness indices on a ridge-and-furrow surface using stereo photogrammetry. *Soil and Tillage Research, 93*[1], 64–76. doi:10.1016/j.still.2006.03.018
- Weiss, C., Frohlich, H., & Zell, A. [2006]. Vibration-based terrain classification using support vector machines. *Intelligent Robots and Systems, 2006 IEEE/RSJ International Conference on* [pp. 4429–4434]. Retrieved from [http://ieeexplore.ieee.org/xpls/abs\\_all.jsp?arnumber=4059113](http://ieeexplore.ieee.org/xpls/abs_all.jsp?arnumber=4059113)

# **Examination of Rigid Wall Biodegradable Packaging Materials**

Róbert VARGA

Department of Material Handling and Logistics,  
Institute of Management and System Engineering,  
Szent István University

## **Abstract**

Internationally and in our country the quantity of plastics which are used for the packaging of goods is continuously growing. To help the alleviation of the environmental loading problems, the development of the biodegradable packaging materials and their application have began already on international and domestic level. I executed examinations with decomposing wrappers which were developed in the Central Environmental And Food Science Research Institute, Budapest. From the different combination of samples I prepared segments and I took pictures from them in a microscope. I was looking for correlation between the compression temperature, the compression time and the breaking force. The results are reported in this study.

## **Keywords**

biodegradable, packaging, pressing, temperature, time, breaking force,

## **1. Introduction**

Internationally and in our country the quantity of plastics which are used for the packaging of goods is continuously growing. Among the packaging materials used in the past few decades, the plastics still represent the fastest growing group. The waste training of plastic packaging materials used in great mass becomes a more difficult problem to environmental pollution.

As a result, the degradation of the chain structure disintegration occurs after a long time. The solving of the environmental loading problems has already begun in an international and domestic level with the development of the biodegradable packaging materials and their application as one of the possible solutions. Biobased food packaging materials are materials derived from renewable sources. These materials can be used for food applications. (Weber, 2000)

In the recent years the Central Environmental And Food Science Research Institute created completely or partially biodegradable rigid packaging materials, which consist domestic raw materials and based on manufacturing technology that is environmentally friendly. These materials are capable of replacing traditional plastic packaging materials in the food packaging area.

The material of the developed products is usually native or modified starch, polylactic acid, or polyhydroxy alcanoats produced by bacteria. The listed materials are not sufficient themselves to constitute packaging materials with appropriate technical characteristics, therefore beside these materials there are also other natural or sometimes synthetic polymers are also used, with a good degradation tendency. Other materials are used too for example the cellulose for improvement of mechanical properties, and triglycerides (fat) to reduce hygroscopic properties of the raw materials. The polymers are large-molecular compounds that consist of the same and repeating units. [Halász L. et al., 1978]

The raw materials of the biodegradable packaging materials can be renewable crude materials: gelatine, casein, keratin by animal origins; starch, cellulose, wheat gluten by plant origins, poly-hidroxi-alcanoats, lactic acid, polylactic acid produced by fermentation, fossil raw material: polyester amid, polyesteruretan, co-polyester, moreover the mix of renewable and fossil raw materials: starch-PVAL and starch- polylactic acid [Biacs et al., 2001].

My research is based on biodegradable, rigid trays that were developed by the Central Environmental And Food Science Research Institute. In this study I have reported results of some production and material test.

## **2. Material and method**

The base material of the biodegradable food trays developed for use in the food industry is finely ground wheat flour. The wheat flour is a very important ingredient because it contains a high proportion of carbohydrates and protein, which promotes biological degradation. It's color is white, which gives a clear decisive tone for the packing material. The other material is the mustard flour that is also finely ground. The yellow mustard flour, which lends a darker shade of the color of the packaging material. The frame material of the ground material is 2-6 mm long chopped wheat straw. For softening the base material drinking water is also added. The raw material components, and other auxiliary materials in suitable proportions were mixed in a special mixing equipment and then pressed by an experimental heated and pneumatically opening and locking tool. Figure 1. illustrates the pressing equipment.



*Figure 1.* Pneumatic opening and closing press equipment tool with tool heating by heating flat

In order to examine the production parameters the pneumatic pressure, and the heating temperature of the device were adjustable. The opening and closing of the tool was carried out by a long-stroke air cylinder with 0,6 MPa pressure, placed on the top. The upper half tool performed vertical movement comparing to the lower, stable half.

The usual extrusion temperature  $T_s$  of the biopolymer materials vary between 120-180 °C, depending on the composition of the base, and because of their heat sensitive additives that can only stand this temperature range. The extrusion temperature should be kept constant, and therefore the temperature of the upper half and the lower half of the mould  $T_f$  and  $T_a$  must be always the same. Thus the press temperature is equal to the temperature of the tool halves.

At a lower temperature than the optimum the production of the biodegradable tray is slower and at a higher temperature than the optimum the production of the biodegradable tray is faster, and quality defects occur in both cases. The reason is that during the production of the rigid biodegradable trays the moulding temperature determines the hardening time. The pressing force:

$$F_s = p \cdot A_{mh} \text{ [N]}$$

where:

$F_s$  – the pressing force [N],

$p$  – the pressure of the material during pressing the working fluid into the cylinder, [Pa],

$A_{mh}$  – the surface of the cylinder [m<sup>2</sup>].

During the production the equipment's maximum pressing force was 3000 N. The time during the product solidifies, and it's shape forms because of heat and pressure is called the press time ( $t_s$ ). According to the literature in case of the thermosetting, not biopolymers, at 15-100 MPa specific pressure assuming wall thickness of 1 mm, the time of the hardening process is from 30 to 60 s [Mondvai, 1991].

In case of thermosetting biopolymers the pressing time is approximately the same, but the pressure is significantly smaller, so the biopolymer materials developed by Central Environmental And Food Science Research Institute counted to 1 mm wall thickness, the required molding time of 40 s, and the pressing pressure 0,6 MPa. The pressing times of the two types of materials are considered to be nearly the same, but in case of thermosetting biopolymers a much less extrusion pressure is sufficient.

The main characteristics of the trays: height 16 mm, length 136 mm, width 136 mm, thickness 3 mm, average weight 22 g.

### 3. Results

During the production process, the long fibre frame material oriented (in case of plastics the textile fibre, in case of biodegradable material the straw). This is illustrated on Figure 2.

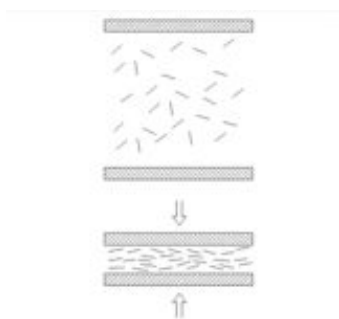


Figure 2. The orientation of the long fibre frame material during pressing [Mondvai, 1991]

The measurements covered the study of the behavior of trays made by different material composition, adding straw and wheat flour. I have prepared some samples of the trays for microscopic examination using a Zeiss Axiostar type microscope, at 20X magnification.

I took the microscopic images with the help of PhD Zoltan Havelda senior researcher at the Agricultural Biotechnology Centre, Gödöllő.

The trays those were made by adding straw and wheat flour can be seen on Figure 3. and microscopic image of the sample (20 X magnification) can be observed on Figure 4. and Figure 5.



Figure 3. Trays made by adding straw and wheat flour



0 1mm → <20X>

Figure 4. The microscopic image of the tray made by adding straw (20 X magnification)

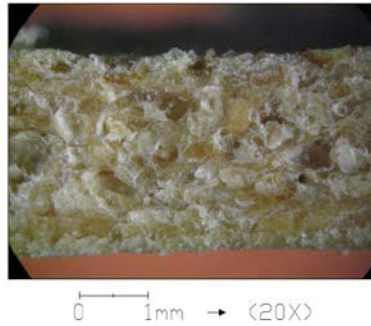


Figure 5. The microscopic segment of the tray made by adding wheat flour (20 X magnification)

The loose structure of the material that can be observed on the microscopic images, suggests low density and low breaking strength. To verify this hypothesis I have performed material tests on tensile machine. I used trays with added straw for the material tests. The aim was to determine the load capacity of the trays.

Figure 6. shows the LLOYD LR5K<sup>plus</sup> computer-controlled universal tensile testing machine prepared for the test. I have placed the tested tray on two blocks with a 100 mm space between them. I have fixed the breaking element in the upper, moving head of the tensile machine. The body of the breaking element facing the test tray was curved. For processing the data of the measurement data collector unit that was connected to the tensile machine, I used the program called NEXYGEN.



Figure 6. LLOYD LR5K<sup>PLUS</sup> computer-controlled universal tensile machine prepared for breaking test  
(Central Environmental And Food Science Research Institute, Budapest)

The breaking diagrams of the trays made by adding straw are shown on Figure 11. In the first series of the experiment I have analyzed 10 pieces of trays of the same size and material composition. For the production of these trays I applied 160 °C of press temperature, 0,6 MPa press pressure and 120 s press time.

The fracture resistance of the samples were measured by the same tensile machine and method as previously described. The results of the experiments graphically illustrated can be seen on Figure. 7.

The measured maximum breaking forces are summarized in Table 1. The breaking forces in the chart and the diagram show that the greatest break resistance was 147,984 N in case of the sample number 6 that appears low even in case of biodegradable packaging materials. The differences between the break resistances can be explained by the different inhomogeneity and orientation of the ground material.

In the second series of the experiment I have analyzed the effect of the pressing temperature and pressing time to break resistance. It has set the pressing temperature between 140 and 200 °C, and the pressing time between 90 and 270 s during the production of the sample trays that were used in the experiment. I have submitted the pressed trays (27 versions) to breaking tests, like in the previous experiment. The measurements were performed in five repetitions.

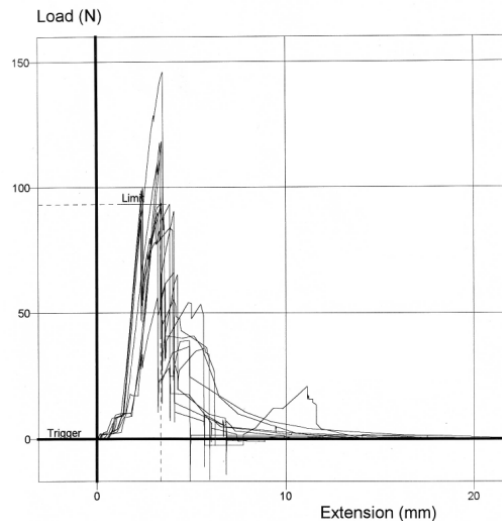


*Figure 7.* Breaking force diagrams of the trays mostly made by adding straw

The measurement results of the second series of experiment are summarized in Table 2., where there are unmarked and marked data, with one, two and three asterisks.

Table 1. Results of the breaking examination

Sample No.	Breaking force $F_t$ [N]
1.	69,854
2.	95,813
3.	100,13
4.	93,460
5.	61,489
6.	147,984
7.	74,838
8.	49,470
9.	94,866
10.	71,550
Average	85,945
Dispersion	27,490

The samples were visually divided into four groups based on their surface, shape, color and hardness.

The unmarked samples were corresponding all of the four properties (surface, shape, color and hardness) of the terms of expectations. It can be said that these samples were not deformed, not cracked, and not even during the removal of the device or during subsequent storage. However, these samples had the highest break resistances (Table 2.). This means that the technology parameters used for their manufacturing (temperature, time), were close to the optimum besides the given product composition.

Table 2. The results of the pressing temperature, pressing time and breaking examination of the fracture [Bakos, 2004]

Pressing temperature $T_s$ [°C]	140	150	160	170	180	190	200
Pressing time $t_s$ [s]	Break resistance $F_t$ [N]						
90	-	-	92,4*	144,2*	164,6	158,6	160,7
120	-	64,2*	129,8	189,8	161,4**	150,1**	122,9***
150	34,3*	78,8*	158,5	153,4**	127,6***	122,1***	-
180	58,8	103,4	121,4**	112,6***	-	-	-
210	79,8	85,2**	75,1***	-	-	-	-
240	61,4**	47,4***	-	-	-	-	-
270	44,8***	-	-	-	-	-	-

The samples marked with one asterisk, have passed the first three criteria (surface, shape, color), but only their upper and lower surfaces solidified. Between the two rinds the material remained soft. These samples were usually difficult to remove without damages from the pressing tool. They contained relatively large amount of water, and often cracks had appeared on them during the removal and they also smeared. Also, because of the high water content of these samples they were deformed more or less during the storage period.

The two asterisk samples were made with a little longer pressing time than it was necessary. These samples were characterized by the burned product color and hairline cracks that appeared during the storage. The samples were deformed, but in their case the occurring deformation was usually significantly below than on the deformation samples marked with one asterisk.

The samples marked with three asterisks were produced with a significantly longer duration and higher temperature than necessary. Therefore the trays burned and on their surface a so-called “wafer” structure was formed, and as a consequence of burn their color changed brown and in some places black. These samples must have been handled very carefully to take them out of the tool. They easily broke, there were a number of hairline cracks on their surface, and on some places there were significant gaps. In case of longer storage time the initial hairline cracks led to product breaks. [Bakos, 2004]

The diagram can be seen on Figure 8. was made from the data of Table 2. that represents the changing of the pressing time in function of the breaking resistance. The curves belonging to the same temperatures are similar. The curves achieve their maximum values at different pressing times. It is interesting that these points belong to the not marked samples that were rated the best on the visual inspection. When increasing the pressing temperature from 140 °C to 170 °C the maximum value of break resistance increased until 170 °C and then it decreased. The diagram illustrates that the highest break resistance belongs to the sample that were produced on 170 °C for 120 seconds. From the diagram it can be concluded that significant quality improvement can be achieved by the correct selection of the break strength, the pressing time and temperature.

To clarify the exact relationship between the parameters and the exploration of the function  $\sigma=f(t_s, T_s)$ , need further experiments.

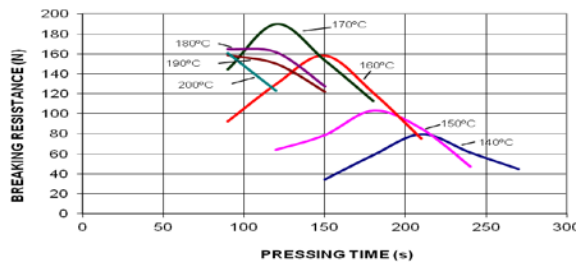


Figure 8. The change of the break resistance in function of the pressing time and pressing temperature

## **Conclusion**

The experiments proved, however, as a result that the breaking strength of the biopolymer test trays are lower than the thermosetting polymer trays. It is probable that a higher pressure, that means a higher pressing force needed in order to produce more compact and higher strength trays. I had no possibility to change the pressing pressure because the applied die-casting machine was not suitable for that. Further studies are required to have new press machine solutions based on the performed experiments. This results in the following article, that I would like to report.

## **Acknowledgement**

The research was supported/subsidized by the TÁMOP-4.2.2.B-10/1-2010-0011 „Development of a complex educational assistance/support system for talented students and prospective researchers at the Szent István University” project.

## **References**

- Bakos P. et al. (2004): Merev falú, keményítő bázisú biológiai úton lebomló csomagolóanyagok fejlesztése, alkalmazástechnikai minősítése, VI. Nemzetközi Élelmiszertudomány Konferencia, Szeged
- Biacs, P. et al. (2001): Biológiai úton lebomló anyagok és eszközök magyarországi bevezetésének előkészítése, MTA tanulmány, Budapest
- Halász, L. et al. (1978): A polimerek feldolgozásának reológiai alapjai. Műszaki Könyvkiadó, Budapest
- Mondvai, I. (1991): Polimerek előállítása és feldolgozása, Tankönyvkiadó, Budapest
- Varga, R. (2007): Biológiailag lebomló csomagolóeszközök laborszintű sajtoló berendezése. Gép, LVIII. 2007/4
- Weber, J. Claus (2000): Biobased packaging materials for food industry – Status and perspectives, Report - EU concerted action project: Production and application of biobased packaging materials, ISBN 87-90504-07-0

## **Basic symmetry properties of thermodynamic cross-effects at coupled diffusion processes through porous media**

Anikó FÖLDI<sup>1</sup> and Csaba MÉSZÁROS<sup>2</sup>

<sup>1</sup>Centre for Energy Research, Hungarian Academy of Sciences,  
Environmental Protection Service  
Budapest, Hungary

<sup>2</sup>Szent István University, Department of Physics and Process Control,  
Gödöllő, Hungary

### **Abstract**

The general nonlinear partial differential equation system describing simultaneous convection and diffusion of multicomponent substances through porous media is discussed in detail on the base of non-equilibrium thermodynamics. After assuming percolative state-dependence of diffusion coefficients instead of classic thermodynamic type, the basic diffusion problem is completely solved analytically in linear approximation. The crucial influence of thermodynamic cross-effects on the final form of the concentration distribution functions of separate components is formally represented by Lommel-type special functions. The solution method leading to expressions containing Lommel-functions is realized in a twofold manner: firstly by direct application of the MAPLE computer algebra system, secondly by its combination with the classical Lagrange's method of variation of constants. It is demonstrated, that presence of thermodynamic cross-effects in a given macroscopic dissipative system naturally eliminates the physically unacceptable existence of infinitely large propagation velocities characteristic for transport processes described by separate parabolic type partial differential equations. Finally, the possible incorporation of our new results into general thermo-hydrodynamic formalism of propagation of disturbances through macroscopic dissipative continua having many important engineering applications is also indicated.

### **Keywords**

diffusion, convection, Lommel-type special functions, propagation of disturbances, computational physics

### **Introduction**

The main motivation for elaborating of this study is that usually applied separate parabolic type partial differential equations (PDEs), which are de facto derived from the linear approximation of the Extended Irreversible Thermodynamics

(EIT) are unsuitable for accurate description of realistic transport processes, because their solutions (which can be correctly set up only within contemporary distribution theory e.g. [Vladimirov, 1984]) imply existence of infinitely large propagation velocities, which fact is in a complete contradiction with the basic physical principles e.g. [Jou et al., 2001]. Historically, Maxwell was the first, who pointed out necessity of taking into account the inertial character of propagation velocities at mathematical modeling of realistic transport processes [Maxwell, 1867]. Later, this problem was resolved by introducing of nonzero relaxation time constants [Cattaneo, 1948], [Cattaneo, 1958], [Vernotte, 1958] in order to ensure presence of inertial phenomena in transport processes. Finally, in 1977, Gyarmati elaborated the most general variant of these separate preliminary studies (leading to application of hyperbolic type PDEs instead of parabolic ones), which became well-known under name of the Wave Approach of Thermodynamics (WAT) [Gyarmati, 1977] and which may be considered as a genuine foundation of the whole EIT.

In the present work we would like to call attention again on another possibility of resolving the infinitely large propagation velocity problem, but without explicit use of the hyperbolic formalism. This method is based on fundamental symmetry properties (usually called Onsager-Casimir symmetries e.g. [Jou et al., 2001]) of conductivity coefficients in linear approximation of the EIT and points out relevance of thermodynamic cross-effects at eliminating of infinitely large propagation velocities even in this approximation. It is based on an earlier paper of one of us [Mészáros et al., 2007], where the Lommel-type special functions [Lommel, 1884-1886] have been applied for the first time in this well-elaborated branch of thermodynamics. In order to demonstrate the general character and possible further applications of our method, we recall here some basic results from non-equilibrium thermodynamics, related to multicomponent diffusion through dissipative continua. Accordingly, if we consider a simultaneous diffusion in a system consisting of “K” number of components, with relative concentrations  $c_k = c_k(\vec{r}, t) \equiv \frac{\rho_k(\vec{r}, t)}{\rho}$ , ( $k = 1, \dots, K - 1$ ) (in the absence of chemical reactions and under isothermal conditions) and without convective motions, the following coupled system of nonlinear partial differential equations is valid:

$$\frac{\partial c_k}{\partial t} = \sum_{j=1}^{K-1} \nabla \cdot (D_{kj} \nabla c_j), \quad (1 \leq k \leq K - 1), \quad (1)$$

(De Groot and Mazur, 1962), (Gyarmati, 1970), (Pascal, 1996) where the diffusion coefficients can be explained by use of the conductivity coefficients  $L_{ik}$  as  $D_{kj} = \sum_{i=1}^{K-1} L_{ki} \cdot \frac{\partial(\mu_i - \mu_k)}{\partial \rho_j}$ , ( $1 \leq k, j \leq K - 1$ ). In this paper we use linear approximation of the EIT and demonstrate, that thermodynamic cross-effects effectively remove the possibility of infinite propagation velocities and may provide a complete novel mathematical method for studying deep relations between the parabolic-, and hyperbolic formalisms of coupled transport

processes. In order to realize this program in a simple manner, we use linear variant of (1) at  $K = 3$ , and consider spatially one-dimensional case, i.e.

$$\begin{aligned}\frac{\partial c_1}{\partial t} &= D_{11} \frac{\partial^2 c_1}{\partial x^2} + D_{12} \frac{\partial^2 c_2}{\partial x^2}, \\ \frac{\partial c_2}{\partial t} &= D_{21} \frac{\partial^2 c_1}{\partial x^2} + D_{22} \frac{\partial^2 c_2}{\partial x^2}.\end{aligned}\tag{2}$$

It was implicitly assumed throughout this introductory section, that we are allowed to work in the so-called energy representation, since the temperature of the system will permanently assumed to be of constant value. Nevertheless, we consider our modelling results in the present work belonging to a domain of the non-equilibrium thermodynamics, which may be considered as the most general [Jou et al., 2001], [Martyushev et al., 2006] physical discipline, whose very powerful methods we intend to apply in a very large scale of open problems, ranging from e.g. modelling of simultaneous transport processes of some measurable chemical components through soil columns e.g. [Bálint et al., 2000], [Bálint et al., 2002] till some very actual global energetic problems related to understanding of possible sustainable states of the Earth biotope e.g. [Annala and Kuismanen, 2009]. The latter one represents a particularly promising area from the point of view of taking into account the thermodynamic cross-effects. Furthermore, if we intend to take effectively into account the possible convective motions (whose incorporation into existing simultaneous heat and mass transfer models usually represents a very difficult task e.g. [Kirschner et al., 2004], [Kirschner et al., 2007]) at such transport problems, it is necessary to elaborate further- and to refine the existing mathematical models of the simultaneous convection-diffusion at both fundamental- [Pascal, 1993], [Pascal, 1996], [Eck et al., 2008], [Mészáros and Bálint, 2011], [Mészáros et al., 2011] and applied numerical e.g. [Knabner and Angermann, 2000] research levels.

### **Symbolic calculation simulation results**

The form of the temperature and moisture-level functions is well-known from the classical literature on thermodynamics and hydrodynamics [Landau and Lifshitz, 2000] and in the simplified, one-dimensional case for e.g. concentration function can be written as (the series expansion coefficients  $k_{jn}$  are constants, and the quantities  $\lambda_{jn}$  ( $j = 1,2$ ) denote the reciprocal values of relaxation time constants of the  $n$ -th harmonics):

$$c_j(\vec{r}, t) \equiv c_j(x, y, z, t) \rightarrow c_j(x, t) = \sum_n k_{jn} c_{jn}(x) \cdot e^{-\lambda_{jn} t}.\tag{3}$$

Substitution of temperature and moisture level functions also represented in this series expansion form into system (2) gives the following equation:

$$\sum_n k_{1n} \left[ (D_{11} - D_{21}) \frac{d^2 c_{1n}(x)}{dx^2} + \lambda_{1n} \cdot c_{1n}(x) \right] \cdot e^{-\lambda_{1n}t} =$$

$$\sum_n k_{2n} \left[ (D_{22} - D_{12}) \frac{d^2 c_{2n}(x)}{dx^2} + \lambda_{2n} \cdot c_{2n}(x) \right] \cdot e^{-\lambda_{2n}t}. \quad (4)$$

Since the equation system (2) is symmetric, we assume, following our earlier basic conception [Mészáros et al., 2007], that spatial harmonics of the same order of different relative concentration functions have identical functional form, i.e.:

$$\frac{d^2 c_{1n}(x)}{dx^2} + \frac{\lambda_{1n}}{D_{11}-D_{21}} c_{1n}(x) = \frac{d^2 c_{2n}(x)}{dx^2} + \frac{\lambda_{2n}}{D_{22}-D_{12}} c_{2n}(x) \propto \Psi_n(x). \quad (5)$$

It is obvious, that homogeneous parts of (5) represent archetypal linear harmonic oscillator equation (for the sake of simplicity we will always assume here, that diagonal diffusion coefficients corresponding to “direct” material flow are always significantly larger than those (i.e. non-diagonal ones) corresponding to thermodynamic cross-effects). For the sake of simplicity, we identify here the functions on their right-hand sides as simplest polynomials of the same order as the order of the relevant spatial harmonic is, i.e.  $\Psi_n(x) \propto x^n, n \in \mathbb{N}$ . In general case, the functions on the right-hand side in the relations (5) must be presented as linear combinations of such elementary polynomials. In order to simplify the forthcoming calculations, we introduce here a unifying notation system valid for both ordinary differential equations (ODE-s) in (5):

$$\{c_{1n}(x), c_{2n}(x)\} \rightarrow y(x), \left\{ \frac{\lambda_{1n}}{D_{11}-D_{21}}, \frac{\lambda_{2n}}{D_{22}-D_{12}} \right\} \rightarrow k. \quad (6)$$

According to this simplifying notation system, the ODEs (5) have the following solution obtained directly, via application of the MAPLE 10 symbolic computer algebra system [MAPLE, 2005]:

$$y(x) = K_1 \cdot \cos(\sqrt{k}x) + K_2 \cdot \sin(\sqrt{k}x) -$$

$$-\frac{x^{1+n}}{k \sqrt{x\sqrt{k}(3n+n^2+2)}} \times \left[ -\frac{1}{(x\sqrt{k})^n} (n+2)(n+1) \cos(x\sqrt{k}) \times \right.$$

$$\times \left( x^{1+n} \sqrt{k} \cos(x\sqrt{k}) - x^n \sin(x\sqrt{k}) \text{LommelS1} \left( n + \frac{1}{2}, \frac{1}{2}, x\sqrt{k} \right) \right) +$$

$$+ \frac{1}{(x\sqrt{k})^n} (n+2) \text{LommelS1} \left( n + \frac{3}{2}, \frac{1}{2}, x\sqrt{k} \right) (x^{1+n} \sqrt{k} \sin(x\sqrt{k}) \cos(x\sqrt{k}) - x^n + x^n \cos^2(x\sqrt{k})) +$$

$$\begin{aligned}
 &+x^{1+n}\sqrt{k}\left(\frac{n}{x\sqrt{k}^n}(n+2)\left(\cos(x\sqrt{k}-1)^2\text{LommelS1}\left(n+\frac{3}{2},\frac{3}{2},x\sqrt{k}\right)\right)-\right. \\
 &\left.-\cos(x\sqrt{k})\sin(x\sqrt{k})\left(\sqrt{x\sqrt{k}}+(n+1)\frac{1+n}{(x\sqrt{k})^n}\text{LommelS1}\left(n+\frac{3}{2},\frac{3}{2},x\sqrt{k}\right)\right)\right). \quad (7)
 \end{aligned}$$

Therefore, this symbolic calculation gave us directly an analytical result explained by Lommel-functions [Lommel, 1884-1886], where  $K_1$  and  $K_2$  are integration constants. In the literature about Lommel-type special functions e.g. [Luke, 1969] there are two types of them, namely  $\text{LommelS1}(\mu, \nu, z)$  and  $\text{LommelS2}(\mu, \nu, z)$ , and both of them are solutions of the ODE  $z^2 \cdot y'' + z \cdot y' + (z^2 - \nu^2)y = z^{\chi+1}$ , where “ $z$ ” is an independent variable. The precise difference between these two basic types of Lommel-functions can be simply explained by special functions, namely by  $\nu$ -th order Bessel-functions of the first ( $J_\nu(z)$ )- and second ( $Y_\nu(z)$ ) kind, and  $\Gamma$ -functions [Luke, 1969], [MAPLE, 2005] in the form of:

$$\begin{aligned}
 \text{LommelS2}(\chi, \nu, z) = &-2^{(\chi-1)} \cdot \Gamma\left(\frac{\chi+\nu+1}{2}\right)\left[-\sin\frac{(\chi-\nu)\pi}{2}\right]J_\nu(z) + \\
 &+\Gamma\left(\frac{\chi-\nu+1}{2}\right)\cos\frac{(\chi-\nu)\pi}{2}Y_\nu(z) + \text{LommelS1}(\chi, \nu, z). \quad (8)
 \end{aligned}$$

The first two terms in (7), multiplied by constants  $K_1$  and  $K_2$ , respectively, give the general solution of the well-known “free” harmonic oscillator problem. Although the solution form (7) is visibly rather complicated (as compared to the usual procedures based on the solutions of ODEs with series expansions techniques), we will retain it here, due to its general character. Earlier, the Lommel-type special functions were very effectively applied e.g. in plasma physics [Randriamboarison, 1997], [Randriamboarison, 1999], [Randriamboarison, 2006], while except our own earlier paper [Mészáros et al., 2007] – according to our knowledge - there have not been other applications of them in the classic theory of transport processes. Despite of this fact and possible usefulness in thermodynamic sense (realized by cross - effects entering solution via coefficients  $D_{12}$ ,  $D_{21}$  and eliminating the infinite velocity propagation problem characteristic for separate parabolic type PDEs frequently used at description of transport processes), this solution function is rather complicated and it is difficult to deal with it at practical calculations. Moreover, another solution form of the same type of the ODE (5) can be represented as

$$\begin{aligned}
 y(x) = &K_1 \cos(\sqrt{k}x) + K_2 \sin(\sqrt{k}x) + \\
 &+\frac{i^n[\Gamma(n+1,-i\sqrt{k}x)(\cos(\sqrt{k}x)-i\sin(\sqrt{k}x))+\Gamma(n+1,i\sqrt{k}x)(\cos(\sqrt{k}x)+i\sin(\sqrt{k}x))]}{2k}, \quad (9)
 \end{aligned}$$

where  $K_1$  and  $K_2$  are again integration constants. Since (9) also contains incomplete  $\Gamma$ -functions, which are very complicated to deal with [Mészáros et al., 2007], we will not use (9) further here, but will prefer (7). In low-order variants ( $n = 2,3$ ) the graphics of the integrals leading to appearance of the Lommel-function in the solution are:

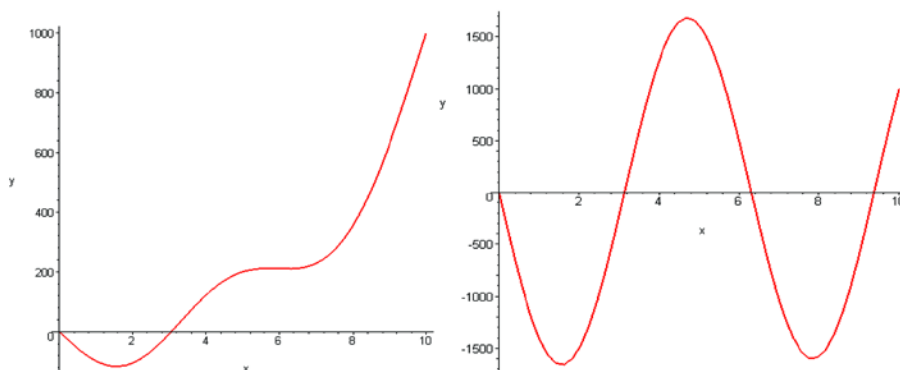


Figure 1.(a-b) Graphics of solutions of the ODE of type (5) for  $n = 2$  and  $n = 3$ , respectively (both graphics are represented in relative units and all constants  $K_1$ ,  $K_2$  and  $k$  are assumed to be equal to one)

Therefore, the oscillatory character of the spatial parts of relative concentration functions described in this section has been obtained without explicit use of the earlier developed WAT [Gyarmati, 1977], which is based on application of the hyperbolic type PDE-s (and their coupled systems) instead of parabolic ones.

### Application of Lagrange's method of variation of constants

The type of the linear ODE, which has to be solved here in its most general form may be represented by:

$$y''(x) + f_1(x) \cdot y'(x) + f_2(x) \cdot y(x) = h(x), \quad (10)$$

and, according to the standard Lagrange's method of variation of constants, it can be solved relatively simply. Let  $y_1(x), y_2(x)$  be two linearly independent solution functions of the homogeneous part of (10). Then, as it is well-known on the base of the classic general theory of variation of constants of ODEs (and their systems) e.g. [Kourensky, 1931], we have the following solution:

$$y(x) = K_1 y_1(x) + K_2 y_2(x) + y_2(x) \int \frac{y_1(x)h(x)}{W(y_1, y_2)} dx + y_1(x) \int \frac{y_2(x)h(x)}{W(y_1, y_2)} dx, \quad (11)$$

where  $K_1$  and  $K_2$  are integration constants and Wronskian of the system is now of the value of  $W(y_1, y_2) \equiv W(\sin(\sqrt{kx}), \cos(\sqrt{kx})) = \sqrt{k}$ . Since in our case  $f_1(x) \equiv 0, f_2(x) \equiv k$ , the integrals appearing on the right-hand side of (11) can be calculated again by MAPLE software package directly and lead to the following finite expressions. In this way we obtained:

$$\int x^n \cos(\sqrt{kx}) dx = \frac{(-1)}{1+n} (-x^{1+n} \cos(\sqrt{kx})) - \sqrt{k} x^{n+2} n (\sqrt{kx})^{-\left(\frac{3}{2}+n\right)} \text{LommelS1}\left(n + \frac{1}{2}, \frac{3}{2}, \sqrt{kx}\right) \sin(\sqrt{kx}) + k \cdot x^{(3+n)} (\sqrt{kx})^{-\left(n+\frac{5}{2}\right)} \text{LommelS1}\left(n + \frac{3}{2}, \frac{1}{2}, \sqrt{kx}\right) \cos(\sqrt{kx}) - \sqrt{k} x^{(n+2)} (\sqrt{kx})^{-\left(n+\frac{5}{2}\right)} \text{LommelS1}\left(n + \frac{3}{2}, \frac{1}{2}, \sqrt{kx}\right) \sin(\sqrt{kx}), \quad (12a)$$

$$\int x^n \sin(\sqrt{kx}) dx = \frac{(-1)}{n+2} (-x^{1+n} (\sqrt{kx})) + \sqrt{k} x^{(n+2)} (\sqrt{kx})^{-\left(\frac{3}{2}+n\right)} \text{LommelS1}\left(n + \frac{3}{2}, \frac{3}{2}, \sqrt{kx}\right) \sin(\sqrt{kx}) + k \cdot x^{(3+n)} (\sqrt{kx})^{-\left(n+\frac{5}{2}\right)} \text{LommelS1}\left(n + \frac{1}{2}, \frac{1}{2}, \sqrt{kx}\right) (n+1) \cdot \cos(\sqrt{kx}) - \sqrt{k} x^{(n+2)} (\sqrt{kx})^{-\left(n+\frac{5}{2}\right)} \text{LommelS1}\left(n + \frac{1}{2}, \frac{1}{2}, \sqrt{kx}\right) (n+1) \cdot \sin(\sqrt{kx}), \quad (12b)$$

i.e. they are represented again by use of Lommel-type special-functions. In order to illustrate the equivalence of the solutions explained by (7) and (11-12a,b), instead of direct and laboursome transformation calculations, we compare them here graphically. Their similarity can be recognized immediately (figures 2-3 are also drawn for  $n = 2$ , and (similarly to figures 1(a-b)) the value  $k = 1$  is taken for the constant in (6)):

Despite of the reversed position of the graphics on the figures 2. and 3. compared to the graphic given on figure 1(a), it can be recognized directly, that the same inflection point appears on all figures 1(a)-2-3 (at the centres of intervals presented on the x-axes).

Since all of the solutions explained explicitly by expressions (7),(8) and (12a-b) show non-monotonic character with clearly visible inflexion points (and differ therefore significantly from simple Gaussian-type curves relevant for solution of separate linear parabolic-type PDEs e.g. [Hörmander, 1983], [Vladimirov, 1984], [Landau and Lifshitz, 2000]), we may state with confidence, that the basic symmetry assumption expressed by (5) leads directly to the result, that

thermodynamic cross-effects are also responsible for effective elimination of infinitely large propagation velocities directly connected to solutions of Fourier's equation of heat conduction or Fick's equation of diffusion. It must also be emphasized, that solution results represented here may also serve as a basis for further refined studies of oscillatory integrals [Hörmander, 1983] being related to simultaneous and coupled diffusion processes in order to give an exact proof for non-existence of singular solutions (explained by use of Dirac-type delta-functions) of coupled transport problems.

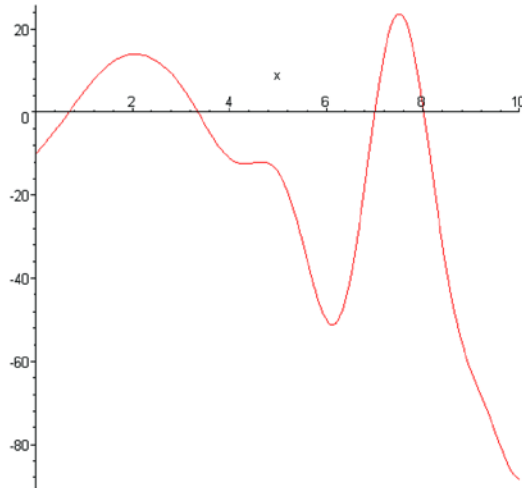


Figure 2. Graphic of solution function of the ODE (5) represented by formulae (11) and (12a-b) for values  $K_1 = +20$  and  $K_2 = -20$  of the integration constants

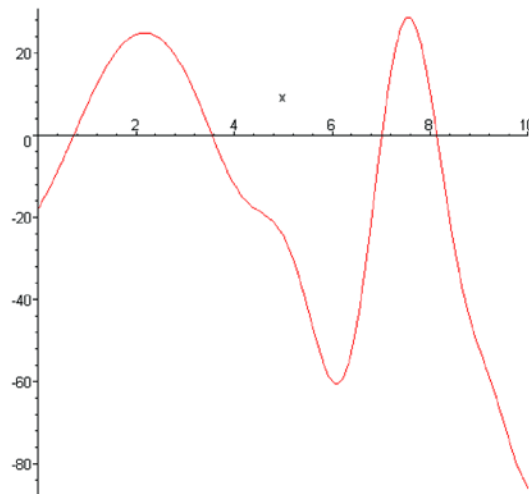


Figure.3. Graphic of solution function of the ODE (5) represented by formulae (11) and (12a-b) for values  $K_1 = +12$  and  $K_2 = -12$  of the integration constants

## **Conclusions**

In the present work a novel approach is presented for effective treating of the infinitely large velocity problem characteristic for idealized transport processes traditionally described by Fourier-, or Fick-equations, which are separate linear parabolic type partial differential equations. After assuming the same solution forms of relative concentration functions on the base of symmetry of the coupled system consisting of two parabolic type linear partial differential equations, the Lommel-type special functions are assigned to a given order of harmonics of the solution functions. It is shown, that this novel – type solution, as well as its possible linear combinations have a completely different shape compared to the classic Gaussian-type solution characteristic for separate linear parabolic-type equations. Then, the same problem is also solved directly by classic Lagrange's method of variation of constants and it is demonstrated graphically, that the two solutions are de facto identical. All calculations have been performed by use of the MAPLE computer algebra system. Further generalization of the method (i.e. if we take into account more than two diffusible components) may give even more accurate description of solutions of the problem and opens new possibilities in modeling and simulation of coupled transport processes through porous media in various engineering problems. Finally, our result may also provide a novel background for studying links about descriptions of propagating disturbances by parabolic-, and hyperbolic-type partial differential equation systems by representation theory of continuous groups.

## **Appendix**

It is well-known from the classic theory of ODEs (e.g. [Ince, 1956]), that general solution of the linear equation  $y'' + \lambda^2 y = f(x)$ , ( $\lambda \in \mathbb{R}$ ) has the following form:

$$y(x) = A \cdot \cos(\lambda x) + B \cdot \sin(\lambda x) + \frac{1}{\lambda} \int_{x_0}^x f(t) \sin[\lambda(x - t)] dt,$$

where  $A = \text{const.}$ ,  $B = \text{const.}$  and  $x_0$  is a suitably chosen value of the independent variable. The integral appearing on the right-hand side is not always possible to solve in closed analytical form. Before widespread use of the computer algebra systems, the general solution of this integral was usually represented by infinite recursive formulae.

## **Acknowledgement**

The research was supported/subsidized by the TÁMOP-4.2.2.B-10/1-2010-0011 „Development of a complex educational assistance/support system for talented students and prospective researchers at the Szent István University” project.

## References

- Annala, A., Kuismanen, E.: 2009, Natural hierarchy emerges from energy dispersal. *Biosystems* Vol. 95, pp. 227 – 233.
- Argyris, J., Faust, G., Haase, M., Friedrich, R.: 2008, *Die Erforschung des Chaos (Eine Einführung in die Theorie nichtlinearer Systeme)* 2. Aufl., Springer-Verlag: Berlin-Heidelberg.
- Bálint Á., Nótás E, Heltai Gy, Tarr Zs, Timári S.: 2000, Transformation of ( $^{15}\text{NH}_4$ ) $_2\text{SO}_4$  fertilizer in brown forest soil in soil core incubation experiment *Bulletin of The Szent István University, Gödöllő*: pp. 93-102.
- Bálint A, Heltai G, Nótás E, Tarr Zs, Jung K.: 2002, Modelling of Environmental Impact of Different N-Sources in Soil/Atmosphere System *Microchemical Journal*, 73:(1-2), pp. 113-124.
- Cattaneo M.C.: 1948, Sulla conduzione del calore. *Atti dei seminario matematico e fisico delli. Università di Modena* Vol. 3, pp. 3 – 21.
- Cattaneo, M.C.: 1958, Sur une forme de l'equation de la chaleur liminant le paradoxe d'une propagation instantane. *Comptes Rendus* Vol. 247, pp. 431-433.
- De Groot, S.R., Mazur, P.: 1962, *Non-equilibrium Thermodynamics*, North-Holland Publ. Co.: Amsterdam
- Eck Ch., Garcke H., Knabner P.: 2008, *Mathematische Modellierung*, Springer-Verlag: Berlin-Heidelberg.
- Gyarmati, I.: 1970, *Non-Equilibrium Thermodynamics (Field Theory and Variational Principles)* Berlin – Heidelberg – New York: Springer-Verlag.
- Gyarmati, I.: 1977, On the wave approach of thermodynamics and some problems of non-linear theories, *Journal of Non-Equilibrium Thermodynamics*, Vol. 2., pp. 233-260.
- Hörmander, L.: 1983, *The analysis of linear partial differential operators I*. Berlin – Heidelberg – New York: Springer-Verlag.
- Ince, E.L.: 1956, *Ordinary differential equations*, New York: Dover Publications Inc.
- Jou, D., J. Casas-Vazquez, and G. Lebon: 2001, *Extended Irreversible Thermodynamics (3rd Ed.)*, Berlin-Heidelberg-New York: Springer-Verlag
- Kirschner, I., Bálint Á., Csikja, R., Gyarmati, B., Balogh, A. and Mészáros, Cs.: 2007, An approximate symbolic solution for convective instability flows in vertical cylindrical tubes, *Journal of Physics A: Mathematical and Theoretical*, Vol. 40, pp. 9361-9369.

- Kirschner, I., Mészáros, Cs., Bálint, Á., Gottschalk, K. and Farkas, I.: 2004, Surface changes of temperature and matter due to coupled transport processes through porous media, *Journal of Physics A: Mathematical and General*, Vol. 37, pp. 1193-1202.
- Knabner, P., Angermann, L.: 2000, *Numerik partieller Differentialgleichungen (Eine anwendungsorientierte Einführung)*, Berlin – Heidelberg – New York, Springer-Verlag.
- Kourensky, M.: 1931, Sur la variation des constants arbitraires pour les intégrales des équations linéaires ordinaires du deuxième ordre, *C. R. Acad. Sci. Paris*, Vol. 192, pp. 1627-1629.
- Landau, L. D., Lifshitz, E. M.: 2000, *Fluid Mechanics*, 2nd Ed. Oxford-Boston-Johannesburg-Melbourne-New Delhi-Singapore: Butterworth-Heinemann.
- E.C.J. von Lommel, Die Beugungerscheinungen einer kreisrunden Öffnung und eines kreisrunden Schirmchens theoretisch und experimentell bearbeitet, *Abh. der Mat. Phys. Klasse k.b. Akademie der Wissenschaften (München)*, 15 (1884-1886) 229 – 328.
- E.C.J. von Lommel, Die Beugungerscheinungen geradlinig begrenzter Schirme, *Abh. der Mat. Phys. Klasse k.b. Akademie der Wissenschaften (München)*, 15 (1884-1886) 529 – 664.
- Luke, Y.L.: 1969, *The Special Functions and Their Approximations Vol. 1.*, New York: Academic Press
- MAPLE 10, 2005, A Symbolic Computation System; Waterloo Maple Inc..
- Martyushev, L. M. and Seleznev, V.D.: 2006, Maximum entropy production principle in physics, chemistry and biology, *Physics Reports*, Vol. 426. pp. 1 – 45.
- Maxwell, J.C.: 1867, On the dynamic theory of gases. *Philosophical Transactions of the Royal Society London* Vol. 157, pp. 49-88.
- Mészáros, Cs., Á. Bálint, I. Kirschner, K. Gottschalk and Farkas, I.: 2007, Mathematical modeling of drying processes using methods of the non-equilibrium thermodynamics and percolation theory, *Drying Technology*, Vol. 25., pp. 1297-1304.
- Mészáros, Cs., Bálint, Á.: 2011, Transient transport processes in deformable porous media, *Chinese Physics B* 20 110507.
- Mészáros, Cs., I. Farkas, K. Gottschalk, B. Gyarmati and Á. Bálint (2011), Surface waves at convection-diffusion processes through porous media, *Mechanical Engineering Letters*, Vol. 6, pp. 95 – 102.
- Pascal, H.: 1993, On a nonlinear convection-diffusion equation. *Physica A*, Vol. 192, pp. 562–568.

- Pascal, J. P.: 1996, Effects of nonlinear diffusion in a two-phase system. *Physica A*, Vol. 223, pp. 99-112.
- Randriamboarison, O.C.: 1997, Impulsive and transient excitation of Bohm-Gross waves in a dissipative plasma, *Physics of Plasmas*, Vol. 4. 2336 – 2347.
- Randriamboarison, O.C.: 1999, Transient Bohm-Gross waves radiated by a point source on the basis of the Klein-Gordon equation, *Journal of Physics A: Mathematical and General*, Vol. 32, 1997 – 2015.
- Randriamboarison, O.C.: 2006, Transient excitation of linear space-charge waves by a punctual source in a drifting cold plasma, *Journal of Physics A: Mathematical and General*, Vol. 39, 9937 – 9960.
- Vernotte, P.: 1958, Les paradoxes de la théorie de l'équation de la chaleur. *Comptes Rendus* Vol. 246, pp. 31-54.
- Vladimirov, V.S.: 1984, *Equations of Mathematical Physics*, Moscow: Mir Publishers

## **Factorial experiment method for determining the efficiency of solar collectors**

István FEKETE<sup>1</sup> and István FARKAS<sup>2</sup>

<sup>1</sup>Department of Technical Engineering, College of Szolnok  
Szolnok, Hungary

<sup>2</sup>Department of Physics and Process Control,  
Szent István University  
Gödöllő, Hungary

### **Abstract**

The efficiency of a solar collector is constantly changing throughout the day, factors such as ambient temperature, fluid temperature and insulation levels play a role in dictating how well a collector converts the sun's energy into usable heat. Most certifications publish information that allows to determine a collector's performance, this performance is often presented as a graph. The corresponding measurement accuracy requires relatively expensive equipment, some accredited institutions are capable of measuring out the efficiency of the collector. In this paper is aimed to introduce a solar collector efficiency curve for determination of normal measuring conditions. The importance of experiments in the fact that the measurement is done in laboratory conditions so that any built collectors can be used. The results of the measurements can appropriate mathematical methods can be evaluated by, so the collector efficiency can be calculated with reasonable accuracy.

### **Keywords**

Solar radiation, collector, temperature distribution, thermal efficiency, structure design.

### **1. Introduction**

The thermal quality of goodness of solar collector is expressed by the efficiency. It must be determined for each apparatus to compare. The efficiency of solar collectors varies a current value, which is primarily dependent on the intensity of solar radiation, alternatively the temperature of the solar collector and its environment.

The efficiency of solar collectors is not categorized as a value, a graph is provided to characterize the efficiency. Typical and constant only in the optical efficiency value can be considered. The efficiency of solar collectors with international standards accepted by Eq. (1) usually given (ISO 9806-2:1995):

$$\eta = \eta_0 - k_1 \frac{\Delta T}{I_g} - k_2 \frac{\Delta T^2}{I_g}, \quad (1)$$

where:  $\Delta T = T_m - T_a$ ,  $T_m = T_{in} + \frac{T_e - T_{in}}{2}$ .

Notations:

- $T_m$  [ K ] – the medium temperature of the heat transfer liquid (calculated),
- $T_a$  [ K ] – ambient air-temperature (measurable),
- $T_{in}$  [ K ] – inlet temperature of the liquid (measurable),
- $T_e$  [ K ] – outlet temperature of the liquid (calculated, (measurable)),
- $I_g$  [ W/m<sup>2</sup> ] – the global radiation, which comes at right angles to the collector (measurable),
- $k_1$  – heat transfer coefficient (heat conductivity) (calculated),
- $k_2$  – heat transfer coefficient (heat radiation) (calculated),
- $\eta_0$  – optical efficiency (calculated).

Some of the incoming solar radiation is lost due to reflection and absorption. The so-called optical efficiency ( $\eta_0$ ) respects of these losses. The collectors give off heat to the environment, heat conduction, and heat convection and by radiation (Killian, 2011). These losses are the heat transfer coefficients  $k_1$  and  $k_2$  is indicated. The energy balance of a type of collector is shown in Fig. 1.

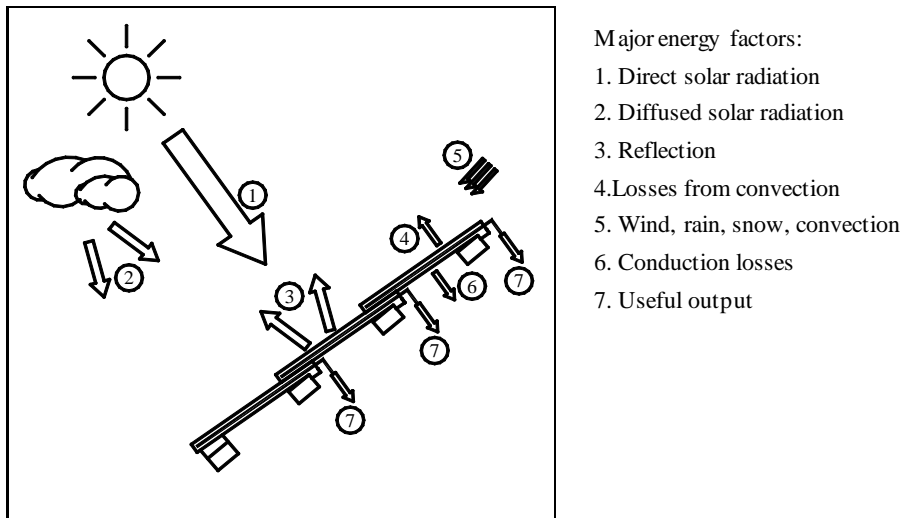


Figure 1. The energy balance of the collector body (own figure)

Heat loss factor and optical efficiency of the collector consists efficiency curve by the Eq. (1) can be calculated. If the collector and the difference between the ambient temperature is equal to zero, the collector does not give off heat to the environment, then the value of the efficiency is maximum, this is the optical efficiency. The optical efficiency and general efficiency curves of the typical collectors are shown in Fig 2.

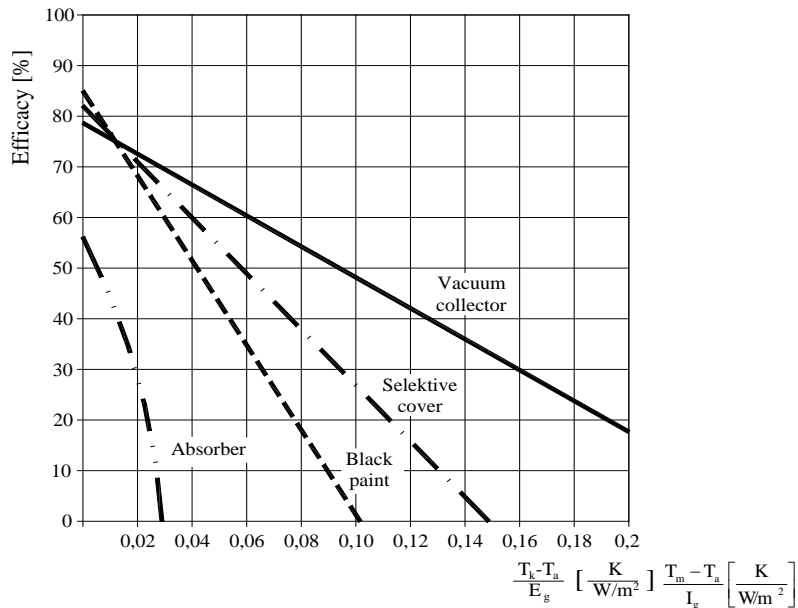


Figure 2. Efficiency-graphs of the different solar collectors (own figure)

The effects of flow rates on the performance and effectiveness of domestic pool solar collector heaters were investigated by Cunio and Sproul (2012). The study shows electrical energy savings in excess of 80% are achievable for typical solar collectors while collector efficiency is only reduced by approximately 10–15%.

The numerical solutions were developed for dynamic solar collector test method. A series of experiments and results are presented for illustration. Analysis of the errors between the predicted and measured fluid outlet temperatures for various test conditions show that the the average error is less than 1°C for unsteady test conditions (Kong et. al, 2012).

The corresponding precision measurement requires relatively expensive equipment. In Europe there are only a few accredited institutions that are suitable for measuring out the efficiency. Most manufacturers of these institutions based on measurement protocols provide the efficiency of solar collector they produce.

In this paper a solar collector efficiency curve determination is shown in normal measuring conditions. As because of the importance of experiments the measurements have been carried out in laboratory environment, so that any built-up collectors can be used.

## 2. Measurement conditions

Factors influencing the efficiency test ( $\eta$ ) parameter: the global radiation ( $I_g$ ), ambient air-temperature ( $T_a$ ), the medium temperature of the heat transfer liquid ( $T_m$ ), inlet temperature of the liquid ( $T_{in}$ ), outlet temperature of the liquid ( $T_e$ ), temperature difference between the medium temperature of the heat transfer liquid and the ambient air-temperature ( $T_m - T_a$ ). The factors listed as having the unit of measurement, while its efficiency is unitless. The optical efficiency than the test parameters are not directly measurable, equal to the values measured by means of extrapolation.

The preliminary measurements to determine the limits of measurement are needed:

- the daily changes in solar radiation intensity and dynamics (see an example in Fig. 3)

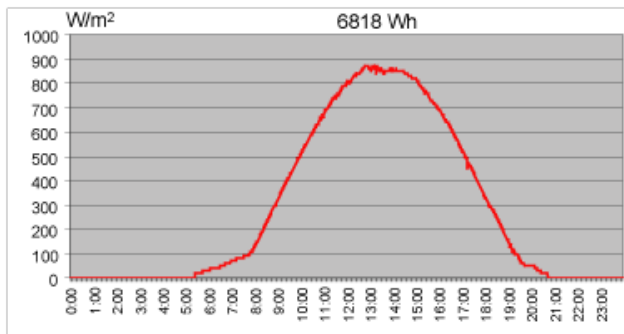


Figure 3. Average summer day solar radiation intensity curve (own figure)

- the daily changes in ambient air-temperature and dynamics (see an example in Fig. 4)

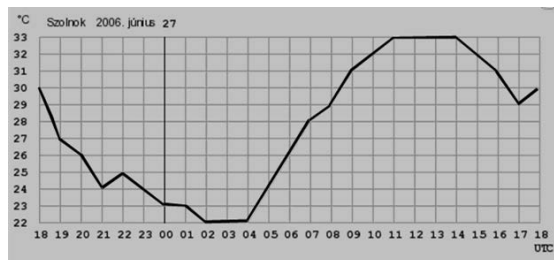


Figure 4. Average summer day temperature curve (own figure)

- the range of inlet temperature of the liquid ( $T_{in}$ ),
- the range of outlet temperature of the liquid ( $T_e$ ),
- determination of the size of the buffer tank,
- mass flow measurement.

During the experiment, temperature rise of the fluid in the collector is measured dependency of the intensity of solar radiation and the rate of flow of the fluid in collector. Then calculate the radiated heat amount, and can be calculated the heat amount absorbed by the collector, so for a given period of time determined by the stabilized collector efficiency.

In this experimental design from the above parameters the solar radiation and the effects of changes in temperature we will attempt to determine to the efficiency:

$$\eta = f(I, \Delta T).$$

*Devices used during the test are as follows:*

- a) Solar radiation is measured on a south direction 45° surface angle with a Kipp & Zonen, CM-5 ventilated piranometer. The device accuracy is within 2%. The piranometer measures the global (total) solar radiation. The measured data is processed in an own developed HC-260-type data acquisition and transferred to PC.
- b) Temperatures are measured with GTH 175/MO type digital thermometer. The device accuracy is  $\pm 0.1^\circ\text{C}$ .
- c) The amount of fluid flowing through the collector hot is measured by a flow + water meter to determine. The measuring accuracy of  $\pm 0.1$  liter.

### 3. Factorial experiment method

When the independent variables in the optimal operating range is relatively simple, linear or quadratic function to look up to, and response factors affecting the number of features is not too large, the factorial experiments are recommended (Antony, 2003). Our goal is for the above listed factors in the efficiency of solar collector change impact analysis, as well as leaving insignificant factor. Follow these steps:

- ( $\eta$ ), as the phenomenon analyzed extreme values for the factors that determine the value,
- given the range of interpretation, the efficiency change, and the relationship between the studied factors ( $\eta = f(I, \Delta T)$ ) determining function.

The factors ( $I$  and  $\Delta T$ ) within the domain of the interpretation, we must take a test range ( $\Delta T_{imin} - \Delta T_{imax}$ ), ( $I_{imin} - I_{imax}$ ). This is necessary because the test results within this range will be valid. In the factor limiting space points set out the experimental settings as in our case, two-factor experiment is therefore the square of the peak. In Fig. 5 the coordinate system is shown in the factor space.

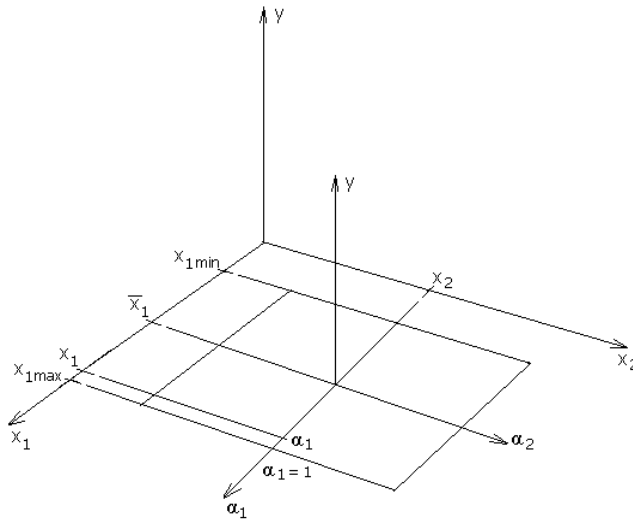


Figure 5. Coordinate system is placed in the center of the factor space

The experimental settings realization check is shown in Table 1.

Table 1. Experimental settings

$\alpha_1$	+		-	
$\alpha_2$	+	-	+	-
Experimental settings	1	2	3	4
Symbol	$a_0$	$a_1\alpha_1$	$a_2\alpha_2$	$a_1\alpha_1\alpha_2$
$\eta_1$				
$\eta_2$				
$\eta_3$				
$\eta_4$				
$\eta_5$				

The last five rows of the measurement results will be added as five-fold repetition of the measurements will be performed.

*Designing the evaluation of experimental results*

Selected according to the experimental design, the relationship between the dependent and independent variables, number of low-degree polynomials can be reached. The model parameters that quantify the effect of each factor, high statistical certainty, independently of each other estimated. Another advantage is that the factors allows simultaneous changes in the detection of interactions between factors such as the information obtained as to what extent the effects of the factors related to setting the levels of other factors (Design of Experiments, 2011).

In order to simplify the subsequent examination, the space factor of the coordinate transformation is performed on both factors, which starts with a basic level to determine the factors by Eqs (2-3):

$$\bar{I} = \frac{I_{\min} + I_{\max}}{2} \quad , \quad (2)$$

$$\overline{\Delta T} = \frac{\Delta T_{\min} + \Delta T_{\max}}{2} \quad . \quad (3)$$

The name of transform factor is  $\alpha_i$ , test range must be fall between -1 and 1. In Fig. 5, the  $I$ ,  $\Delta T$  factors, and  $\alpha_i$  (transformed factor) relationship by the Eqs (4-5):

$$\frac{I - \bar{I}}{I_{\max} - I} = \alpha_1, \quad (4)$$

$$\frac{\Delta T - \overline{\Delta T}}{\Delta T_{\max} - \overline{\Delta T}} = \alpha_2. \quad (5)$$

Of both factor conducting the transformation the test parameter  $\eta$  in the Eq.6 develops:

$$\eta = f(\alpha_1, \alpha_2). \quad (6)$$

Therefore, in the transformed factors range between -1 and 1, and the experimental settings in these locations is created (-), (+).

The accuracy of the test model, of the factor space center also should be a series of measurements. Such results is shown in Table 2:

Table 2. The factor space center measurement series

N	1	2	3	4	5
$\eta_{0n}$					

From the table we get the efficiency ( $\overline{\eta_0}$ ) and variance ( $S_0^2$ ) values.

*The approximate mathematical model*

The form of model can be written as:

$$\eta = \eta_0 - k a b_1 k + b_2 N + b_{12} k N. \quad (7)$$

The results obtained during measurements of Legendre's principle curve is must be a fit. The phenomenon of trying to factor in a linear model approach, which forms the Eq. (8):

$$\eta = b_0 + b_1 I + b_2 \Delta T + b_{12} I \Delta T. \quad (8)$$

The efficiency of transformed coordinate system according to the form of Eq. (9):

$$\eta = a_0 + a_1 \alpha_1 + a_2 \alpha_2 + a_{12} \alpha_1 \alpha_2. \quad (9)$$

*Creating the transformation table*

The data are shown in Table 3, which is the last column of the above table has been specified value calculated from the measured averages.

Table 3. The transformation matrix

Coefficients	$a_0$	$a_1$	$a_2$	$a_{12}$	measuring results
number	-	$\alpha_1$	$\alpha_2$	$\alpha_1 \alpha_2$	$\eta$
1	+	+	+	+	$\eta$
2	+	+	-	-	$\eta$
3	+	-	+	-	$\eta$
4	+	-	-	+	$\eta$
$a_i$	$\bar{a}_0$	$\bar{a}_1$	$\bar{a}_2$	$\bar{a}_{12}$	

The experimental values for the option are expected to Eq. (10).

$$a_i = \frac{\sum_{j=1}^N \alpha_j \eta}{N}, \quad (10)$$

where:

$$N = 2^2 = 4,$$

$$a_0 = 1/N[+\eta_1 + \eta_2 + \eta_3 + \eta_4], a_1 =$$

$$= 1/N[+\eta_1 + \eta_2 - \eta_3 - \eta_4], a_2 = 1/N[+\eta_1 - \eta_2 + \eta_3 - \eta_4],$$

$$a_{12} = 1/N[+\eta_1 - \eta_2 - \eta_3 + \eta_4].$$

The original curve is approximated get it, according to the transformed factors  $\alpha_i$  are replaced respectively by substituting the transformation context.

*The approximate margin of error function*

The variance in each experimental setting can be defined by as:

$$s_j^2 = \frac{1}{n-1} \sum_{i=1}^n (\eta_{ji} - \bar{\eta}_j)^2, \quad (11)$$

where:

N – the number of repeated measurements (n = 5).

*The approximate variance functions*

The variance is calculated from the equation of:

$$s_\varepsilon^2 = \frac{\sum_{j=1}^N s_j^2}{N}. \quad (12)$$

The margin of error amount, the *Student test* using 5% significance level with 95% probability:

$$\Delta\varepsilon = t \cdot s_\varepsilon ; - \text{ where: } - t: \text{ by table 2,571 } \quad (f = 5 \text{ degrees of freedom}).$$

*The variance analysis of the agreement*

The *Fisher's test* under the different experimental settings, to variances of the same theoretical variance, the Eq. (13) is, if:

$$F_k = \frac{s_{\max}^2}{s_{\min}^2} \leq F_{\text{tabl}} \quad (13)$$

where:

–  $F_{\text{tabl}}$  value 5,1.

$F_k$  if it is less than the tabulated value, the *Fisher test* under the different experimental settings belonging to the same theoretical variance within the variance. If the *Fisher test*, there is no agreement, then *Bartlett's test* should be used:

$$c = 0,4343 \left[ 1 + \frac{1}{3(N-1)} \left[ \sum_{j=1}^N \frac{1}{f_j} - \frac{1}{f_0} \right] \right], \quad (14)$$

where:  $f_0 = \sum f_j$  ,

$$B = \frac{1}{C} \left[ f_0 \lg s_\varepsilon^2 - \sum_{j=1}^N f_j \lg s_j^2 \right]. \quad (15)$$

By table  $f = N - 1 = 5 - 1 = 4$  degrees of freedom:  $\chi^2 = 9,488$ .

If  $B < \chi^2$ , the empirical test of theoretical variance within the same variance.

The coefficients significance test are performed:

$$\Delta a_j = \frac{t s_\varepsilon}{\sqrt{N}}. \quad (15)$$

For example, if the  $a_{12} < \Delta a_{12} = \Delta a_j$  the basis of correlation coefficient is not significantly different from zero, and therefore may be omitted, in which case the function can be written in the approximate equation:

$$\eta = \left[ \overline{a_0} + \overline{a_1} \alpha_1 + \overline{a_2} \alpha_2 \right]. \quad (16)$$

If this is satisfied, then the equation describing the phenomenon that the test range, depending on factors transformed,  $\Delta\varepsilon$  a margin of error of 95% probability.

The accuracy of the analysis models

As a first step, if the simplification fails, the previous point-in-context, if not, then the transformed coordinate system, the original form should be replaced with the transformation in relationships:

$$\eta = \overline{a_0} + \overline{a_1} \cdot \frac{\Delta T - \overline{\Delta T}}{\Delta T_{max} - \overline{\Delta T}} + \overline{a_2} \cdot \frac{I - \overline{I}}{I_{max} - \overline{I}}. \quad (17)$$

After settling of the equation, the original function of the factors, it is known relationship describing the phenomenon. In the case when some member coefficient calculated nipper rather, there is a possibility that these members is omitted after certain checks. In this case, the first step is to verify that the simplified approximation functions, the limits of error, describe the phenomenon, then this function belonging to fit variance to be determined.

The different experimental settings, the function Eq. (18) takes the following values, respectively substituting  $\Delta T_{min}$ ,  $\Delta T_{max}$ ,  $I_{min}$ ,  $I_{max}$ .

The different function values calculated for each experimental setting:

$$\begin{aligned}
 \eta_{\text{fl}} (\Delta T_{\text{max}}, I_{\text{max}}) &= (\Delta T_{\text{max}} + I_{\text{max}}), \\
 \eta_{\text{fl}} (\Delta T_{\text{max}}, I_{\text{min}}) &= (\Delta T_{\text{max}} - I_{\text{max}}), \\
 \eta_{\text{fl}} (\Delta T_{\text{min}}, I_{\text{max}}) &= (-\Delta T_{\text{max}} + I_{\text{max}}), \\
 \eta_{\text{fl}} (\Delta T_{\text{min}}, I_{\text{min}}) &= (-\Delta T_{\text{max}} - I_{\text{max}}).
 \end{aligned} \tag{18}$$

The fit variance is defined as:

$$s_{\text{ill}}^2 = \frac{\sum_{j=1}^N (\eta_{\text{fl}} - \overline{\Delta \eta_j})^2}{N - (k + 1)}. \tag{19}$$

If the fit variance, due to lower than the approximate variance functions ( $s_e$ ) then the function surely describes the phenomenon, belonging to each experimental setup. The second step is to check that the approximating function, quadratic members should be taken into account. This was done to approximate the function factor to determine the value of the factorial space center:

$$\eta_{f0} = (\overline{\Delta T_0}, \overline{G_0}). \tag{20}$$

If the  $\eta_{f0}$  average value of this setting is within the margin of error ( $\Delta \varepsilon$ ), then:

$$\eta_{f0} \pm \Delta \varepsilon. \tag{21}$$

In this case, the presence of members of the squares assumed to approximate the function is not justified.

*Of the factorial experiment after expected results:*

- studies exploring factors are negligible,
- ( $\eta$ ), as a determining factor of the phenomenon extreme values are set,
- the efficiency ( $\eta$ ) change in the interpretation of the range, and the factors studied ( $I, \Delta T$ ) to set up connections between functions.

#### 4. The results of the efficiency determination

The measured and calculated values are shown in tabular form (Table 4). Based on the results generated charts and characteristics, are shown in Figs 6-7. The measurement and the calculation precision of the values monitored.

Table 4. The temperature measurement, calculation results

I	m	T <sub>in</sub>	T <sub>e</sub>	T <sub>e</sub> -T <sub>in</sub>	T <sub>m</sub>	T <sub>a</sub>	T <sub>m</sub> -T <sub>a</sub>	(T <sub>m</sub> -T <sub>a</sub> )/I
[W/m <sup>2</sup> ]	[kg/h]	[°C]	[°C]	[K]	[°C]	[°C]	[K]	[K m <sup>2</sup> /W]
804	141	20.2	27.5	7.3	23.85	24.0	-0.15	-0.00019
786	141	20.2	27.2	7.1	23.75	24.0	-0.25	-0.00032
752	141	20.2	27.0	6.8	23.60	24.0	-0.40	-0.00053
721	141	20.2	26.7	6.5	23.45	23.0	0.45	0.00062
841	141	44.9	51.3	6.4	48.10	23.0	25.10	0.02985
894	140	44.9	51.7	6.8	48.30	23.0	25.30	0.02830
817	141	44.9	51.1	6.2	48.00	23.0	25.00	0.03060
889	141	44.9	51.6	6.8	48.30	23.0	25.30	0.02846
943	141	68.6	74.5	5.8	71.50	22.0	49.50	0.05249
945	141	68.6	74.5	5.9	71.55	22.0	49.55	0.05243
956	141	68.6	74.5	5.9	71.55	22.0	49.55	0.05183
969	141	68.6	74.7	6.1	71.65	23.0	48.65	0.05021
946	141	68.6	74.6	5.9	71.55	22.0	49.55	0.05238
932	141	92.0	96.2	4.3	94.15	21.0	73.15	0.07849
936	142	92.0	96.3	4.3	94.15	20.0	74.15	0.07922
898	141	92.0	96.0	4.0	94.00	21.0	73.00	0.08129
928	141	92.0	96.2	4.3	94.15	21.0	73.15	0.07883

Q <sub>liquid</sub>	Q <sub>flow</sub>	η	(T <sub>m</sub> -T <sub>a</sub> )/I <sub>800</sub>	function values	difference
[W]	[W]	[-]	[K / W; m <sup>2</sup> ]		%
1196	1537.2	0.778	-0.1	0.777	-0.1
1166	1502.8	0.776	-0.3	0.778	0.3
1116	1437.8	0.776	-0.4	0.779	0.3
1066	1378.6	0.774	0.5	0.774	0.0
1045	1608.0	0.650	23.9	0.644	-0.9
1109	1709.3	0.649	22.6	0.652	0.4
1012	1562.1	0.648	24.5	0.641	-1.2
1110	1699.8	0.653	22.8	0.650	-0.4
951	1803.0	0.527	42.0	0.536	1.6
967	1806.8	0.535	41.9	0.537	0.3
967	1827.9	0.529	41.5	0.539	1.9
999	1852.7	0.539	40.2	0.547	1.4
967	1808.8	0.535	41.9	0.537	0.4
706	1782.0	0.396	62.8	0.404	2.0
707	1789.6	0.395	63.4	0.400	1.2
657	1717.0	0.382	65.0	0.390	1.8
706	1774.3	0.398	63.1	0.402	1.1

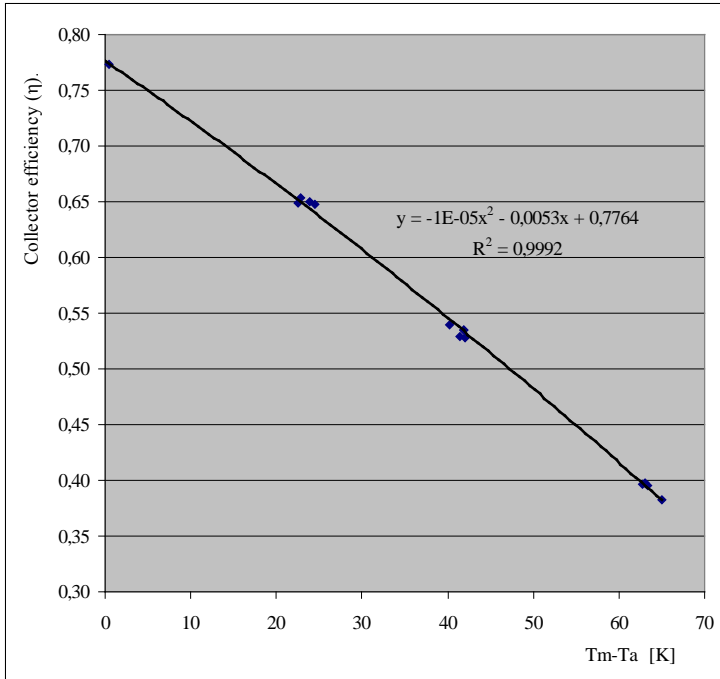


Figure 6. Collector efficiency curve ( $T_m - T_a$ )

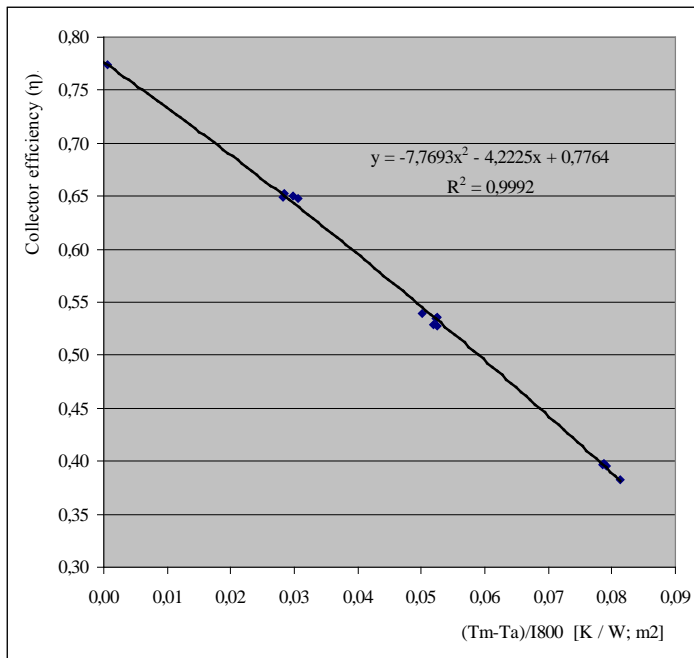


Figure 7. Collector efficiency curve ( $(T_m - T_a) / 1800$ )

The collector efficiency is determined by the operating conditions, as shown in Fig. 7. The optical efficiency of the collector within  $\eta_0=0,776$ , indicating the losses, calculated heat loss coefficient  $k_1=4,24$  (thermal conductivity),  $k_2=0,008$  (thermal radiation).

## Conclusions

Analysis of the efficiency of solar collector has been introduced using calculation and measuring methods. The exact design measurements and the measurement results to the appropriate mathematical methods are shown to be not only a high-precision instruments, laboratory results may be technically correct, ratings are achieved.

Investigations and modeling of the questions raised by the current collector efficiency formula is suitable for the calculations. The change affects the intensity of the radiation collector efficiency. The formula used in medium temperature collector based on the actual value does not reflect the full extent of efficiency. Temperature distribution inside the collector and the collector connected efficiency is important to determine the impact of a more precise control and greater energy gain.

Beside the calculation approach intensive measurements have been carried out including the daily changes of solar radiation and ambient temperature dynamics, the inlet and outlet temperatures of the liquid medium and the value of mass flow rate.

A factorial experimental method has been introduced and explained in details in order to determine the most important factors to characterize the efficiency of solar collectors.

Finally, the collector efficiency curves were determined. This included the optical efficiency, the heat loss coefficient and also the thermal conductivity and thermal radiation factors, as well.

## Acknowledgement

The research was supported/subsidized by the TÁMOP-4.2.2.B-10/1-2010-0011 „Development of a complex educational assistance/support system for talented students and prospective researchers at the Szent István University” project.

## References

- Antony, J., Design of Experiments for Engineers and Scientists, Elsevier 2003, ISBN-10: 0750647094
- Cunio, L.N., Sproul, A.B., Performance characterization and energy savings of uncovered swimming pool solar collectors under reduced flow rate conditions, Solar Energy, Vol. 86, No 5, 2012, p. 1511-1517.

Design of Experiments for Test and Evaluation, Factorial experiments  
[http://kisterv.kkft.bme.hu/download/DOE\\_BME\\_2011.pdf](http://kisterv.kkft.bme.hu/download/DOE_BME_2011.pdf), (in Hungarian)

ISO 9806-2:1995, Test methods for solar collectors, Part 2: Qualification test procedures, International Organization for Standardization, Geneva, Switzerland

Killian, A.V., Solar Collectors: Energy Conservation, Design, and Applications. Nova Science Publishers, 2009, p. 349.

Kong, W., Wang, Z., Xing, L., Xin, L., Ning C., Theoretical analysis and experimental verification of a new dynamic test method for solar collectors, Solar Energy, Vol. 86, No 1, 2012, p. 398-406.

## **Performance of solar collectors by reflected spectral measurements**

Ivett KOCSÁNY, István SERES  
Department of Physics and Process Control,  
Institute for Environmental System,  
Szent István University

### **Abstract**

At the Department of Physics and Process Control, Szent István University, Gödöllő various solar applications were installed for educational, demonstrational and research purposes, such as PV and solar thermal units, transparent wall insulation and solar dryer unit. The solar energy application possibilities give opportunity to reduce the consumption of traditional energy resources by the solar thermal systems. The performance of solar collectors is influenced among them by the intensity of the incoming solar radiation, the active part of the absorber surface, the reflection and absorption of the glass cover of the collectors, the utilization of the system, etc. Reflection measurements were carried out under natural radiation circumstances at summer time in Gödöllő. In this experiment five different types of color filters and a radiometer (designed especially for solar power) were used. The color filters are absorbing the various wavelengths of the spectral ranges.

### **Keywords**

Wavelength, reflection, efficiency, color filters, solar radiation

### **1. Introduction**

The Earth is naturally illuminated by electromagnetic radiation from the Sun. The peak solar energy is in the wavelength range of visible light (between 0,4 and 0,7 nm). Other substantial parts of incoming solar energy are the invisible ultraviolet and infrared radiation. Just a small amount of solar radiation extends into the microwave region of the spectrum. The relative movement of the sun on the sky causes solar intensity change during the day and the year, as the incoming radiation is modified by several processes in the atmosphere like:

- refraction and diffraction,
- absorption,
- scattering,
- reflection.

Longwave radiation is originating from sources at temperatures near ordinary ambient temperatures and thus substantially all at wavelengths greater than 3nm.

To separate the useful range of the spectra of the incoming radiation classification was used based on the traditional physical wavelength ranges. The used classification can be seen in Table 1 as follows.

Table 1. Different ranges of the solar spectra

Range	Wavelength [nm]
Infrared	above 780
Red	640-780
Orange	600-640
Yellow	570-600
Green	490-570
Blue	430-490
Violet	380-430
Ultraviolet	below 380

The radiation could be emitted by a collector, by the atmosphere, by any other body. The intensity of sunlight is reduced in any case of absorption or reflection.

Our measurement shows that not only the intensity but the spectrum of the radiation is changing in time. As the length of the route of the solar radiation through the atmosphere varies during the day (it is longer in the morning and in the evening, and it depends on the season as well), the scattering effect of the air causes spectral difference in the radiation. Based on spectral measurements (see Fig 1. for a sunny and cloudy day) the intensity of the different ranges (IR, red, etc.) were separated and they are planned to compare to the actual efficiency values, to find the most important wavelength range. Based on such observation data analysis was elaborated for understanding the behavior of different technologies. From the measured data the energy production data under low radiation (morning and evening hours, cloudy days - it can be seen on Fig.1.) were analyzed separately from the data under high radiation conditions.

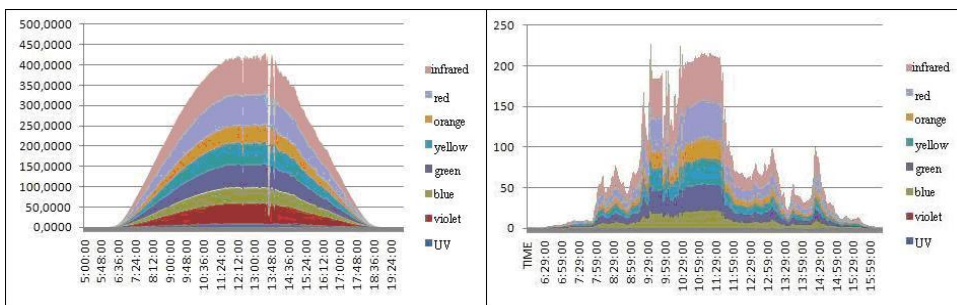


Figure 1. Spectral data of a cloudiness (left side) and cloudy day (right side)

## 2. Materials and methods

### 2.1. Color filters

Color filter is an optical element that partially absorbs incident radiation selective with respect to wavelength (such as color). The different color filters absorb different range of the solar spectral distribution. These filters can be used in field of photography, optical instruments, and illuminating devices to control the amount and spectral composition of the light.

The material of the filters are variable it can be made of plastic (usually cellulose acetate) for economy, of glass for maximum permanence, of liquid solutions in cells with transparent faces for flexibility of control. Material of the filters are defined the users group. Color filters can be classified according to their type of spectral absorption: short-wavelength pass, long-wavelength pass or band-pass; diffuse or sharp-cutting; monochromatic or conversion. Every filter is one band pass filter in terms of the portion of the visible part of the spectrum. Sharp and diffuse denote the sharpness of the edges of the filter band pass.

In a special lab at Szent István University, Institute of Mechanics and Engineering, Department of Agriculture and Food Machinery (MEGI) parameters of our color filters (transmission, reflection of the filters) were measured, the used equipment is shown in *Fig.2*. The measurement results are shown later in the discussion part.



*Figure 2.* The special spectrometer from MEGI

### 2.2. Measurements and the spectrometer

For the measuring the incoming solar radiation a special equipment, a solarimeter was used (*Fig. 3.*). The model SL 200 can measure the radiation in a resolution of  $W/m^2$ . There is opportunity to make a longer experiment for example a more than one day series of measurements. Solar radiation data are updated in every minute. Data base of the meter can be read and also a graphical

approximation can be made. By a transfer data software the measured values can be directly loaded to the computer. The spectrometer is easy to use for evaluation of the produced electric power and also for optimum orientation of solar panels and performances follow-up. It can store and save the average values of power.



Figure 3. Technical data of the used spectrometer

In our measurement the optoelectronic sensor of the meter has been covered by a black cardboard in order to the reflected radiation from the flat plate collector can be measured precisely (only reflected radiation from one direction is measured on this way). The length of the shading cardboard paper is 14 cm and the distance between the sensor and the flat plate collector was 50 cm.

The experiments were carried out at Gödöllő, Szent István University, Department of Physics and Process Control (*Fig. 4.*).

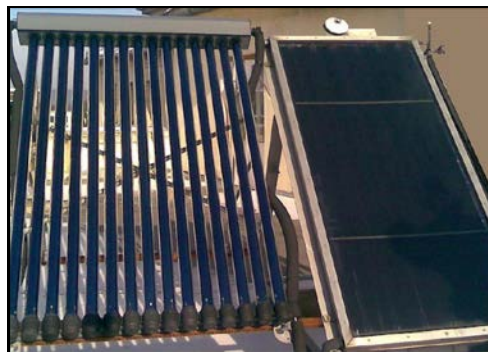


Figure 4. Measurement place  
(Szent István University Physics and Process Control Department)

For the first time the intensity of the direct solar solar radiation was measured without and with using the different type of colour filters (red, blue, green,

yellow and cyclamen). Thereafter this process was repeated with the radiation reflected from the collector surface.

### 2.3. Results and discussion

Based on the measured data, the rate of reflected radiation is principally depends on the angle of incident radiation (Esfamichael et al, 2000). When the angle between the incoming radiation and the normal direction of the surface is small the reflection is less than otherwise. Solar radiation includes both beam and diffuse components. Three types of scattered radiation are known as specular (the angle of incoming radiation is equal to the reflected), diffuse (obliterates all directional characteristics of incident radiation) and general (Shah, 2004.). In general, the magnitude of the reflected intensity a particular direction for a given surface is a function of the wavelength and the spatial distribution of the incident radiation. At this stage of the work the reflection of the total radiation is considered without wavelength dependence.

As it was mentioned earlier the wavelength ranges pass through the filters was measured preliminary in a special lab. The measurement results for the reflectance of the colour filters made in a blackroom circumstances can be seen on *Fig. 5*.

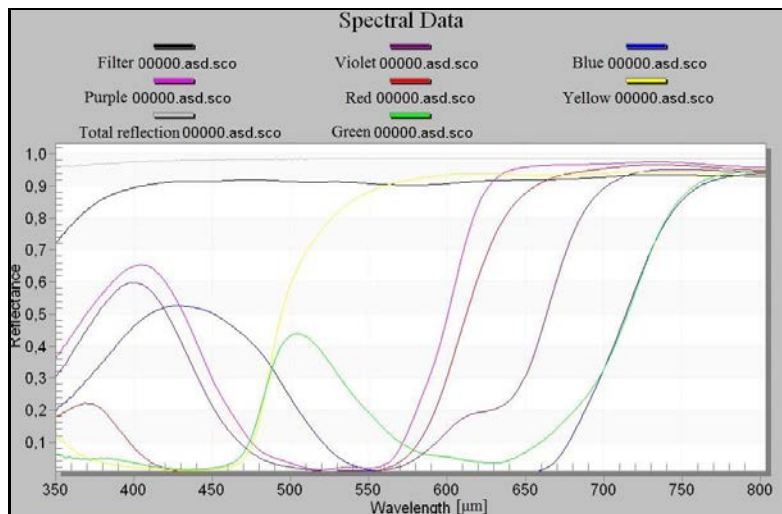


Figure 5. Measured spectral data of the different type of colour filters by Institute of Mechanics and Engineering Department of Agriculture and Food Machinery

From the measurement results, it can be seen, that all the reflectance spectrum lines are going on the same way, increasing from about 0 to 0,95 as the wavelength increases above 800 nm. From these results it can be concluded, that if a special range of the spectra is aimed to investigate, it can be done by subtracting of the data of two filters. The reason for this the reflectivity of the

yellow filter is growing up at the wavelength about 500 nm, while the same effect for the red filter can be noticed at about 650 nm. So in the 500 nm - 650 nm range the red filter transmit much more radiation as the yellow one. The sensitivity graph of this method can be shown as the reflectivity difference of the two mentioned filters, as follows in *Fig. 6*.

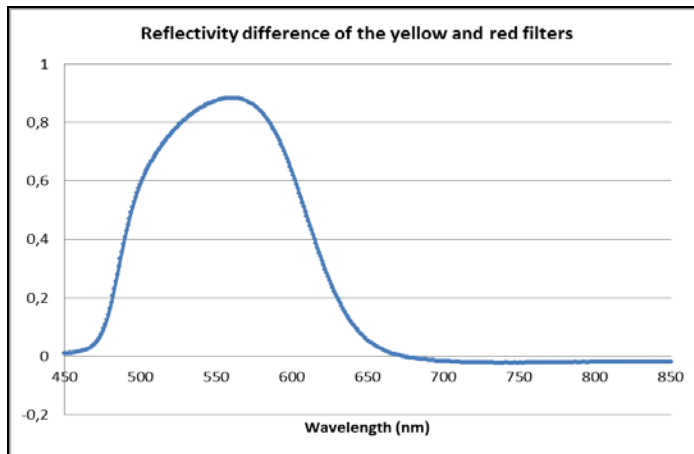


Figure 6. The difference of the reflectivity of the yellow and red filters in the visible range

The same method can be used for the 600 – 750 nm range by the difference of the red and blue filters (*Fig. 7*.)

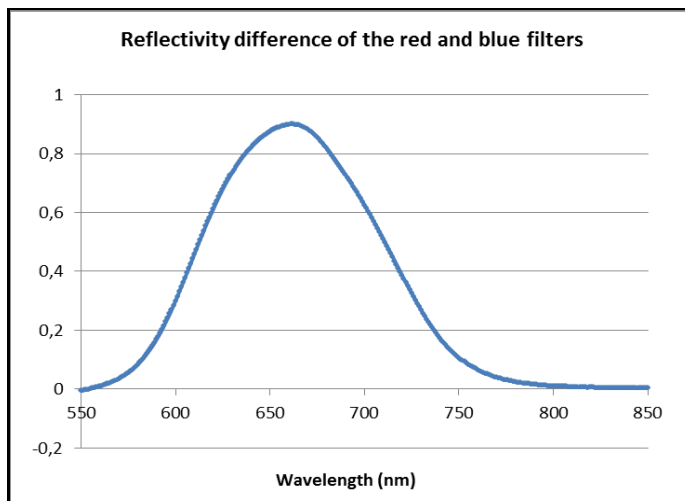


Figure 7. The difference of the reflectivity of the red and blue filters in the visible range

External measurement results can be seen at the following graphs. The rate of the filtered (colour filter) and non filtered incoming direct solar radiation can be seen in Fig.8 at different times of a day.

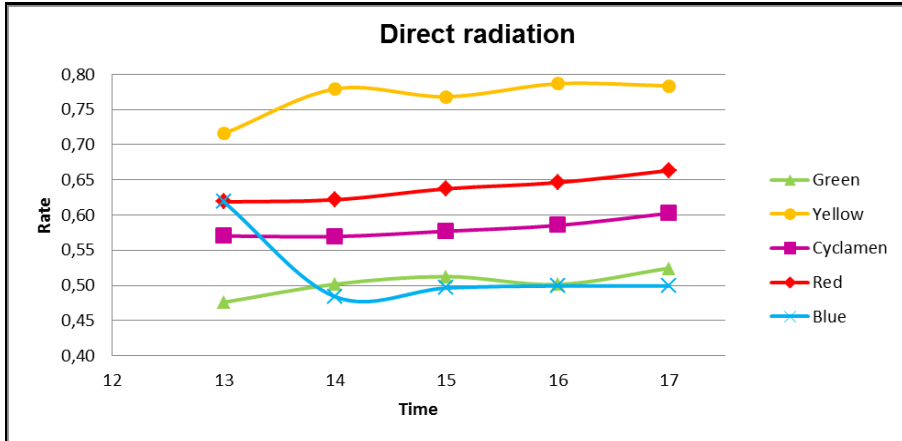


Figure 8. Rate of the direct and filtered solar radiation

For the analysis the difference of the measured power values were investigated, too. For example if the difference of the direct solar power behind a red and a blue filter is graphed, the Fig. 9. figure can be seen.

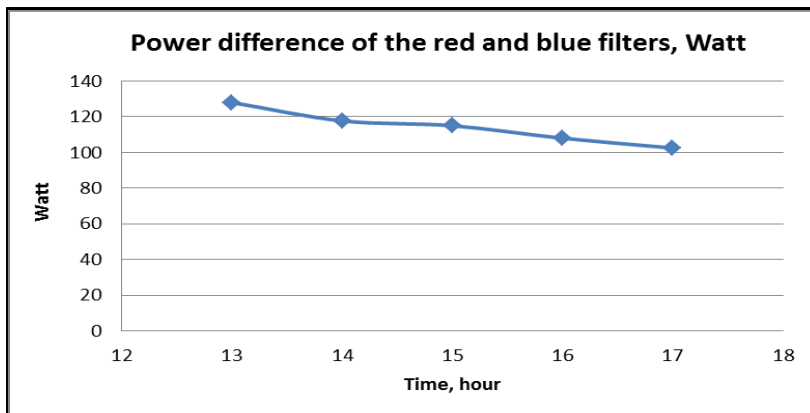


Figure 9. Difference of the red and blue filtered solar power in Watts

From the graph, it can be seen, that the difference is decreasing against the time. It is logical, as when the sun is going lower, the sunrays has to cross longer air layer which cause bigger scattering in the light, such as higher red and lower blue component part. But than the red filter is reflecting more radiation back

which cause less energy through the red filter, as it is shown by measurement in *Fig. 9*.

If the same method is checked for the difference of the reflected light from a solar glass surface, the result are not so definit. The possible reason for it, that in this case the measured values are much lowers (about one tenth of the direct radiation – which shows high – above 90 % - transmitticity of the solar glass in this range) and the sensiticity of the used meter is not low enough for the precise analysis.

## **Conclusion**

During the spectral analysis of the solar equipment the spectral effect of the solar cover (glass or plastic) were tested by the help of color filter slides. First the reflection functions of the used filters were determined. With the help of the spectral distribution of the reflectance the change of the spectra of the direct solar radiation was checked by a solar power meter. The same test were done with the light reflected from the surface of a plain solar collector, but in that case the sensitivity of the used meter was not enough for measuring the small changes.

## **Acknowledgement**

The research was carried out with the support of the OTKA K84150 project.

## **References**

- Cooper P. I. (1969). The absorption of solar radiation in solar stills. *Solar Energy*, Vol. 12, p. 3.
- Esfamichael T, Wackelgard E. (2000). Angular solar absorptance and incident angle modifier of selective absorbers for solar thermal collectors. *Solar Energy* Vol. 68, No. 4, pp. 335–341.
- Shah L.J, Furbo, S. (2004). Vertical evacuated tubular-collectors utilizing solar radiation from all directions, *Applied Energy*, 78, pp. 371–395.

## Solar energy utilization in solar air conditioning systems

Attila SZILÁGYI<sup>1</sup>, István SERES<sup>2</sup>

<sup>1</sup>Department of Vehicle and Agricultural Engineering, College of Nyíregyháza

<sup>2</sup>Department of Physics and Process Control,  
Institute for Environmental Engineering Systems  
Szent István University

### Abstract

Nowadays the energy consumption of the air conditioning during the summer is comparable to the energy consumption of the heating systems in winter. This energy demand would be decreased with solar air conditioning devices reducing the energy consumption and the environmental impact of the power plants.

The heat energy demand of the solar air conditioning of the households can be fulfilled by the solar energy as the energy production is proportional to the consumption, so there is no need for storing the solar energy as it occurs in lot of solar applications. For this purpose a solar collector combined with an absorption cooler can be a proper solution. On the output side of the installation a heat exchanger and a fan is used.

However the idea is used in industrial applications, the household usage is not solved yet. During our first measurements the energy output of a vacuum tube collector was determined as a function of the volume current of the solar liquid. The installation of the heat exchanger to the system is introduced, too.

### Keywords

solar energy, vacuum tube collector, solar cooling, air conditioning

### 1. Introduction

The energy from the Sun is indispensable for the life (living world) in our planet. Besides this energy utilization assure the comfort for the people environmental friendly way.

The incoming solar irradiation maximum value is  $1.360 \text{ kW/m}^2$ , at the boarder of the Earth's atmosphere. This irradiation reaching the Earth surface direct or/and indirect form with the maximum value of  $1 \text{ kW/m}^2$ . The indirect radiation is caused especially by clouds and fogs. The hours with sunshine are variable on the Earth. In Hungary this value is 1200...1400 kWh/m<sup>2</sup> per year. [3]

We can measure the solar radiation with the following devices [1]:

- pyrheliometer (direct radiation: Abbot-, and Angström-pyrheliometer),
- actinometer (relative radiation: Michelson-Martin-, and Linke-Feussner-actinometer),

- pyranometer (direct and indirect radiation: Kipp&Zonen-, and Moll-Gorczyński-pyranometer ),
- pyrgeometer (infra-red radiation),
- pyrradiometer (total radiation), and
- Campbell-Stokes-recorder (record the hours of sunshine).

At Szent István University, Department of Physics and Process Control (Gödöllő, Hungary) the measurement of the solar radiation is done with several Kipp & Zonen pyranometers and the data are stored on a computer.



*Figure 1.* Kipp & Zonen CM-11 pyranometer (SZIU, Department of Physics and Process Control)

## **2. Solar energy utilization**

We can utilize the solar energy with active and passive form. In our case we are using the active form, with collectors, which are utilizing the heating effect of the solar energy.



*Figure 2.* Vacuum tube collector (SZIU, Department of Physics and Process Control)

The collectors have two main forms [2]:

1. concentrated collectors (by solar power plants), and the
2. flat collectors.

The flat collectors' two main types are the flat plate collector and the vacuum tube collector. These collectors are used especially in households. This installation is very simple and we can make hot water, and can use for them heating and cooling. The typical transfer fluids are: water, water and propylene glycol, rarely thermal oil, and air.

### 3. Air conditioning and absorption cooling

In summer we can cool in our house with some kind of environmental forms. These are passive and active forms. The first is architectural solution for example the correct choice of the building's structure, materials (walls, doors and windows, required heat insulation, etc.) and other ways like the natural shading (with plants, trees) and other shading. The second is the using of the air conditioning devices. The most environmental friendly solution is the application a solar collector with an absorption cooling system. For the air changing we can use air to air heat exchanger, with which we can save energy (in winter and in summer).

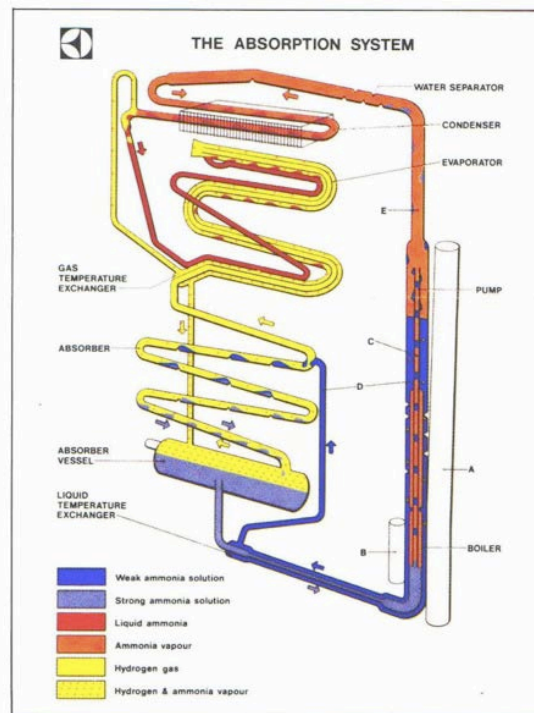


Figure 3. Absorption cooling cycle [II]

The absorption cooling system works with heat energy and make cold with a chemical process. This technology was invented by Edmund Carré and Ferdinand Carré in 1850s. This technology developed by H. Geppert in 1890s and the final form made by two Swedish engineers, Baltzar von Platen and Carl Munters in 1922. Their device operated without pump, used a neutral gas (hydrogen) and air cooling. This was bought by Electrolux in 1925. [4]

#### 4. Measuring unit and results

We have measured a vacuum tube collector operated by the way shown in Fig. 4. The collector useful surface is  $1.485\text{m}^2$ , the solar energy was utilized as heat through a heat exchanger, the transfer fluid was water.

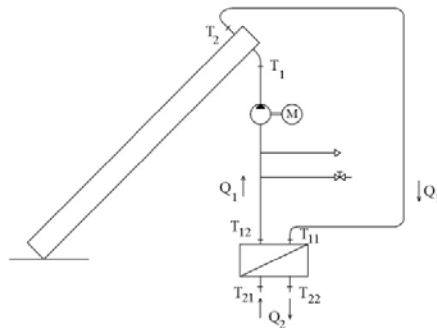


Figure 4. The scheme of the used equipments during the measurement

In Fig. 4. the  $T_1$  and  $T_2$  are the inlet and outlet temperatures of the collector,  $T_{11}$ ,  $T_{12}$  the inlet and outlet temperatures of the of the primer and  $T_{21}$  and  $T_{22}$  the inlet and outlet temperatures of the secondary side of the heat exchanger.  $Q_1$  and  $Q_2$  are the mass currents of the collector loop and the cooler loop.

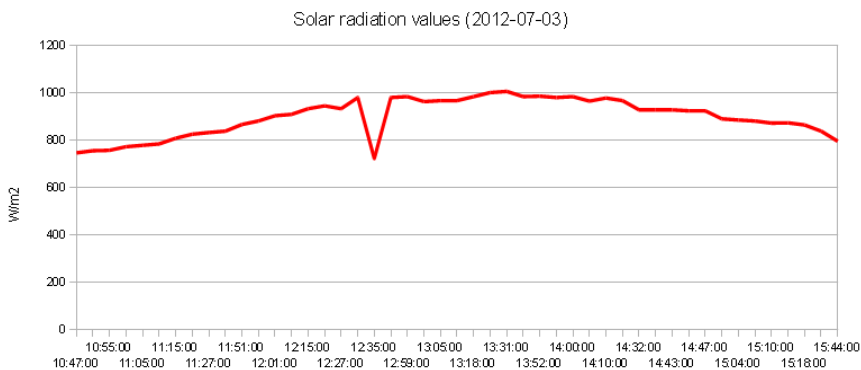


Figure 5. Solar radiation values in a typical sunny day in Hungary

The temperatures were measured at four point with PT1000 sensors, Fig. 4. shows this inlet and outlet measurement points. The other main parameter was the fluid flow rate, which we could change in the primer and in the secondary cycle. The actual, daily solar radiation values were recorded by a pyranometer (Fig 5.).

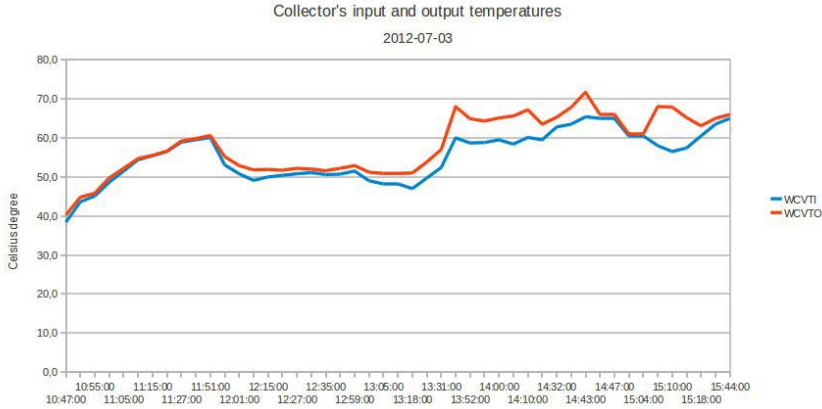


Figure 6. The vacuum tube collector's inlet and outlet temperature values

Fig. 6. shows the difference of the inlet and outlet temperatures. To determinate the collector's heat performance (P), the following formula was used:

$$P = \dot{Q} = \frac{c \cdot m \cdot \Delta T}{d} = c \cdot \dot{m} \cdot \Delta T = c \cdot \rho \cdot \frac{d}{d} \cdot \Delta T = \frac{V}{t} \cdot c \cdot \rho \cdot Q \cdot \Delta T \quad (1)$$

where c is the special heat capacity [kJ/kg K], m is the mass [kg], ρ is the density [kg/m<sup>3</sup>], ΔT is the difference of the temperatures [°C], and Q is the fluid flow rate [m<sup>3</sup>/s]. The water's main parameters are: the c = 4.2 kJ/kg K, ρ = 1000 kg/m<sup>3</sup>. So we can see that the collector's heat performance is depend on two parameters: the fluid flow rate and the difference of temperatures.

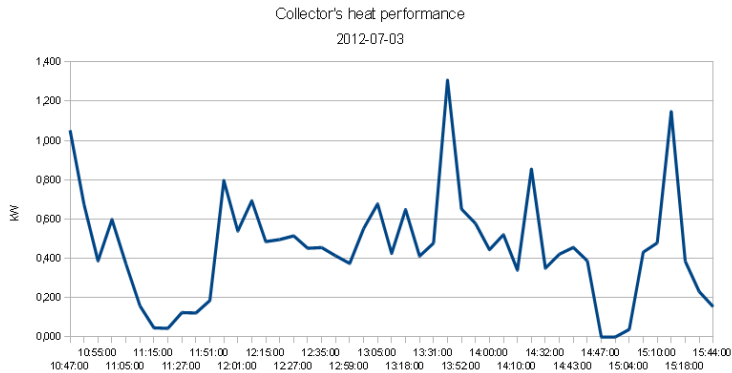


Figure 7. The vacuum tube collector's heat performance

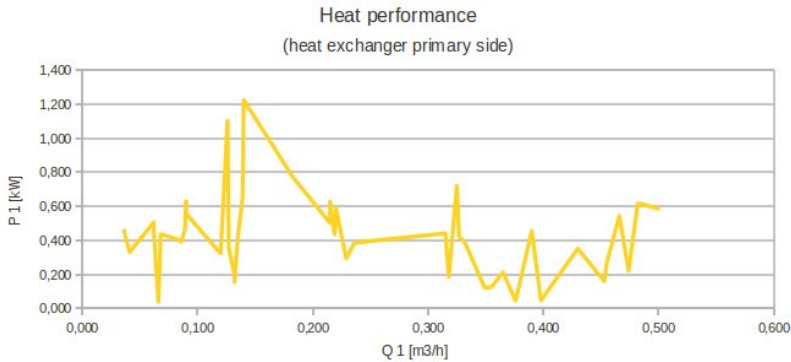


Figure 8. The heat exchanger's heat utilization

## Conclusion

The incoming solar radiation was converted with an about 50% efficiency to heat by the vacuum tube collector (it is a bit lower, then the usual efficiencies of these type of collectors, because of the relatively high output temperature – we had more heat loss in the tubes, valves and other elements, but high temperature is important for the effective operation of the absorption unit).

From the heat exchanger, about 300 W heat power was utilized (which is about 25% of the incoming radiation), so the heat exchanger had the thermal efficiency of 50%. The reason of this high loss is due to the experimental setup, no insulation was used on the heat exchanger.

It was recognized that the efficiency of the heat conversion depends on the fluid flow, the slower fluid flow means higher utilization values, the maximum values were measured between 0.1 and 0.2 m<sup>3</sup>/h flow rate.

The power demand of the planned experimental cooling system can be fulfilled with the introduced system by using of the optimal setting point.

## Acknowledgement

The research was supported/subsidized by the TÁMOP-4.2.2.B-10/1-2010-0011 „Development of a complex educational assistance/support system for talented students and prospective researchers at the Szent István University” project.

## References

- [1] Beke János: Műszaki hőtan mérnököknek, Mezőgazdasági Szaktudás Kiadás, Budapest, 2000., 527-535. oldal (in Hungarian)
- [2] Gyurcsovics Lajos: A napenergia hasznosítása az épületgépészetben, Műszaki Könyvkiadó, Budapest, 1982. (in Hungarian)

- [3] Kacz Károly – Neményi Miklós: Megújuló energiaforrások, Mezőgazdasági Szaktudás Kiadó, Budapest, 1998., 11-43. oldal (in Hungarian)
- [4] Komondy Zoltán – Halász László: Hűtőgépek, Tankönyvkiadó, Budapest, 1970. (in Hungarian)
- [5] Zsebik Albin, Csata Zsolt, Torma József, Váradi Szabolcs, Ioannis Moumoulidis: Fűtés és hűtés napenergiával, Energiagazdálkodás, 2010/2., 3-8.oldal (in Hungarian)
- [I] <http://meteor.geo.klte.hu/hu/doc/> (Debreceni Egyetem, Meteorológiai Tanszék, napsugárzás)
- [II] <http://www.treehugger.com/renewable-energy/steinway-installs-solar-powered-air-conditioning.html>

# **Modelling of meteorological parameters for city Pécs in photovoltaic energy simulations**

István Ervin HÁBER<sup>\*</sup>, Tamás BOTKOS<sup>\*\*</sup>, István FARKAS<sup>\*\*\*</sup>

<sup>\*</sup> Department of Technical Informatics, University of Pécs, Pécs, Hungary

<sup>\*\*</sup> Hungarian Meteorology Service, Pécs, Hungary

<sup>\*\*\*</sup> Department of Physics and Process Control,  
Szent István University, Gödöllő, Hungary

## **Abstract**

Meteorology parameters such as environmental temperature, solar irradiation and the wind speed are influencing the production of photovoltaic (PV) arrays, while these are modifying the efficiency of the PV cells. Averages of meteorology parameters from 10 years back have been collected to make a regression analysis on them and produce a function on each parameters. These functions can give the ingoing data for the previously made block oriented energy model on photovoltaic array, which gives back the correct temperature of the PV modules, and through this, the most accurate actual efficiency can be calculated.

## **Keywords**

ambient temperature, solar radiation, parameter estimation, performance, efficiency

## **1. Introduction**

Photovoltaic (PV) modules are producing energy from sunlight, and since they are made from half conducting materials, like Silicon as the most popular, their production is highly influenced by the temperature of its basic elements, the PV cells. All of the manufactured modules are rated after the Standard Test Conditions (STC). The STC is universally applied to rate peak power output of a solar cell in a laboratory or a module out in the field, but rarely occur in real outdoor applications. Generally, the irradiance (insolation power) is smaller and the temperature higher. Both factors reduce the power that can be delivered by the module to the matched load (Luque and Hegedus, 2011).

The PV cell temperature can be reduced passively by appropriate placing of the modules, since the absorbed sunlight big in percentage will be converted into heat, but this heat can be used for cooling through the naturally induced (bouyancy driven) flows as it is shown in Fig. 1 simulated by CFD. The actual temperature field is shown in K (Háber and Farkas, 2011).

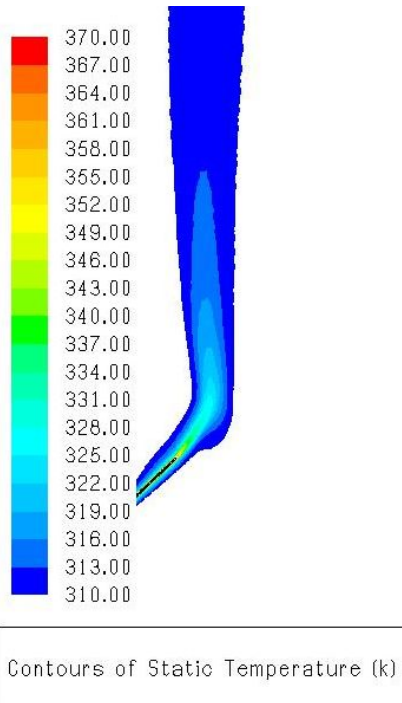


Figure 1. Naturally induced flow at the top of a PV module

Passive cooling can also occur if wind is blowing and it can flow around the module. The cooling rate can be basically given by the heat transfer coefficient ( $\alpha$ ,  $\text{Wm}^{-2}\text{K}^{-1}$ ), and it is increasing by the wind velocity in the most cases. The most popular placing situations (pitched roof, flat roof, facade installation and free standing modules) were investigated by Computational Fluid Dynamics (CFD), to produce functions on the heat transfer coefficients in relation with the wind velocity.

Through these functions if they are used with a heat resistance model, since they are dynamically modifying the wind controlled heat transfer rate, the instantaneous cell temperature can be given. The benefit of this is that we have a complete model for the heat transfer circumstances of a PV module.

This model can be used also to predict the energy production of a whole PV plant very precisely, if we know how the meteorology parameters will evolve.

The meteorology parameters can be presented also as a function following the method described by Farkas and Rendik (1993).

Our whole research is based on the PV system, which can be found on the top of the main building of University Pécs, Faculty of Engineering (Boszorkany str. 2., Pécs, Hungary), and the whole PV energy model evaluation is also based on this. So we have to make the functions of the meteorological parameters, based on the collected climate data's by the Hungarian Meteorology Services local meteorology station located at the airport of Pécs-Pogány.

Our goal is, that at the end, we will have only one ingoing parameter to the PV energy model, which is the number of the day in the year, or a time interval if we want to show the energy production through a year for example.

Based on the literature of this specific field, this could be the most precise model for a PV plant energy prediction, since it takes the wind effects widely into consideration, and not just one condition (1 ms<sup>-1</sup> wind velocity) like the NOCT (Nominal Operating Cell Temperature model), and it is describing the heat transfer in the PV modules structure.

Modeling the meteorological parameters in Pécs can be useful for other engineering applications, such as predicting yield for solar thermal collectors, calculating energy balance at houses, etc.

The modeled parameters can be useful at controlling these systems also.

## 2. Modeling the environmental temperature in details

At the modeling of the environmental temperature the first step is to fit a function on the daily averages, through the year. All the data's the fitting based on, are the averages of the last 8 years (2004-2011), which are official measurements of the Hungarian Meteorology Service.

As the averages of a year were shown in a chart, we can see immediately that an exponential function could be eligible to describe the trend.

The average temperature ( $t_a$ ) function which have to be parameterized is the following way (Farkas and Rendik, 1993):

$$t_a = \left[ a_4 N_{\text{day}}^2 + a_5 N_{\text{day}} + a_6 \right] \exp \left[ - \left[ \frac{N_{\text{day}} - a_7}{182.5} \right]^2 \right], \quad (1)$$

$a_4$ - $a_7$  are the parameters to be identified while  $N_{\text{day}}$  means the actual day number in the year.

The tool *gnuplot* under Unix/Linux systems is a very easy and friendly tool to define parameters of functions fitted on discrete data. It uses the Marquart-Levenberg algorithm, since it is non-linear regression, this method will define the minimum places of the data (Koniarczyk, Adam, 2003).

The computer based approximate minimum search procedures essentially operate in the following manner: First, we estimate a value of the desired parameters: the initial value of the fitting parameters. Then the algorithm from the initial values of the parameters steps in the direction where the amount is most reduced, and calculates that such a small change causes a cash to minimize the loss in the value of the desired quantity. If this is a small reduction below of the threshold, i.e. the procedure is completed, the algorithm converges, and the resulting solution is returned as parameter values.

As initial values we have chosen the already defined parameters to Budapest given by I. Farkas (Farkas, Rendik, 1993).

On Fig 2. we can see the plot of the result of the parameter fitting.

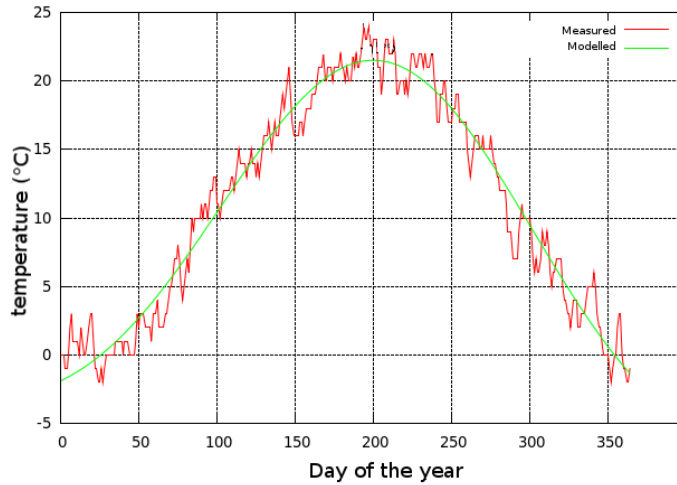


Figure 2. Fitting curve on the daily averages of the environmental temperature

The procedure in *gnuplot* is the following:

```
gnuplot> fit ((a4*x**2+a5*x+a6)*exp(-((x-a7)/182.5)**2)) "homerseklet_napi-at1.csv"
using 1:2 via a4,a5,a6,a7
After 9 iterations the fit converged.final sum of squares of residuals : 850.386rel.
change during last iteration : -1.39304e-07
degrees of freedom (FIT_NDF) : 361
rms of residuals (FIT_STDFIT) = sqrt(wssr/ndf) : 1.53481
variance of residuals (reduced chisquare) = wssr/ndf : 2.35564
Final set of parameters Asymptotic Standard Error
a4 = -0.000804383 +/- 1.427e-05 (1.774%)
a5 = 0.305511 +/- 0.005871 (1.922%)
a6 = -7.31937 +/- 0.6528 (8.919%)
a7 = 212.189 +/- 3.119 (1.47%)
correlation matrix of the fit parameters:
a4 a5 a6 a7
a4 1.000
a5 -0.924 1.000
a6 0.641 -0.878 1.000
a7 -0.128 -0.188 0.539 1.000
VARIABLES:
a4=-0.000804383
a5=0.305511
a6=-7.31937
a7=212.189
```

Figure 3. The result screen of the *gnuplot* fitting procedure

The *gnuplot* calculates the parameters (Fig. 3) and gives back a lot of useful information also, like the Standard Error, and how the single parameters influencing it, degrees of freedom characterizes the goodness of fit (the data pairs are the difference between the number of the seeking parameters). The result contains also a table showing the correlation of the data.

Needed to know that the tables top left and bottom right corner are of one, while the other numbers value close to 0, then the model parameters (in our case,  $a_i$ ) be considered as truly independent data. The closer are the non-diagonal elements to zero, the more accurate the fitted data was considered the error estimation. And of course we get the final values of the parameters  $a_i$ ,  $i=4,5,6,7$ .

Now we have to define the daily changes of the temperature, and sit it on the yearly curve.

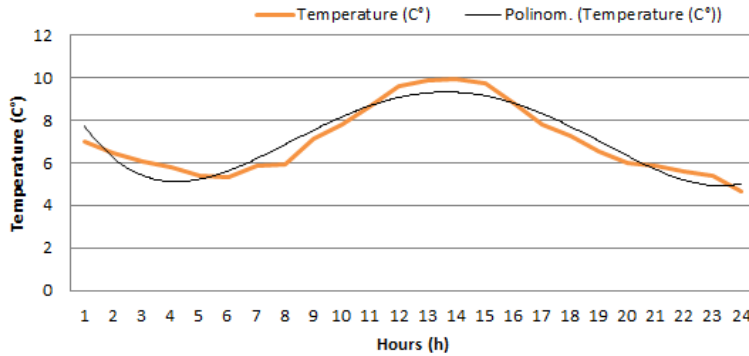


Figure 4. Fitting curve on the hourly averages of the environmental temperature (321<sup>st</sup> day of the year)

Figure 4 shows a possible solution for the fitting made by Excel, but we have the specific function for the ambient temperature, where we have to define the parameters (Farkas and Rendik, 1993):

$$t_w(\tau) = t_m \cos[\alpha(\tau - \tau_0)] + t_a, \quad (2)$$

where  $\alpha = 2\pi/24$ ,  $\tau_0 = a_8$  and  $t_m$  (the amplitude of the cosines function):

$$t_m = [a_1 N_{\text{day}}^2 + a_2 N_{\text{day}} + a_3]. \quad (3)$$

The way is the same as described before, so finally the calculated parameters are:

$$\begin{aligned} a_1 &= -0.0001298, \\ a_2 &= 0.04555, \\ a_3 &= 2.689, \\ a_4 &= -0.000804383, \\ a_5 &= 0.305511, \\ a_6 &= -7.31937, \\ a_7 &= 212.189, \\ a_8 &= 14.0. \end{aligned}$$

According to these, the whole function can be plotted in *gnuplot* as shown on Fig 5.

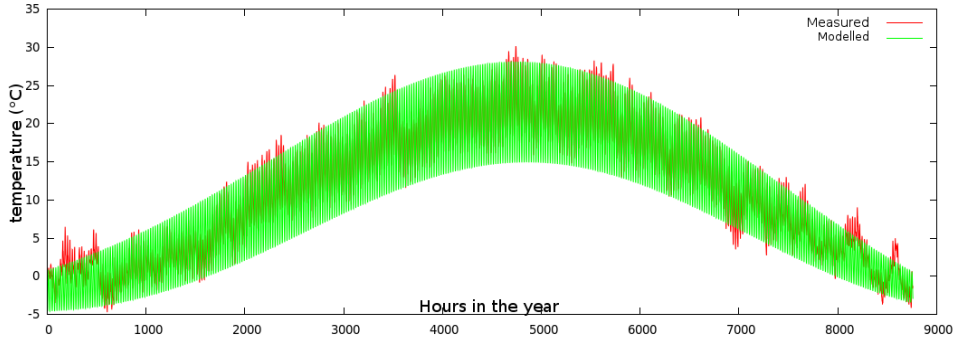


Figure 5. Fitting curve on the annual distribution of the environmental temperature

### 3. Modeling irradiation and wind velocity

The modeling of the irradiation is been made as described above, but we have other initial function. With this irradiation model we can predict the global irradiation comes to a horizontal plane (Hungarian Meteorological Service, 2012).

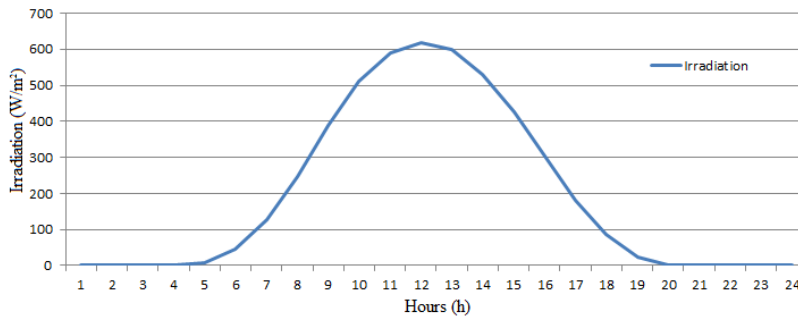


Figure 6. Typical daily distribution of global irradiation

For prediction of the solar irradiation we can use a combination of a cosines and a second order exponential equation (Farkas and Rendik, 1993):

$$I(\tau) = \begin{cases} I_m \cos[\beta(\tau - \tau_0)] \exp\left[-\frac{\tau - \tau_0}{\tau_h}\right], & \text{if } |\tau - \tau_0| \leq \tau_h \\ 0, & \text{if } |\tau - \tau_0| \geq \tau_h \end{cases} \quad (4)$$

where  $\beta = \pi/2\tau_0$

We have to define the function for the maximum daily averages  $I_m$  (5) for the interval halving  $\tau_h$  (6) and for the time delay  $\tau_0$  (7) accordingly (Farkas and Rendik, 1993).

$$I_m = [c_1 N_{\text{day}}^2 + c_2 N_{\text{day}} + c_3] \exp \left[ - \left[ \frac{N_{\text{day}} - c_4}{182.5} \right]^2 \right], \quad (5)$$

$$\tau_h = [c_5 N_{\text{day}}^2 + c_6 N_{\text{day}} + c_7], \quad (6)$$

$$\tau_0 = c_8. \quad (7)$$

The initial values are the already defined parameters to Budapest similarly to the case of temperature approximation. The fitting procedure was performed with *gnuplot* again the same way described above. The parameters calculated for Pécs are the following:

$$c1 = -0.0148689$$

$$c2 = 4.93699$$

$$c3 = 572.477$$

$$c4 = 180.789$$

$$c5 = -0.00013$$

$$c6 = 0.004$$

$$c7 = 3.657$$

$$c8 = 11.5$$

For prediction of the wind velocity we will use the following equation:

$$w(\tau_h) = e^{a(N_{\text{day}})(\tau_h - b(N_{\text{day}})^2) + c(N_{\text{day}})}, \quad (8)$$

where the estimation of the single parameters is:

$$a(N_{\text{day}}) = d_a \cos(e_a N_{\text{day}} - f_a) + g_a, \quad (9)$$

$$b(N_{\text{day}}) = d_b \cos(e_b N_{\text{day}} - f_b) + g_b, \quad (10)$$

$$c(N_{\text{day}}) = d_c \cos(e_c N_{\text{day}} - f_c) + g_c. \quad (11)$$

Based on these functions the fitting with *gnuplot*, the solution for the parameters are the following:

$$da = 166.4$$

$$db = 0.3593$$

$$dc = -0.4763$$

$$ea = 0.000199$$

$$eb = 0.02387$$

$$ec = 0,01881$$

$$\begin{aligned}fa &= 0.03667 \\fb &= 4.368 \\fc &= 4.348 \\ga &= -166.4 \\gb &= 13.15 \\gc &= 2.635\end{aligned}$$

## Conclusion

In this paper the modeling of the meteorological variables especially the ambient temperature and the solar radiation has been made for the location of city Pécs. The parameters of the applied approximation functions have been identified by non-linear regression using Marquardt-Levenberg algorithm along with gnuplot fitting procedure. With these functions the solar PV energy model is complete, and ready for yield simulations.

## Acknowledgement

The research was supported/subsidized by the TÁMOP-4.2.2.B-10/1-2010-0011 „Development of a complex educational assistance/support system for talented students and prospective researchers at the Szent István University” project.

## References

- Luque, Hegedus: (2011), The Handbook of Photovoltaic Science and Engineering, John Wiley & Sons Ltd.
- Háber, I., Farkas, I. (2011), Combining CFD simulations with blockoriented heatflow-network model for prediction of photovoltaic energy-production, Journal of Physics 268, IOP Publishing
- Farkas, I., Rendik, Z. (1993), Handling of solar climatic data, The International Journal of Ambient Energy, Vol. 14, No. 2 April 1993, pp. 59-68.
- Koniorczyk, M., Adam, P. (2003), Introduction to computer processing of measured data, Pécs University Press, Pécs (in Hungarian).
- Solar radiation data, Hungarian Meteorological Service, 2012, Pécs-Pogány.

# **Spectral irradiance effects on exergetic performances of photovoltaic module: initial study**

Dani RUSIRAWAN<sup>1</sup> and István FARKAS<sup>2</sup>

<sup>1</sup>Department of Mechanical Engineering,  
Institut Teknologi Nasional (ITENAS) Bandung  
Bandung, West Java – Indonesia

<sup>2</sup>Department of Physics and Process Control,  
Szent István University  
Gödöllő, Hungary

## **Abstract**

The performance of photovoltaic (PV) systems is influenced by spectrum of solar irradiance even under the same solar irradiance conditions. In term of wavelength ( $\lambda$ ), the spectrum (light) of solar irradiance can be divided into three main regions i.e. ultraviolet region with  $\lambda < 0.4 \mu\text{m}$  ( $\sim 5\%$  of the irradiance), visible region with  $0.4 \mu\text{m} < \lambda < 0.7 \mu\text{m}$  ( $\sim 43\%$  of the irradiance) and infrared region with  $\lambda > 0.7 \mu\text{m}$  ( $\sim 52\%$  of the irradiance). Physically, light with energy too high or low is not usable by a PV systems to produce electricity. In this paper, effects of spectral irradiance on the exergetic performances of PV modules will be initialized, under Gödöllő climatic conditions. As a research subject, two PV modules technologies i.e. poly-crystalline silicon – pc-Si (ASE 100 type) and amorphous silicon – a-Si (DS 40 type), as components of 10 kWp grid connected PV array system at Szent István University were used.

## **Keywords**

Spectrum solar irradiance, visible light, efficiency exergy of PV, poly-crystalline silicon and amorphous silicon

## **1. Introduction**

Presently, direct conversion of solar energy into electricity is being accepted as an important form of power generation. This electricity generated by a process known as the photovoltaic effect using photovoltaic (PV) system, which are made from semiconductor materials.

The outputs of PV systems operating under real working conditions are influenced by two main factors: spectral irradiance distribution and module temperature. When the photon strikes on the PV cell (as smallest of PV system), it can produce electrical energy if the photon energy is greater than or equal to

an energy band gap of the material. Each PV cell has a different energy band gap; for example, amorphous silicon (a-Si) has an energy band gap of 1.7 eV whereas poly-crystalline silicon (pc-Si) has 1.1 eV. PV cells have different spectrum responses at different ranges of wavelength ( $\lambda$ ). As an illustration, the spectrum responses of a-Si and pc-Si lie between 305 – 820 nm and 305 – 1200 nm, respectively (Sirisamphanwong et al., 2012).

It is well known that most of the radiation absorbed by a PV system is not converted into electricity (electrical energy) but also contributes to increase the temperature of the cells or modules (thermal energy), thus reducing the PV system performance or electrical efficiency.

In applications level, the PV module is a basic building block to construct PV systems, and through its connection (both in series or parallel), desired current ( $I$ ) or voltage ( $V$ ) can be obtained.

In thermodynamic point of view, PV module performance can be evaluated in terms both energy and exergy (availability). Energy analysis (energetic) is based on the first law of thermodynamics and exergy analysis (exergetic) is based on both the First and the Second Laws of Thermodynamics. Unlike energy, exergy is not subject to a conservation law (except for ideal or reversible processes). Exergy is consumed or destroyed, due to irreversibility in any real processes. The exergy consumption during a process is proportional to the entropy created due to irreversibility associated with the process.

A lot of studies were conducted on the performances of PV modules, but most of them using energy analysis method.

In this paper, effects of spectral irradiance on the exergetic performances of PV modules will be initialized. As a research subject, two PV modules technologies i.e. pc-Si (ASE 100 type) and a-Si (DS 40 type) as components of 10 kWp grid connected PV array system at Szent István University were used. Beside as comparison purpose, further outcome of this research is trying to find a possibility to increase the performance both PV modules.

## 2. System description

A grid-connected PV array system at Szent István University (SZIU) was installed on the flat roof of Dormitory building of SZIU, and are structured into 3 sub-systems. Sub-system 1 consists of 32 pieces of ASE-100 type modules from pc-Si (wafer based crystalline silicon technology), and sub-system 2 and 3 consists of 77 pieces of DS-40 type of modules from a-Si technology (thin film technology), respectively. The total power of the system is 9.6 kWp with the total PV surface area 150 m<sup>2</sup>. Every sub-system uses a separate inverter (Sun power SP3100-600 for sub-system 1 and SP2800-550 for others sub-system), that will convert the production of DC electrical energy to the 230 V AC, 50 Hz electrical grid (Farkas et al., 2008). The schematic installation of grid-connected PV array at Szent István University can be seen in Fig. 1. The arrays had a 30° tilt with respect to the Earth's surface and were facing 5° East of South.

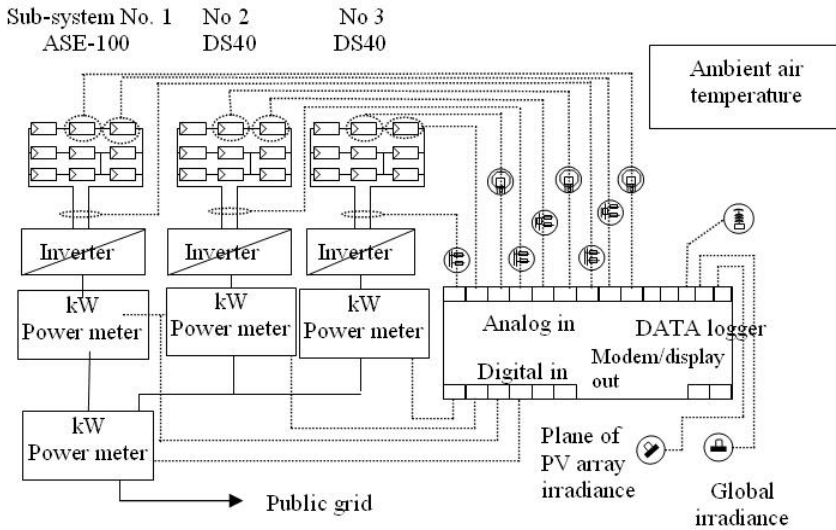


Figure 1. Schematic diagram of a 10 kWp grid-connected PV array at Szent István University, Gödöllő

### 3. Photovoltaic performances

As a general performance parameter, theoretically the energy efficiency of PV system is dependent upon four parameters, namely: the global solar radiation,  $G$  ( $\text{W}/\text{m}^2$ ), the PV area,  $A$  ( $\text{m}^2$ ), the voltage at maximum power,  $V_{mp}$  (V) and the current at maximum power,  $I_{mp}$  (A). The efficiency energy of the PV system can be defined as (Akyuz et al., 2012):

$$\eta_{PV} = \frac{I_{mp} V_{mp}}{GA} \quad (1)$$

Furthermore, the above equation is defined as relative energy efficiency of PV module.

In other way, solar energy can be viewed as photonic energy from the sun. Energy conversion of PV system relies on the quantum nature of light, whereby light is perceived as a flux of particles – photons – which carry the energy (J) as follow:

$$E_{ph}(\lambda) = hf = \frac{hc}{\lambda} \quad (2)$$

where  $h$  and  $c$  are physical constants;  $h$  is Planck's constant ( $\approx 6.626 \times 10^{-34}$  J.s);  $c$  is speed of light in vacuum ( $2.998 \times 10^8$  m/s);  $f$  is the frequency of wave (Hz) and  $\lambda$  is wavelength of the light (nm).

The number of photons falling per second on one square centimeter area on earth for a clear sky day is  $4.4 \times 10^{17}$  (for per square meter area on earth it is  $4.4 \times 10^{21}$ ). Assuming the solar radiation as the solar constant ( $1367 \text{ W/m}^2$ ) for a clear day, the number of photons falling per second on per square meter area can be calculated for a given solar radiation as follow:

$$N_{ph} = \left( \frac{G}{1367} \right) 4.4 \times 10^{21} \quad (3)$$

In order to obtain exergy efficiency of the PV system, the exergy input and output should be known. Exergy means the capacity to work, i.e. the maximum work which the system can perform on passing from a given state to a state of equilibrium with all components of the environmental, which is regarded as a source and receiver of any flows of energy carriers and energy (Sventitskii et al., 2009).

Before make analysis based on experimental, as initial approaches, some correlation as follow can be implemented in order to evaluation of effect spectral irradiation on efficiency exergy of PV module:

$$\dot{E}n_{ph}(\lambda) = En_{ph}(\lambda) \times N_{ph} \times A, \quad (4)$$

$$\dot{E}n_{chemical} = \dot{E}n_{ph}(\lambda) \times \left( 1 - \frac{T_c}{T_s} \right), \quad (5)$$

$$\dot{E}x_{chemical} = \eta_{pc} \times \dot{E}n_{chemical}, \quad (6)$$

where  $N_{ph}$  is the numbers of photon falling per second per unit area on Earth ( $1/\text{m}^2 \cdot \text{s}$ );  $\dot{E}n_{ph}(\lambda)$  is the photonic energy falling on the PV system (W);  $\dot{E}n_{chemical}$  is available photonic energy or Chemical potential (W) or exergy of the solar radiation;  $\dot{E}x_{chemical}$  is exergy rate available from chemical potential (W) and furthermore this term is known as exergy of PV system;  $T_c$  and  $T_s$  are cell/module and sun temperatures, respectively (K); and  $\eta_{pc}$  is efficiency of power conversion (Joshi et al., 2009).

#### 4. Results and discussion

As a general performances, the change in relative efficiency of two PV module respect to variation of the solar radiation and the ambient temperature, are given in Figs. 2 and 3 (simulation by PV\*SOL 3.0 software packages). Principally, at  $T = 25^\circ\text{C}$  and  $G = 1,000\text{W/m}^2$ , the relative efficiency is 1.0, and usually this condition used as reference or standard test conditions (STC).

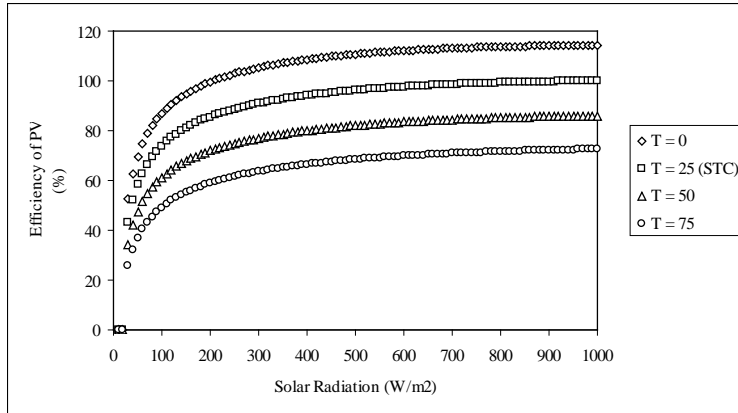


Figure 2. Relative efficiency of PV module at different temperatures for ASE – 100

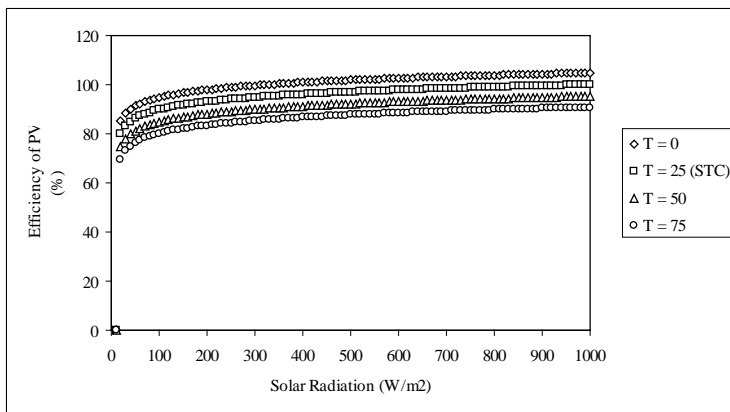


Figure 3. Relative efficiency of PV module at different temperatures for DS 40

Both figures shows that the relative efficiency of module is nearly constant over a wide range of intensities, and only dropping sharply below 20% of the standard 1,000 W. Variations in temperature cause the curve to shift upwards (if colder) or downwards (if warmer). It clear also that ASE-100 (wafer based crystalline silicon technology) is more sensitive to temperature-changes than DS-40 (thin film technology).

Figs 2-3 not show a specific contribution of each solar radiation spectrum on the PV performance. Variability of solar radiation spectrum (in term of wavelength) on the available of photonic energy (chemical potential) and exergy of PV modules (corresponding to the available of photonic energy) during a year can be seen in Figs 4-5, which is calculated based on Eqs (2-6). Data for these calculations are taken from PV\*SOL 3.0 software packages, with efficiency of power conversion 11.94 for ASE-100 and 4.91 for DS-40 (Rusirawan et al., 2012).

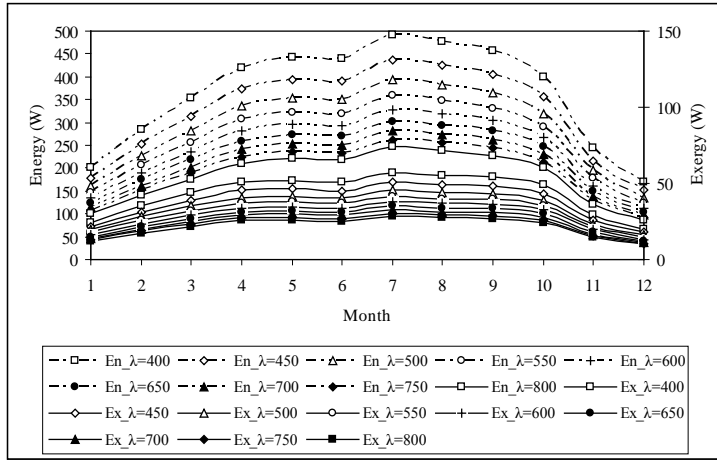


Figure 4. Photonic energy (exergy of solar radiation) and exergy of PV module (ASE-100) at different wavelength –  $\lambda$  (nm)

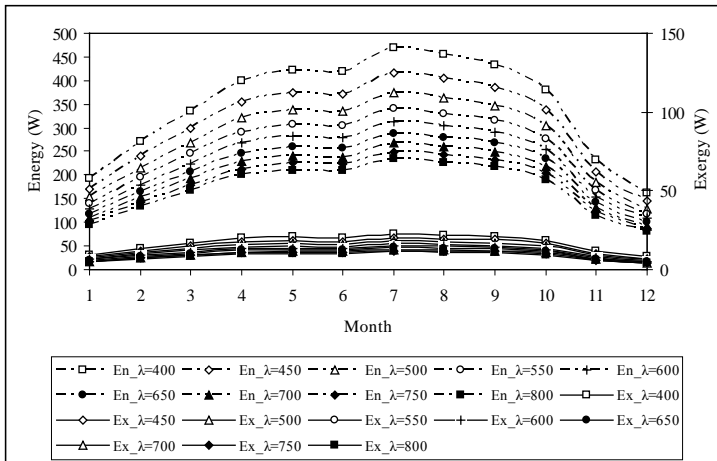


Figure 5. Photonic energy (exergy of solar radiation) and exergy of PV module (DS-40) at different wavelength –  $\lambda$  (nm)

Based on Figs. 4-5, it can be seen that the available of photonic energy ( $\dot{E}n_{chemical}$ ) and the exergy of PV system ( $\dot{E}x_{chemical}$ ) of each PV modules are highest at lowest of wavelength.

In order to get real phenomena and correlation about effects spectral on the PV performance in term of exergetic, spectral solar irradiance data in Gödöllő, that available at Dept. will be used. The solar spectral have recorded at wavelength range between 360 – 1100 nm by using a spectro – radiometer (MS-710), in period 2 months in 2009. Sample of measured spectral data is shown in Fig. 6 (Seres et al., 2009).

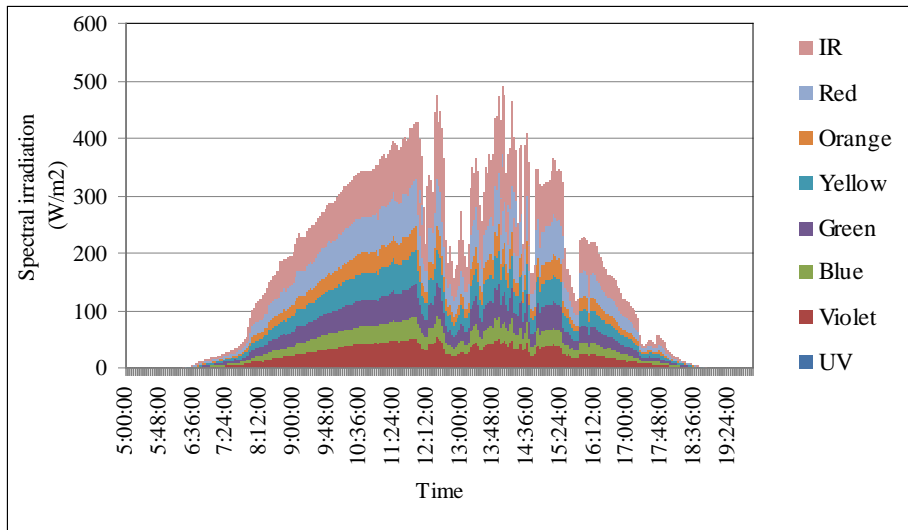


Figure 6. Spectral irradiation data for one day in Gödöllő (data in September 18, 2009)

Based on above figure, it clear that although the red spectral irradiation (in visible region) and infra red (in invisible region) have the lower energy (and exergy), as a consequences of high wavelength, nevertheless both are more important than the rest due to their give big distribution on the whole day (not just in solar peak hours).

## Conclusion

Study of spectral irradiation effect on exergy performance of PV module had initialized. First of all, as a general performance, relative efficiency energy of PV module characteristics is evaluated, theoretically. In term of these, the results showed that ASE-100 (wafer based crystalline silicon technology) is more sensitive to temperature changes than DS-40 (thin film technology).

All the PV modules (in this case ASE-100 and DS-40) showed that the highest exergy of solar radiation (available of photonic energy) and exergy of PV modules can be generated by spectrum of solar irradiance with short wavelength, and vice versa. Based on these characteristics, it can be predicted that change of the wavelength of the spectrum, will great affects on the performance of the PV modules, particularly in exergy efficiency of PV. Deep analysis based on experimentals spectral irradiation measured data still need to performed, in order to get better correlation between energy and exergy efficiencies of PV. Other parameters such as average photon energy (APE) which represent the average energy per photons included in a spectrum, need to be considered in evaluation.

## **Acknowledgements**

This research is carried out with the support of OTKA K 84150 project, Szent István University Kocsis Károly Research Grant and the Ministry of National Education of the Republic Indonesia.

## **References**

- Akyuz, E., Coskun, C., Oktay, Z. and Dincer, I. (2012): A novel approach for estimation of photovoltaic exergy efficiency. *Energy* (44) 1059 – 1066.
- Farkas, I. and Seres, I. (2008): Operational experiences with small-scale grid-connected PV system. Szent István University Faculty of Mechanical Engineering, R&D in Mechanical Engineering Letters (1), 64-72.
- Joshi, A.S., Dincer, I. and Reddy B.V. (2009): Performance analysis of photovoltaic systems: a review. *Renewable and Sustainable Energy Reviews* (13) 1884–1897.
- Rusirawan, D. and Farkas, I. (2012): Availability of the photovoltaic modules in view of photonic energy. *Scientifich monograph: Applications of physical research in engineering part 1*, pp. 42 – 61.
- Seres, I., Farkas, I., Kocsany, I. and Weihs, P. (2009): Comparison of PV modules under different spectral conditions. Szent István University Faculty of Mechanical Engineering, R&D in Mechanical Engineering Letters (3), 81-89.
- Sirisamphanwong, C. And Ketjoy, N. (2012): Impact of spectral irradiance distribution on the outdoor performance of photovoltaic system under Thai climatic conditions. *Renewable energy* (38) 69 – 74.
- Sventitskii, I. I. and Grishin, A. P. (2009): Measurement of solar radiation exergy. *Russian Agricultural Sciences* (Vol. 35, No. 6) 434 – 437.

# **Predictive modeling for low power photovoltaic systems**

Zoltán KAPROS

Department of Physics and Process Control for Szent István University

## **Abstract**

The research work aims the integration of autonomous or grid connected PV systems could be more safely and more cheaply, as presently possible. The obstacles to the spread of PV systems, which need for accurate 15-minute schedules, but the PV technology can not able to give these. The accurate knowledge of more several small systems' power production is not known for the system operators. During the research, analyze and appreciate the opportunity to how can be produced information on the total average PV performances in a micro-region based on measurement and evaluation of a chosen reference photovoltaic system. Further expected result is the errors between the average performances according to analytical programs and the actual measurable values are able to make predictive forecasting. The paper shows a new method which could be suitable for short-term forecast.

## **Keywords**

photovoltaic systems, modeling schedule, smart grids

## **1. The timeliness topic and its importance**

The grid stability requires knowledge of the actual performance of short and long-term modeling of precise estimates. In ideal conditions, or the statistically expected analytical modeling have solved a scientific sense. The weather and radiation conditions vary, so typically only significant deviation follows the statistically expected values. These differences are analytically modeled electricity production is expected to lead to significant errors in comparison.

The demand to spread the low power building integrated photovoltaic systems connected to the grid is increased significantly. By the EU proposed decarbonisation "Energy Roadmap 2050" the electricity generation by 2050 from the renewable energy will minimum 64% and maximum 97%. Another statement that the proportion of electricity consumption in the "gross final energy consumption" in 2050 almost wills doubles reaching 36 to 39% of share.

The co-operation of the various electricity systems, the coordination of balance of energy production and consumption demand has become an essential goal.

Therefore there is need for a scientifically – technically clear methods to combination of small systems (in particular, photovoltaic systems) which can predict the simultaneous production of electrical energy.

## **2. Assumptions**

The autonomous and the grid connected systems with the quarter-hour average performance data can be characterized. The main objective is to develop a new method which able to give the joint performances with minimum requirements measurement. If a chosen reference photovoltaic system has continuous measurement and assessment will be able produced acceptable data for other similar systems operation too. The analytical models can estimated by a large number of unknown factors the 15-minute average performances, but this error and the spreading of this error are important and useful.

From the behavior of standard reference system can be inferred with reasonable accuracy the similar systems behavior. The predictive model is also possible in a period of near-average performance because of the determinative and durable physical effects. Because the expected values of the analytical modeling of a photovoltaic system, especially the meteorological conditions and the radiation fluctuations cause the errors and inaccuracy by the model calculations systems have only slightly responsible. The error due to external factors considered significant deterministic, so that examining a reference system operation by the same type of solar photovoltaic systems can be produced more information specific to the operation of the systems.

## **3. The error measurement and interpretation**

The analysis is based on an examination of the difference between the actually measured and the expected (modeled) average power production. The actual mathematical error measurement and explicit formula for determining the appropriate required. The main aspects are as follows:

- to be relative numbers because of different rating systems in comparison with the performance goal
- to be a relative value, and whose denominator and the ratio values characterized by transparency the different conditions of the periods of the year and the different systems.

The simplest possible to form factor of the relative error that the differences in the relative performance and the expected performance. However the numerator and denominator values would not say anything about the utilization of the system.

The equivalent peak load hour [Sharma, Tiwari, 2011] in a given time shows a value kind of performance. Thus, the actual performance of the system could be illustrated in relation to utilization. In the energetic the peak load hour is typically with hours / year dimension and that means under the continuous

operation with the nominal power how long time would be required to the system may produce that the energy actually produced in a year,

The peak load hour is related to a time period and the energy production, but the equivalent peak load hour is characterized by energy-generating operating capacity in a given moment.

By sizing a PV system is the equivalent peak load hour defined as follows:

$$h_{ekv} = \frac{\zeta_{real}}{I_P} \quad (1)$$

Where  $h_{ekv}$  is the equivalent peak load hour, in h,  $\zeta_{real}$  is total specific amount of solar electricity in kWh/m<sup>2</sup>,  $I_P$  is current value of the global radiation intensity during in kW/m<sup>2</sup>.

In a micro region which is typically exposed to the same environment effects the relative error based on the effective peak load number could be useful indicator.

#### 4. Cell efficiency prediction

The average cell Efficiency adopted by the following equations [Tian et al, 2007]:

$$\eta_m = \eta_r(1 - \beta(T_c - T_a) - \beta(T_a - T_m) - \beta(T_m - T_r) + \gamma \log_{10} I) \quad (2)$$

Where  $\eta_m$  is the average monthly cell efficiency in %,  $\eta_r$  is the reference efficiency in %.  $\beta$  is the solar angle,  $T_c$  is the PV module temperature in °C,  $T_a$  is in the sun (daytime) period the average air temperature in °C,  $T_m$  is the monthly mean temperature in °C,  $T_r$  is the reference temperature in °C,  $\gamma$  is temperature coefficient,  $I$  is calculated factor.

The value of the average cell efficiency could be determined with the cell efficiency calculation and the thermal analysis data for all the characteristics period of current knowledge of global radiation data. So the expected energy production values can also be defined.

#### 5. Modeling based on reference system analysis

A direct reference system based on system monitoring of the operation without significant costs can correct the errors by the analytical methods.

The basic idea is that with the analysis of a selected reference plant and with the differences of the expected and actual values for energy production also can be established a model which is suitable for other plants.

The model assumes that these errors in some way for the operation of each photovoltaic power station are deterministic. So these are typical value by the same technical solutions (e.g., crystalline or amorphous type solar cell) systems. Therefore necessary:

- a database for future expected energy production by analytical model (under the same influence of the weather in the same micro region)
- a specific measurement by reference plant which on the deviation as an error is determined
- developing a model based on the relative error factors to determine actual performance of the photovoltaic systems in the same micro-region. (The micro-region is in a narrow geographic zone in which typically the same climatic conditions.)

## 6. System performance prediction based on past behavior

By a photovoltaic system the amount of electricity produced is compared to the forecasted conditions there are differs, because the actual environmental conditions data (temperatures, solar radiation spectrum, wind, direct and diffuse radiation ratio) and analysis of analytical data used there is always a difference. The variations as interference signal affect the expected production and it is cause errors in the forecasts.

The interference mainly not arise from the characteristics of the systems essentially there are standard components assembled in standard way, so dependent on natural conditions. The determining factor is the combination of interference by a reference system.

Due to The interference effects' complexity it is difficult and expensive to make analytical model with practical benefits, but some numerical methods could be suitable for using. One new model used the 15-minute mean expected performance data and expected energy production during this period characterizing the current operating status.

The performance, expressed as an equivalent peak load number can be expressed as follows:

$$h_{ekv,t}(t) = \frac{(g_{PV}(t) \times \eta(t) \times A)}{I_P} \quad (3)$$

Where the  $h_{ekv,t}$  is equivalent peak load hour in t time by the expected modeled global radiation data,  $g_{PV}$  is amount of daily global radiation in kWh/day,  $\eta$  is the PV efficiency, A is the PV useful surface area in  $m^2$ ,  $I_P$  is the current value of the global radiation intensity in  $kW/m^2$ .

Always sunny weather expected and actually measured equivalent peak load numbers are determined. Table 2 shows the relative error factor can be seen:

Table 1. Sample Data Table

$t_0$	$\Delta t$	$h_{ekv,t0}$ (expected)	$h^*_{ekv,t0}$ (measured)	$f_{t0} = (h-h^*)/h$
$t_1$	15 min	$h_{ekv,t1}$	$h^*_{ekv,t1}$	$f_{t1}$
$t_2$	15 min	$h_{ekv,t2}$	$h^*_{ekv,t2}$	$f_{t2}$
$t_3$	15 min	$h_{ekv,t3}$	$h^*_{ekv,t3}$	$f_{t3}$
...	...	...	...	...
$t_n$	15 min	$h_{ekv,tn}$	$h^*_{ekv,tn}$	$f_{tn}$
...	...	...	...	...
$t_m$	15 min	$h_{ekv,tm}$	$h^*_{ekv,tm}$	$f_{tm}$

A numerical model can be set up a polynomial function for the  $f(1), f(2), \dots, f(n)$  predictive values. So that the model is able to determine an specified expected average performance data for the following  $\Delta t$  short-term periods.

So based on error analysis of an reference power plant operation may be suitable for giving the 15 minutes average predictive performance data in the same micro region

The prognosis means directly a fault factor prognosis. However, with this prognosis the specified value is counted from the expected performances of analytical model,

## Conclusion

The research work aims the integration of autonomous or grid connected PV systems could be more safely and more cheaply, as presently possible. The obstacles to the spread of PV systems, which need for accurate 15-minute schedules, but the PV technology can not able to give these. The accurate knowledge of more several small systems' power production is not known for the system operators.

During the research, analyze and appreciate the opportunity to how can be produced information on the total average PV performances in a micro-region based on measurement and evaluation of a chosen reference photovoltaic system.

The research thesis is expected that the average performances of the systems can be modeled with reasonable accuracy with an on-line examination of a reference system.

Further expected result is the errors between the average performances according to analytical programs and the actual measurable values are able to make predictive forecasting.

## Acknowledgement

The research was supported/subsidized by the TÁMOP-4.2.2.B-10/1-2010-0011 „Development of a complex educational assistance/support system for talented students and prospective researchers at the Szent István University” project.

## **References**

- TIAN, W.-WANG, Y.-REN, J.-ZHU, L. (2007): Effect of urban climate on building integrated photovoltaics performance, *Energy Conversion and Management* 48. pp. 1–8.
- SHARMA, R.-TIWARI, G.N. (2011): Technical performance evaluation of stand-alone photovoltaic array for outdoor field conditions of New Delhi, *Applied Energy*, Article in press

# **Landfill gas quality and quantity parameter changes depending on precipitation intensity**

Tamás MOLNÁR

Institute of Plant Sciences and Environmental Protection  
University of Szeged, Faculty of Agriculture

## **Abstract**

Landfill gas production and methane generation are affected by the physiological conditions and main abiotic factors of the microbes involved in the degradation process: nutrient content, temperature, moisture content and pH values [Bánhegyi, 1993]. Micro-organisms need nutrients for the sustenance of their vital functions to be able to provide the energy content necessary for their cell activities [Zehnder 1988]. The anaerobic degradation processes are affected by the change in pH, which also affects methane generation; a neutral pH = 7 is the best [Szabó, 1994a]. One of the most important factors in the development of the landfill gas is the temperature of the waste, while the outside temperature changes only have an impact in the upper few meters of the landfill, but with some delay it is displayed inside the waste. The moisture content of the waste is an important factor for micro-organisms, it is necessary for metabolism and biochemical processes [Tabasaran, 1980]. The optimum moisture content levels range widely; on wastewater treatment plants biogas was produced even out of materials containing 0,1-1,0% solid. The upper limit of the landfill by 60% solids content, if anaerobic conditions can be reached by compression, landfill gas can be obtained. Literature data indicate that 40 to 50% dry matter content of the landfill is most suitable for ensuring the best anaerobic environment, however, significant differences can be observed in the values of landfill gas generated in dry and wet waste [Olessák-Szabó, 1984].

## **Keywords**

Landfill gas, abiotic factors, anaerobic degradation, municipal solid waste,

## **1. Introduction**

In our country and world-wide the amount of waste is growing rapidly due to economic development. It is true that the amount of selectively collected waste is also increasing and also the quantities of secondary materials as recycled materials quantities – so they can get back into the manufacturing process – however it is an important task to dispose of the waste at an up-to-date and environmentally friendly location.

The theoretical and practical phenomenon confirms that processing the generated waste by modern European Union-compliant technology systems can be used as alternative energy instead of fossil energy sources to produce electricity and heat. The other aspect is to protect the environment, and therefore use measures and technologies, which provide possibility for minimizing the potential environmental problems during the placement and disposal of waste. The issue of landfill gases from the anaerobic decomposition of municipal waste has been dealt with since it was demonstrated that natural and anthropogenic methane, carbon dioxide emissions contribute to the development of the greenhouse effect phenomenon. The objective of my research is to examine and assess the factors influencing the development of landfill gas production at a waste disposal site that is characteristic of a given region. The landfill gas extraction was examined under operating conditions and it was found out which changes in the parameters caused the change of quantity and quality characteristics of the energetically utilized landfill gas.

## 2. Material and Method

The examinations were carried out on the communal solid waste refuse dump of the „A·S·A Hódmezővásárhely Köztisztasági Ltd.” in the outskirts of Hódmezővásárhely on the area No. 01957/1 between 31.01.2007 and 31.12.2007 at 11 gas wells, where the precipitation quantity data provided by the weather station were examined together with the landfill gas qualitative and quantitative parameters I measured. During the research, test groups were formed out of the daily rainfall groups and the methane contents of the associated gas wells (Table 1). The data were statistically processed with SPSS for Windows 11.0 program was used. The data were processed by the method of analysis of variance. Homogeneity was examined with Levene-test. When comparing the group-couples Tamhane test (in case of heterogeneity), and LSD test (in case of homogeneity) was applied. The tightness between variables was determined by linear regression analysis; the test results were illustrated in tables and in graphical form. I determined which group pairs show significant differences and, regarding all gas wells, what the impact of rainfall change is on the methane contents of the landfill gas and the quantity of the produced landfill gas.

Table 1. Precipitation quantity groups and their operational parameters

Rainfall groups	Rainfall quantity [mm/day]
<b>1. group</b>	0
<b>2. group</b>	0,1 - 1
<b>3. group</b>	1 - 3
<b>4. group</b>	3-5
<b>5. group</b>	>5

## 2. Results

### 2.1 Quantity and quality changes of landfill gas by precipitation quantity

In case of all gas wells I tried to find relationships between the daily precipitation data provided by the meteorological station and the methane content of the landfill gas. Since there can be significant differences in the gas production of the dry and wet landfill, the examination of this field is significant considering the whole landfill gas verticum. The results are presented in Table 2, where the minimum and maximum values of methane content are between 1-68%. The best values can be observed in groups 3-4. , which was 1-5 mm/day precipitation intensity and 54,65-50,14% methane contents. With the highest element number in group 1, with 0 mm/day precipitation intensity 48,91% methane content was measured, while the least favourable 48,44% methane content was measured in Group 5 above 5 mm/day precipitation intensity.

Table 2. The results of the correlation between precipitation and methane contents

Rainfall groups	Raifall quantity [mm/day]	N [db]	CH <sub>4</sub> Mean [%]	CV% [%]	Deviation [%]	95% Confidence Interval for Mean		Min. [%]	Max. [%]
						Lower Bound	Upper Bound		
<b>1. csoport</b>	0	286	48,91	29,91	14,63	47,21	50,61	1	68
<b>2. csoport</b>	0,1 - 1	77	49,78	27,43	13,65	46,68	52,88	17	66
<b>3. csoport</b>	1 - 3	55	54,65	22,33	12,20	51,35	57,95	20	67
<b>4. csoport</b>	3-5	33	50,14	30,21	15,15	44,77	55,51	1	64
<b>5. csoport</b>	>5	66	48,44	29,83	14,45	44,89	51,99	6	68
	Összesen	517	49,67	28,79	14,31	48,43	50,90	1	68

Based on the above relationships it can be observed that correlation can be found between the methane content and the precipitation of the landfill in case of precipitation quantity groups 3-4, the results presented in Figure 1. In case of groups 1 and 2 (0-1mm/day) precipitation quantity domain the average methane content values decreased significantly (48,91-49,78%), as the moisture content value necessary for the anaerobic catabolism decreased. In case of group 5 it could be observed when the precipitation quantity reached of exceeded the value of 5 mm/day then the biological conditions deteriorated; the surroundings of the gas wells got wet, and their productivity and methane content significantly decreased. In this domain the leachate must be stopped to get back in order to maintain landfill gas production.

The variance coefficient was CV%=22,33%, the deviation was s=12,207, the sample number was n=55db in Group 3 (3-5mm/day) in the precipitation quantity domain. In this case I measured the most favourable methane content (CH<sub>4</sub>=54,65%), and the minimum and maximum values were 17-66%. The

variance analysis showed significant results between the group pairs with significance level  $P < 5\%$  in the examined parameters. The sample proved to be homogenous by the homogeneity examinations so I use LSD test. The results of the analysis of the various groups are shown in Table 3. The statistical analysis proved 5,736% and 6,208% methane contents difference between the group pairs 3.-1. and 5.-3. Significant differences can be observed in these groups. The significance levels of 3.-1. group pair shows a deviance of ( $\text{sig}=0,007$ ),  $P < 5\%$  between the groups 5.-3. there is significant deviance ( $\text{sig}=0,018$ )  $P < 5\%$ .

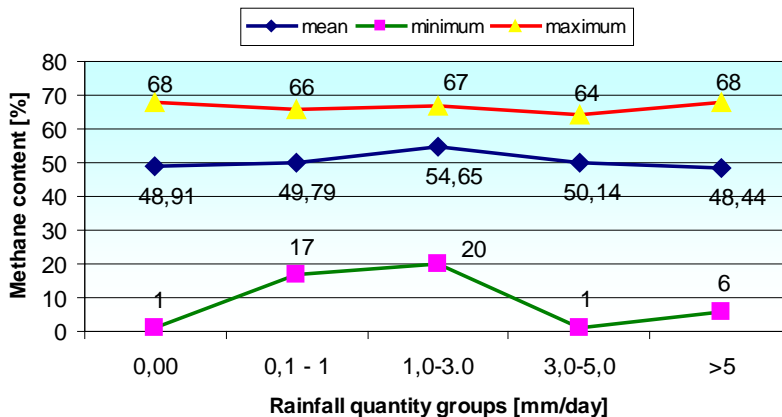


Figure 1. The results of the correlation between precipitation and methane contents

Table 3. Differences in the methane content of the examined groups and the results of the group pairs

Rainfall groups	Rainfall quantity [mm/day]	1. group 0 [mm/day]	2. group 0,1-1 [mm/day]	3. group 1-3 [mm/day]	4. group 3-5 [mm/day]	5. group >5 [mm/day]
1. group	0	-	ns	*	ns	ns
2. group	0,1 - 1	0,866	-	ns	ns	ns
3. group	1 - 3	5,736	4,870	-		*
4. group	3-5	1,230	0,364	4,506	-	ns
5. group	>5	0,472	1,338	6,208	1,702	-

ns = not significant, \* =  $P < 5\%$ , \*\* =  $P < 1\%$

The precipitation data provided by the meteorological station and the methane quantities of landfill gas from all gas wells were put together and presented in Table 4. The changes of methane contents and the quantity values of the landfill gas are influenced significantly by the amount of the precipitation.

When processing the data I found that the most favourable period with regard to the values of methane content and also the quantity values of landfill gas is May and June. The average temperature values are higher and also the increasing precipitation quantity is favourable for the biological processes in the landfill.

Table 4. Quantity and quality changes by the precipitation quantity

Month	Landfillgas CH <sub>4</sub> [%]	Landfillgas quantity [m <sup>3</sup> /month]	Peak hours [h]	Rainfall quantity [mm/ month]
January	53,91	18150,41	292,50	26,5
February	53,60	24764,41	335,25	35,20
March	47,05	20416,65	325,75	48,80
April	49,12	21562,23	332,25	10,30
May	54,92	27859,25	358,25	98,30
June	53,65	25998,36	339,25	111,00
July	49,24	22771,35	396,81	32,80
August	51,19	23175,18	290,54	52,50
September	46,30	16407,71	233,84	68,80
October	46,98	22846,56	326,82	51,60
November	46,89	22998,25	353,62	66,90
December	48,14	22966,35	328,95	23,50
Total	49,67	269916,71	3913,8	52,2

A statistical analysis was necessary this is why a linear regression examination was carried out with the monthly average methane content values of all gas wells [CH<sub>4</sub> %] and also the precipitation quantity data [mm/month], the results of which are presented in Figure 2. The relationship between the methane contents of all gas wells and the precipitation at the landfill can be described with the equation  $y = 0,0442x + 47,263$  the  $R^2 = 0,1964$ . The tightness of the relationship shows intermediate correlation, the value of the correlation coefficient is  $r=0,44$ . In case of positive correlation the methane content of the landfill gas can grow together with the growing precipitation amount.

Further linear regression examinations were made to find the relationship between the monthly changes of landfill gas quantities [m<sup>3</sup>/month] and the precipitation amount [mm/month]. The results are shown in Figure 3. The relationship between the monthly changes of landfill gas quantities and the precipitation amount can be described with the following equation:  $y = 58,304x + 20117$  the  $R^2 = 0,5026$ . That means the precipitation quantity has a in 50,26% influence on the quantity of the landfill gas produced from the gas wells. The value of the correlation coefficient is  $r=0,71$ , an increase in precipitation results in the increase in the landfill gas quantity.

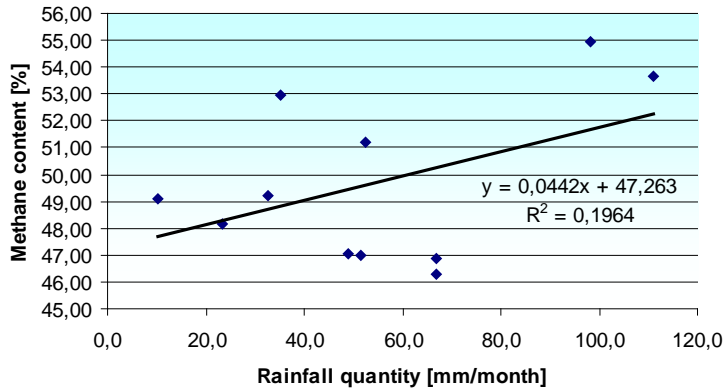


Figure 2. Precipitation intensity changes on the methane content of the landfill gas

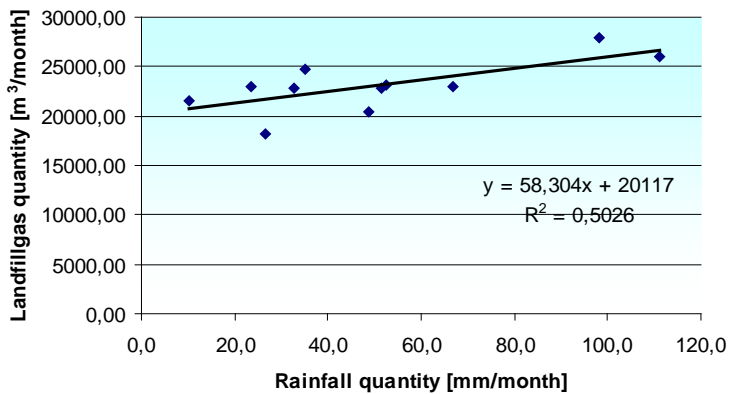


Figure 3. Precipitation intensity changes on the quantity of landfill gas

## Conclusion

I found that the rainfall quantity rates influence the processes taking place in a landfill, so the amount of landfill gas and its methane content. The relationship between methane content and rainfall intensity can be described with the equation  $y = 0,0442x + 47,263$  where  $R^2=0.1964$  and the correlation coefficient is  $r=0,44$ . The relationship between rainfall intensity and the quantity of landfill gas can be described with the equation  $y = 58,304x + 20117$  where  $R^2=0.5026$  and the correlation coefficient is  $r=0.71$ . I suggested when the rainfall intensity is less, then the water from the leachate reservoirs should be directed to the top of the waste with irrigation systems, so that the moisture content is maintained and that dust concentration is reduced. In the rainy period the area near the gas wells should be prevented to get wet because of the gas production and methane content can significantly decrease so in this case the leachate should be evaporated with the heat generated by waste heat from engines.

## **Summary**

The landfill sites have two fundamental problems to deal with, one is the rainfall leaking through the body of the waste and the other is landfill gas quantity from the anaerobic decomposition of waste. Current regulations require landfills to have drainage systems for leachate for landfill gas deflectors in order to meet environmental standards. The depletion of fossil fuels and also their polluting effect have drawn the attention to the exploration and practical application of alternative energy sources [Farkas, 2010]. The issue of landfill gases from the anaerobic decomposition of municipal waste has been dealt with since it was demonstrated that natural and anthropogenic methane, carbon dioxide emissions contribute to the development of the greenhouse effect phenomenon [Farkas, 2010]. The objective of my research is to examine and assess the factors influencing the development of landfill gas production at a waste disposal site that is characteristic of a given region. The landfill gas extraction was examined under operating conditions and it was found out which changes in the parameters caused the change of quantity and quality characteristics of the energetically utilized landfill gas. Overall, in a particular landfill, the meteorological parameters are always changing; the organic matter input parameters are characteristic of the region therefore the extraction efficiency can only be changed by the control of the exhaust capacity. Therefore, research has great importance in this area of research to show which landfill gas parameters are generated with the climatic parameters and organic matter intake. Both the existing and proposed landfill sites might use the results of my doctoral research for the best available landfill gas extraction and methane content.

## **Acknowledgement**

The research was supported/subsidized by the TÁMOP-4.2.2.B-10/1-2010-0011 „Development of a complex educational assistance/support system for talented students and prospective researchers at the Szent István University” project.

## **References**

- Bánhegyi, I. (1993): *Biológiai hulladékkezelés. Hulladékgazdálkodás* (szerk. Árvai J.), Műszaki Könyvkiadó, pp.39-423.
- Olessák, D.–Szabó, L.(1984): *Energia hulladékokból*. Műszaki Könyvkiadó, Budapest.
- Szabó, I. (1994): *A hulladéklerakók aljzatszigetelő rendszerének kialakítása*, Műszaki irányelv tervezet. Kézirat, Budapest.
- Tabasaran, O. (1981): Gas production from landfill. In: Bridgewater AV, Lidgren K, editors. *Household waste management in Europe, economics and techniques*. New York: Van Nostrand Reinhold Co.; 1981. p. 159–75.

Zehnder, ABJ.(1998): *Biology of Anaerobic Microorganisms*. New York: John Wiley and Sons.

Farkas F.(2010): Climate change – biofuels. „Natural and artificial ecosystems in Somes-Cris-Mures-Tisa rives basins”. Nemzetközi konferencia, Arad, 2010. május 7-8. p. 172.

# **Comparative analysis of destructive forces acting on the structure of off-road towed vehicles**

László GURMAI<sup>1</sup> and Péter KISS<sup>2</sup>

<sup>1</sup>Szent István University, Faculty of Mechanical Engineering,  
Institute of Process Engineering,

<sup>2</sup>Department of Automotive Technology  
Gödöllő, Hungary

## **Abstract**

Trailers towed on terrain are exposed to extreme stress. The spectral density of terrain profiles' stochastic activating function provides a basis for studying the destructive effects of vibration on structures. Knowledge of the spectral density and the vehicle's characteristic frequency range permits a comparative examination of the different terrain conditions. From this we can diagnose the extent to which roads with different surface profiles damage the test structure at different towing speeds. The results can be used to design test tracks where vehicles suffer the kind of damage that occurs in regular working conditions.

## **Keywords**

terrain profile, spectral density, characteristic frequency

## **1. The relevance of the subject and objectives**

Fatigue tests of vehicles traversing terrain in many cases result in faults that differ from those observed in actual field conditions. This is because existing test systems do not – or not with sufficient accuracy – model the mechanical effects that vehicles experience in actual use. The damage-causing effects experienced by vehicles towed over terrain may be determined by performing series of measurements. Using the measurement results, we can produce a comparative method allowing the determination of force relations occurring in reality. The method permits the development of a fatigue testing system that causes fault phenomena equivalent to those which occur on vehicles used in the field.

The objective of the research is thus to analyse the relationships between vehicles traversing terrain and the conditions of that terrain. A further objective is to investigate and describe the excitation forces acting on vehicles due to the terrain profile, i.e. the micro and macro obstacles.

## 2. Theoretical background to terrain condition modelling

The research involved measuring the relationship between vehicle and terrain. The approach was based on the methods and theoretical considerations of vehicle-terrain theory. Of the four models of wheel-track relations, the most appropriate was identified as deforming wheel on deforming surface model, on the basis of the discussion in Laib: *Vehicles moving on terrain* (2002). The model takes account of the effects on vehicle motion of the mechanical behaviour of the deforming soil and the vibrational properties of the terrain profile and the vehicle. The forces arising from the interaction of the two systems under various terrain conditions may be determined by measurements.

The causes of vibrational accelerations divide into macro-obstacles, comprising the relief forms of the terrain, and the micro-obstacles that cover the soil surface. The micro-obstacles have a much more complex effect on the structure than the macro-obstacles, and their profiles can only be described by statistical functions. The unevenness on the soil surface may, according to Gedeon (1981), be described by the mathematical representation of stochastic, i.e. random processes. A stochastic processes is a group of random, physically-related events or forms which have the same statistical parameters.

Because of the stochastic nature of terrain unevenness, the forces acting on the vehicle will also be stochastic. This permits the inference that measurement results must be evaluated using an analytical method using numerical calculations to produce statistical results.

The stochastically-distributed excitation function derived from the terrain profile permits determination of the spectral density based on the destructive effect of the vibrations on the structure. The lifetime determination method permits real loads to be mapped to a combination of obstacles that may be used for accelerated fatigue tests.

The spectral density function is formally equivalent to the Fourier transformation relation:

$$S(f) = \lim_{T \rightarrow \infty} \frac{1}{2T} \left( \int_{-T}^T \left( \xi_t(\omega_0) e^{-ift} \right) dt \right)^2 \quad [\text{m}^3] \quad (1)$$

- $\xi_t(\omega_0)$ : realisation function of the specific machine  
 $f$ : frequency  
 $T$ : half period

## 3. Determination of resonant frequency of trailers

Measurements are required to determine the destructive effect of various terrain conditions. The magnitude of forces generated on the vehicle by the excitation of

profiles, however, depends on the vibrational properties of the vehicle structure. For the structure shown on figure, we must establish its vibrational characteristics before we can measure the mechanical effects of a specific terrain. We must know the centre of mass, mass, number of elastic and dampening elements and their properties, and the period of the trailer's characteristic angular frequency. These properties may be determined by measurement and used to calculate the system's inertial moment and resonant frequency.



Figure 1. Trailer adapted for acceleration measurements

A basic assumption for determination of the trailer's natural angular frequency and critical resonant frequency range was that the structure behaves similarly to a physical pendulum, i.e. its period of vibration is constant, and that the vibration of a vehicle brought into vibration will gradually attenuate.

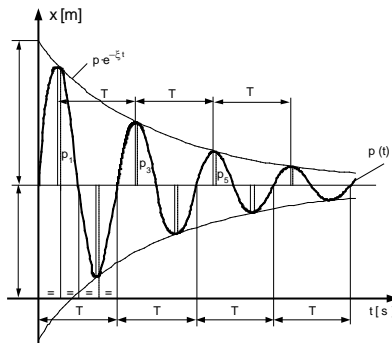


Figure 2. Damped vibration

In its general form, attenuated vibration is described by the function:

$$x(t) = x_0 \cdot e^{-ct} \cdot \sin(2\pi \cdot f \cdot t + \alpha) \quad [m] \quad (2)$$

Displacement:  $x$  [m]

Initial displacement:  $x_0$  [m]

Frequency of damped vibration:	$f$	[Hz]
Phase angle:	$\alpha$	[°]
Time:	$t$	[s]
Attenuation coefficient:	$c$	[Ns/m]

The characteristic angular frequency ( $\alpha$ ) is derived from the trailer's characteristic attenuation curve, which we determine by drop tests. The measurement involved recording the vibrational curve of the trailer's suspension system. The elastic characteristics of the trailer's tyres were determined at three different inflation pressures.

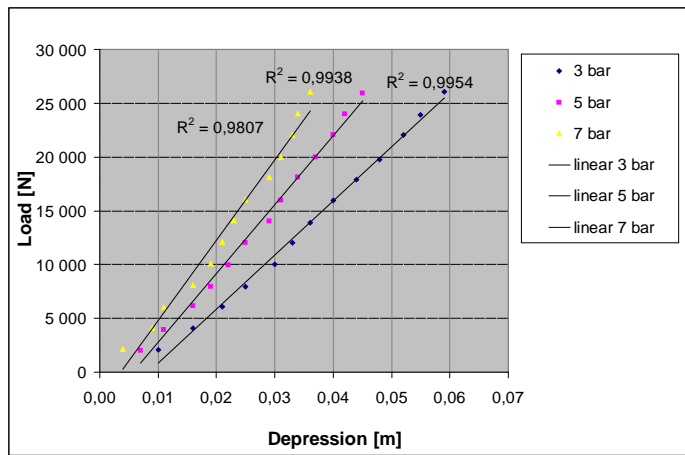


Figure 3. Tyre elastic characteristics at three different pressures

We determined the attenuation curve by a “swing test”, which measures the period and changing amplitude of free vibration of the trailer structure after the application of a small excitation force. From the resulting attenuation curve for each setting, we can determine the logarithmic decrement, the parameter characterising the attenuation.

The logarithmic decrement ( $\Lambda$ ) is the natural logarithm of the ratio of successive amplitudes.

$$\Lambda = \ln \frac{A_n}{A_{n+1}} \quad [-] \quad (3)$$

From the logarithmic decrement, we can calculate the Lehr attenuation number ( $D$ ), the attenuation of the system divided by the critical attenuation of a system whose other parameters are similar. This tell us whether the system will go into periodic or aperiodic vibration. The Lehr attenuation number is given by:

$$D = \frac{\Lambda}{\sqrt{4\pi^2 + \Lambda^2}} \quad [-] \quad (4)$$

Amplitude (vibrational acceleration):  $\Lambda$  [m/s<sup>2</sup>]

The logarithmic decrement is also used to calculate the system attenuation coefficient (c).

$$c = \frac{\Lambda}{\pi} m \alpha \quad [\text{Ns/m}] \quad (5)$$

The characteristic angular frequency of the trailer ( $\alpha$ ) is:

$$\alpha = \sqrt{\frac{k}{m}} \quad [1/s] \quad (6)$$

As given by Ludvig (1973), the characteristic frequency of an excited vibrational system is the frequency at which a system vibrates after being left to itself after a transfer of energy (excitation). When vibrated at the characteristic frequency, the system assumes a higher amplitude than at other frequencies. Characteristic frequency:

$$f = \frac{\alpha}{2\pi} \quad [\text{Hz}] \quad (7)$$

Finally, we can determine the frequency range in which resonance can occur in a trailer. Resonance arises if the system attenuation is small and excitation is close to the characteristic frequency. If the amplitude is sufficiently high, a condition of resonance catastrophe occurs, potentially causing the rapid destruction of the entire system, in our case the trailer. This can occur in the range

$$D < 0.1 \text{ and } 0.8 \cdot \alpha < \omega < 1.3 \cdot \alpha$$

Thus the trailer used in the measurement, depending on adjustment, could resonate at frequencies between 2.7 and 6.3 Hz. The largest change to the characteristic frequency is caused by changing the mass of the trailer.

#### **4. Measurements on the trailer**

After determining the trailer's vibrational characteristics, we measured the forces caused by the terrain conditions. This involved measuring, in eleven

different speed ranges, the trailer's traction demand and accelerations which the terrain conditions caused in the trailer structure. The latter were measured at the points shown on figure 4.

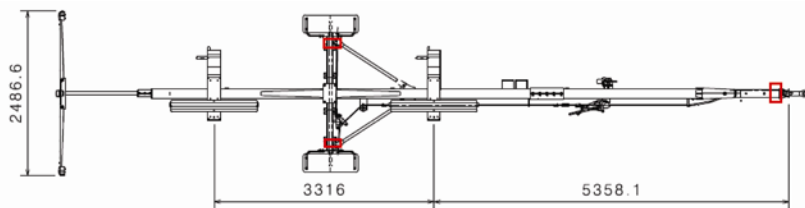


Figure 4. Positions of acceleration sensors on the measurement trailer

As the trailer traversed the selected field at pre-determined speeds, and in fatigue-bench tests, measurements were taken at a frequency of 300 Hz over a period of 200 seconds and forwarded by the data collection unit (SPIDER 8) to the data storage computer.

The measurements consisted of two distinct phases. The first series was performed under real operating circumstances by towing the trailer along five tracks of different characteristics. The first was a high-quality surfaced road, and the second a low-quality surfaced road. The remainder were agricultural dirt tracks of three different soil types.

The second phase of measurements involved a comparison of two different accelerated endurance test systems (figure 5), one involving a rolling testbench, and the other a circular track.



Figure 5. Measurements on circular track and rolling testbench

## 5. Measurement results, and discussion

In the first stage, the terrain profiles were recorded for each stretch of road traversed. The method devised by Gedeon was used to produce a spectral density function from the recorded data (figure 6), permitting the comparison of various profiles.

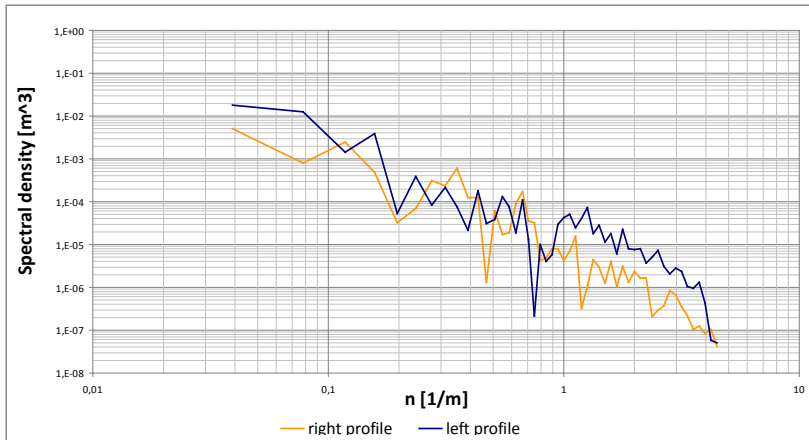


Figure 6. Spectral density for pebble-gravel road

The destructive effect of terrain on vehicles depends on the magnitude and frequency of forces arising from surface unevenness.

Fourier transformations were used to permit the accelerations recorded in various speed ranges to be compared in the frequency domain. As seen on figure 7, the form of the trailer's frequency curve is the same at each speed on a given road section, but the amplitudes steadily increase with speed. Different colours on the graph indicate different speeds. The bottom (red) curve corresponds to a traction speed of 3.6 km/h, and the top (purple) curve to a speed of 25 km/h.

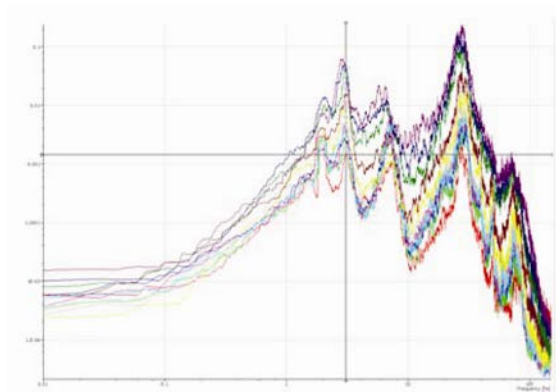


Figure 7. Fourier transform of accelerations for different speeds

Comparison of the Fourier transforms of the time-varying accelerations recorded in different field conditions shows local maxima corresponding to the trailer's characteristic frequency, repeated at harmonics higher up in the frequency range.

We also calculated and compared the RMS values of accelerations recorded during traction at various speed ranges on different field conditions.

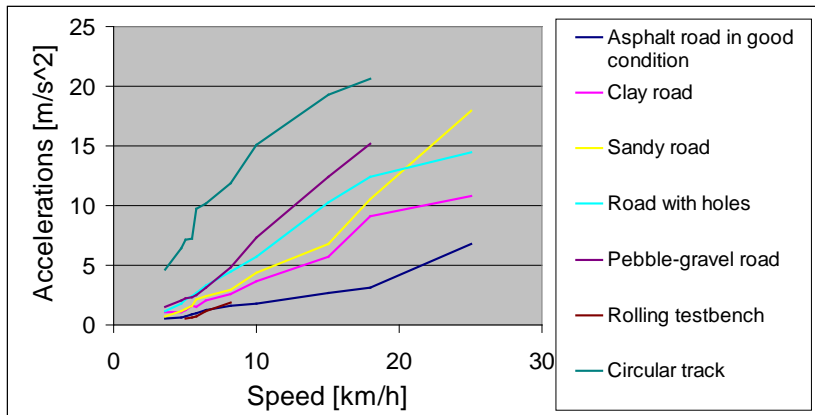


Figure 8. RMS values of accelerations measured on left side of towed structure on various road types and at various traction speeds

Figure 8 clearly shows that more extreme field conditions result in higher acceleration values. The RMS values measured during circular-track fatigue tests were extremely high compared with an ordinary road.

## Conclusion

The measurements show that the resonant frequency of the vehicle may be found independently of the road type, and that travelling at the wrong speed on a particular road may result in undesirable resonances in the vehicle. Generation of resonance by artificial obstacles on a test vehicle travelling and at a properly-selected speed is a potentially good basis for an accelerated fatigue test.

Further research is required to explore the relationship between the spectral density function and the Fourier transform of the vehicles' vibrational accelerations. This requires a simulated vibration test to determine the relationship between the two curves. Also required further measurements and refinement of the vibrational model, and these form the subject of ongoing and future research.

## Acknowledgement

The authors would like to express their thanks for the assistance in carrying out the measurements provided by the Hungarian Institute of Agricultural Engineering, (Gödöllő, Hungary) and CLAAS Hungaria Kft.

## **References**

- Laib, L. (2002): Terepen mozgó járművek, Szaktudás Kiadó Ház, Budapest, pp. 222-272
- Gedeon, J. (1981): Mechanika IV/1 Lengéstan. Budapest Műszaki egyetem Közlekedésmérnöki Kar, Tankönyvkiadó, pp. 13-76.
- Ludvig, Gy. (1973): Gépek dinamikája, Műszaki könyvkiadó, Budapest, pp. 83-110.

# Analysis of Governing Process of the Underload Gear Shifting

Attila SZEGEDI, Antal LENGYEL

College of Nyíregyháza, Faculty of Technology and Agriculture  
Department of Vehicle and Agricultural Machine Technology

## Summary

Differing requirements make complex demands towards the agricultural machines of our day. An effective operation calls for an efficient and versatile drivetrain system being connected to a modern diesel engine, considering that the engine power must be transmitted to the wheel-ground contact with minimum possible loss. Moreover, the momentary ratio should enable an optimal engine load even in a wide vehicle speed range to achieve low fuel consumption. To this end, most frequently modern PowerShift transmissions are used. Their critical point of operation is the gear change process under load. In our research, we investigate this shifting process starting with the signal controlling the gear change, including the pressure changes of hydraulic operation components, and ending with the traction force change in time.

## Keywords

Tractor transmission, Powershift,

## 1. Introduction

On a worldwide scale, the main aim of research on transmission design is reducing the drivetrain losses. In his research, *Molari et al.* [1] determined friction losses of the same type of transmission which was especially fitted to the tractor examined in the present paper. Making the gear change process speed-dependent presents a vigorous research area too. *Tanelli et al* [2] have researched automatic tuning possibilities of gear shift parameters. *Bietresato et al.* [3] also researched energy losses of tractor transmissions by using acceleration tests. During the gear change, the power transmitted is decreased by friction losses which also depend on the process and speed of ratio change. With increased shifting duration, the kinetic energy loss of the power machine goes up due to speed reduction. In order to disclose the connections of these processes, the chronological progression of the gear change process has to be looked into accurately and in detail—this can be indicated with the characteristics of control signals in a most reliable way. Our experiments deal with these control signals and later on, based on our measurement results, we formulate our conclusions.

Our final aim is the energetic optimization of shifting process by modified governor signal accordance with working speed and traction force.

## 2. Measurement method and the equipment applied

The detailed examination has been carried out using a New Holland T7040 type tractor. The longitudinal section drawing of its power transmission system is shown in figure 1.

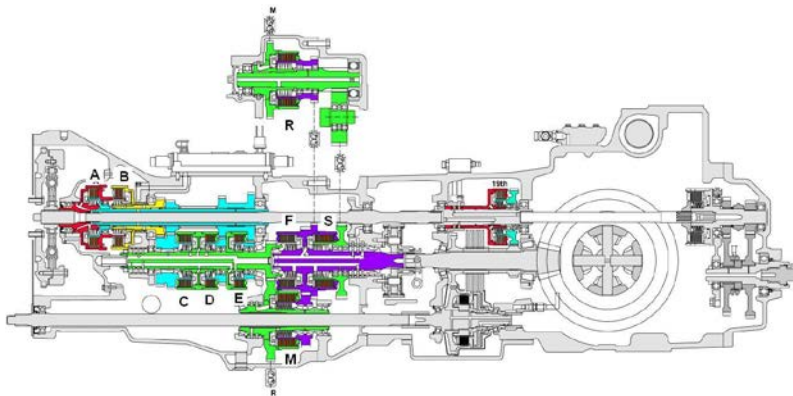


Figure 1. Longitudinal section of the transmission

It is a Full Powershift transmission enabling to shift 19 forward and 6 reverse gear ratios under load. By this transmission, speeds of 3-9 km/h, as well as 5-13 km/h, at soil cultivation and around 40 km/h at transport operations, can be provided. The gear change is done by 9 hydraulically controlled multi-plate wet clutches. As a special characteristic of the clutch, during transportation a good efficiency direct drive can be imparted from the flywheel through the TLT drive shaft while the 19th gear is engaged. This diminishes heating and friction losses [1].

The measurements were executed on the outskirts of the Hungarian town Szerencs on the 4th of May 2010 hauling a 9800 kg gross weight trailer on public roads. In an acceleration cycle of the investigation, the indirect measurement of the traction force were carried out by a hydraulic master cylinder placed in the towing-device [4]. Over the course of the measurement the control current as well as the pressure values of the hydraulics actuating the clutch, responsible for gear change, were recorded as a function of time.

The first measurements were executed in two phases.

***In measurement phase one***, we read the electrical signal of the control unit actuating the hydraulics directly out of the control circuit through the CAN bus of the tractor, via the OEM software of New Holland (New Holland Electronic Service Tool). With the software, we saved the chronological current

progression to be sent to the solenoid valve of the hydraulically controlled multi-plate clutch.

*In* measurement phase two, we examined the hydraulic pressure changes. For measuring the pressure actuating the clutch, we applied a Hydac type hydraulics monitoring device /measurement&data storage/ during the ratio change. The Hydac HDA 3444-A-600-000 pressure transmitters were connected to the pressure measurement service terminals of the clutches marked B, D and E on the control unit of the transmission. Within the hydraulic control circuit, this is located directly after the proportional selector valve, this way, we managed to examine the extent of the pressure actuating the individual clutches. We obtained precise data on what time-related and curve steepness deviations they are between the electric control current and the pressure controlled by it. The measured pressure values were recorded via Hydac HMG 2020 gauge&data collector, and after exporting them to a PC the data became ready to be evaluated.

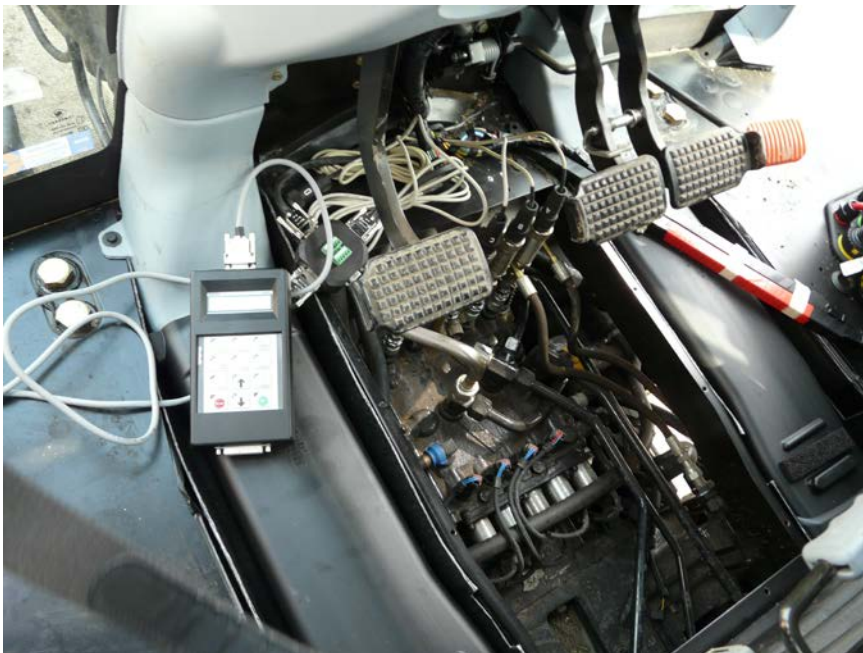


Figure 2. Connecting the pressure transmitters and the gauge&data collector to the control unit

### 3. Measurement results

Control signals, the number of which reached 80000 during the investigation, were recorded at every single clutch. In a gear change process, the current change based on the measured data is shown in figure 3.

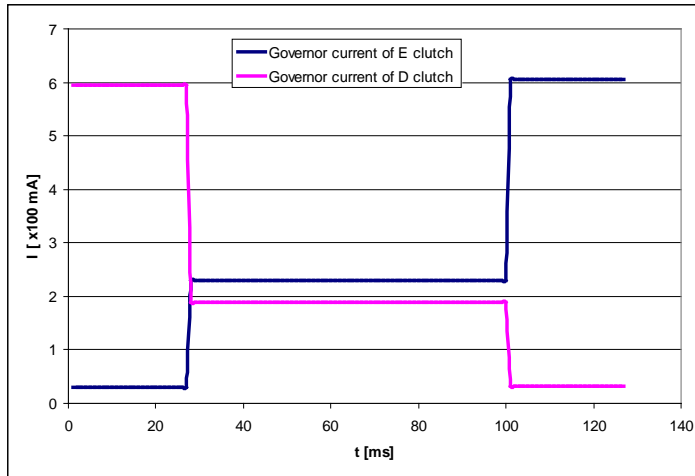


Figure 3. Chronological progression of electrical control signals of the sequential gears during shifting

While clutch D is engaged, the governor current of the hydraulic system of 0,6 A drops to 0,2. A during the time of the gear change. Simultaneously, an equal governor current starts to activate the selector valve of the hydraulic clutch in order to engage the next gear. After a certain period of time which can be set in the software operating the shifting system (in the present case 47 ms), clutch D fully disengages, while its control current comes down to 0,05 A. In contrast, clutch E reaches a fully engaged stage, consequently its governor current increases to 0,6 A. For analysing the connections of the control process, the electrical signal as well as the hydraulic control pressure measured at a given clutch were plotted in the same time diagram.

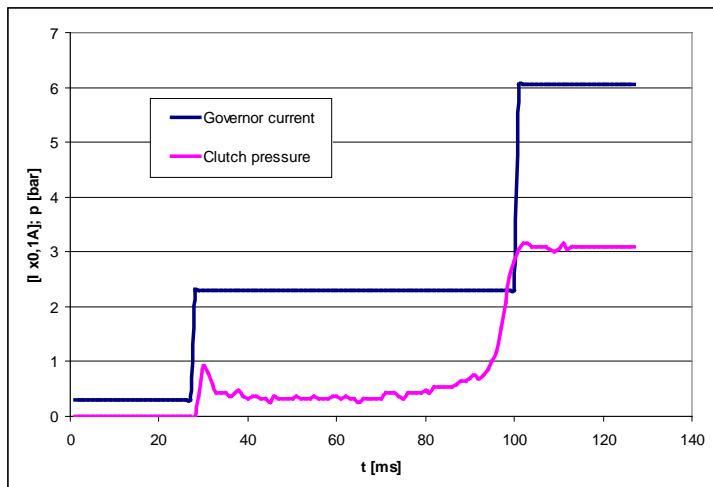


Figure 4. Chronological progression of the electrical control current and hydraulic actuating pressure of clutch E during shifting

It is clearly shown in figure 4 that the hydraulic pressure build-up takes place with a delay of 10-15 milliseconds, following the control current changes. The explanation lies in the facts that it comes to certain time consuming movements while pushing together the clutch lamellas and on the other hand, the integrated hydraulic accumulator needed for exetuting a jolt-free gear change has to be filled up.

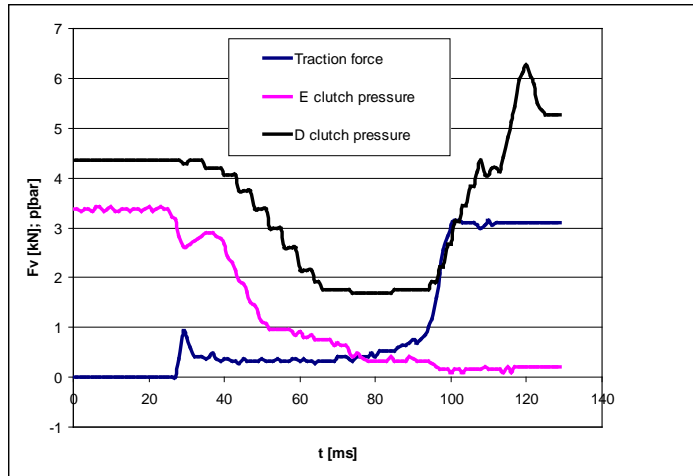


Figure 5. Chronological progression of hydraulic actuating pressures and traction force during shifting

In figure 5 the change of the measured traction force is shown. From the diagram it can be ascertained that the control pressure of the clutch is accurately followed by the traction force exerted by the power machine.

The delay of several milliseconds is primarily attributable to the mass inertia of the power machine since the traction force were not examined between the wheel and the ground but between the tractor and the trailer. The traction force peak at the end of the gear change clearly reflects the additional force required for re-accelerating.

## Conclusions

Power machines need to exert variable traction forces in a wide speed range. Based on the data measured by us, connections between the electrical control signal and the shifting process can be revealed. We have determined that the power machine operates with control signals featuring equal duration and current strength regardless of the velocity and traction force exerted. From an energetic point of view, it would be expedient to differentiate the hydraulic pressure controlling the process of the gear change under load, depending on traction force and driving speed. Using this modified control, slight fuel savings would occur, moreover, due to minimised friction, there could be an increase in

life expectancy of clutch components, a reduction in lubricant operating temperature as well as an improvement in shifting comfort depending on operating conditions. Continuing our research, we aim to make a contribution to creating an optimised series of shifting control signals.

With the currently most widely used modern transmission shiftable under load (PowerShift), the critical point of operation is the gear change process under load. In our research, we investigate this process starting with the signal controlling the gear change, including the hydraulic operating pressure, and ending with the traction force change in time. Based on the measured data it can be ascertained that the changes of the electric control signal are followed by the hydraulic operating pressure with a delay of several milliseconds. The changes of the traction force show similar results. The peak of the traction force, appearing at the end of the shifting, indicates the additional force required for re-accelerating. From an energetic point of view, it would be expedient to differentiate the hydraulic pressure controlling the process of the gear change under load, depending on traction force and driving speed. Using this modified control, slight fuel savings would occur, moreover, due to minimised friction, there could be an increase in life expectancy of clutch components, a reduction in lubricant operating temperature as well as an improvement in shifting comfort depending on operating conditions. Continuing our research, we aim to make a contribution to creating an optimised series of shift control signals.

### **Acknowledgement**

The research was supported/subsidized by the TÁMOP-4.2.2.B-10/1-2010-0011 „Development of a complex educational assistance/support system for talented students and prospective researchers at the Szent István University” project.

### **References**

- [1]. Molari G. –Sedoni E.: (2008) Experimental evaluation of power losses in a power shift agricultural tractor transmission Biosystems Engineering Vol. 100 pp.177-183.
- [2]. Tanelli M. et al. (2011) Transmission control for power-shift agricultural tractors: Design and end-of-line automatic tuning Mechatronics Vol 21. pp.285-297.
- [3]. Bietresato et al. (2012) Assesment of the efficiency of tractor transmissions using acceleration tests Biosystems Engineering Vol. 112 pp.171-180.
- [4.] Lengyel A. – Szegedi A. (2011): Terhelés alatti áttételváltás folyamatainak elemzése Járművek és Mobil Gépek online folyóirat nyomtatásban megjelent különszáma, 139-145. o., ISBN 978-963-269-227-2

# Examination of the cob cracker adapter manufacturers' performance in Hungary

Aдриенн GODA<sup>1</sup>, Viktor MEDINA<sup>1</sup>, László ZSIDAI<sup>2</sup>

<sup>1</sup>Institute of Engineering Management

<sup>2</sup>Institute of Industrial Technologies  
Szent István University

## Abstract

The Hungarian cob cracker adapter manufacturers can be aggregated in three main groups: individual, series and mass product manufacturers. The performance of these companies could be analyzed by an Importance-Performance Analysis (IPA). Before the IPA we have to make a SWOT (Strengths-Weaknesses-Opportunities-Threats) analysis to know the most important internal factors. We determined 39 internal factors (strengths and weaknesses) of the sector and their importance and performance. Then it was also examined the influence of the external factor to the internal factors to be able to determine the performance of the cob cracker manufacturer sector, which has a good performance based on the results of this research.

## Keywords

Manufacturing, performance analysis, IPA, SWOT, cob cracker adapter

## 1. Introduction

The Hungarian cob cracker adapter manufacturers can be aggregated in three main groups: individual, series and mass product manufacturers. [1] The performance of these companies could be analyzed by an importance-performance analysis (IPA). [2] Before the IPA we have to make a SWOT analysis to know the most important internal factors.

During a SWOT analysis we need to ask and answer questions that generate meaningful information for each category (**strengths**, **weaknesses**, **opportunities**, and **threats**) in order to maximize the benefits of this evaluation and find competitive advantages. [4]

**Strengths** (characteristics of the business, sector or project team that give it an advantage over others) and **weaknesses** or limitations (characteristics that place the team at a disadvantage relative to other, or the customers, partners get unsatisfied) are internal factors, **opportunities** (chances to improve performance, e.g. make greater profits, in the environment) and **threats** (elements in the environment that could cause trouble for the business or project) are external factors that are important to achieving the objectives of the

company. [5] The companies have direct effect to the internal factors and indirect influence to the external ones.

The examination of the Hungarian cob cracker adapter manufacturer sector with an internal and external factor analysis allows the analysis of the manufacturers' strengths and weaknesses and the mapping of the possible dangers and difficulties. The main focus of the SWOT analysis is to examine the innate abilities of the Hungarian cob cracker adapter manufacturer sector, and the environmental impacts. The internal factors are essentially determined by the sector or the company because the branch is converting them to strengths or weaknesses. But the external factors cannot be controlled by the firm or the sector, because these are given by environmental opportunities and threats.

After determining the internal factors we evaluated the importance of strengths and weaknesses. Based on these results we prepared the industry's performance-importance matrix and determined four special areas (See figure 1.) [6]:

1. Keep level areas (Keep up the good work)
2. Area requiring special attention (Concentrate here)
3. Area of low priority (Low priority)
4. Low-priority area displaying as strength (Possible overkill).

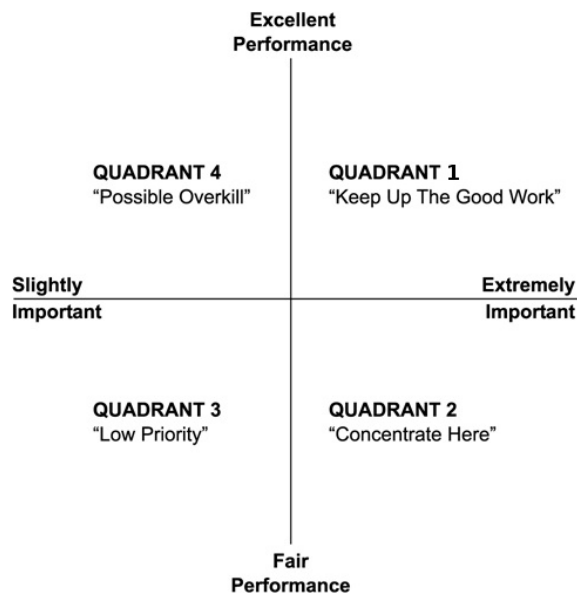


Figure 1. Importance-performance analysis

(Source: own editing on the basis of John A. Martilla, John C. James [2])

The companies usually operate in a rapidly changing environment, and the external conditions are constantly influenced by the efficiency of the use of internal resources. Therefore, we should analyze the environment at all levels in which a SWOT analysis can help us.

In the present paper we examined the influence of the external factor to the internal factors too. This investigation could give interesting results, because an external coefficient could have a positive or negative effect to the different internal factors. This means that the same external factor could be an opportunity or a threat on the same time depending from its effects to the strengths and weaknesses.

## **2. Results**

At the beginning phase of the research we determined the internal factors (see table 1.). After collecting 39 possible strengths and weaknesses based on a qualitative research we analyzed the performance of the companies and the influence of the internal factors for the three manufacturer groups (individual, series and mass producers). The performance was rated between 1 and 5. The value 1 means fair performance and 5 means excellent performance. Rating numbers above 3 mean strength, below 3 ones mean weakness. We averaged the three manufacturer groups' performances and made a rating from the most significant strength to the most remarkable weakness (see table 1. and 2.).

The results of the average comparing to the individual groups show us notable differences and deviances. This means that there are important differences in the performance of the groups. After analyzing this question it can be established that although there are variances among the companies the averages can be suited to general comparison of the different internal factors' role. The certificate of quality and the transport distances are the best performed strengths. In all the three groups received the maximum point. The product quality, the reliability and number of suppliers have also good rating. In all of these strengths the second group, series manufacturers was rated the best.

The distribution network, the substitutability of raw materials and components are the most significant weaknesses. In this case all three groups received the minimum points. The interest of the production units in the turnover and the pollution of the production mean also notable vulnerability for the sector. In the three groups' rating there were not too many differences among the groups.

After examining the performance of the internal factor we made a qualitative research to be able to determine their importance. The importance was rated also between 1 and 5. The value 1 means low weight, the number 5 means high significance.

The most important internal factors are the certificate of quality, the product quality, the satisfying the costumer, the profitability, the packing of the final product and the distribution network. All this factors received the maximum priority in all cases, which means that the companies have to focus to these areas. Fortunately all this elements are strengths except the distribution network, which is the most important weakness. It is interesting that the other most important weakness was evaluated as the less important factor from the 39.

Table 1. Importance-performance analysis of the strengths  
(Source: own research)

	Production type	Individual		Series		Mass		Average	
		Perf.	Imp.	Perf.	Imp.	Perf.	Imp.	Perf.	Imp.
1	Transport distance	5	3	5	3	5	3	5	3
2	<b>Certificate of quality</b>	5	5	5	5	5	5	5	<b>5</b>
3	Number of suppliers	4	3	5	5	4	3	4,3	3,7
4	Reliability of supplier	4	3	5	5	4	4	4,3	4
5	<b>Product quality</b>	4	5	5	5	4	5	4,3	<b>5</b>
6	<b>Satisfying the costumer</b>	4	5	5	5	4	5	4,3	<b>5</b>
7	Product differentiation	4	5	4	2	4	2	4	3
8	Flexibility for the orders	5	5	3	1	4	5	4	3,7
9	Price comparing with the substitutes	5	5	3	2	4	5	4	4
10	Professional experiences	2	3	5	5	5	5	4	4,3
11	Great number of buyers	3	5	4	2	4	3	3,7	3,3
12	Suitability of the produced adapters for different combines	5	5	1	1	5	5	3,7	3,7
13	Ability of growth	4	5	4	3	3	4	3,7	4
14	Flexibility of production capacity	3	5	5	3	3	4	3,7	4
15	<b>Profitability</b>	4	5	4	5	3	5	3,7	<b>5</b>
16	Recycling	3	1	4	5	3	1	3,3	2,3
17	Flexibility of order deadlines	5	5	1	1	4	5	3,3	3,7
18	International affairs	2	4	5	5	3	3	3,3	4
19	Raw material supply	3	4	5	5	2	4	3,3	4,3
20	<b>Packing of the final product</b>	3	5	4	5	3	5	3,3	<b>5</b>

After the rating of the performance and importance of the internal factors we make the importance-performance analysis. Graphically illustrating in a frame of reference the rating values of the importance and performance we can determine a strategy based on the four quadrants (see figure 2.). In the most important quadrant where those internal factors are which is important but the performance is low there are only three elements (second quadrant). The distribution network is the factor which needs the most intervention. The other areas which must be in our focus are the loss of time and the professional trained staff. In these cases it is not so urgently the intervention but the manufacturers have to build up a strategy how they can better their performance with exception of series manufacturers.

The mass and individual producers have to reduce the loss of time and to make more rational and planned their production. The manufacturer companies have to introduce more efficient production management systems, because the loss of time has an unfavourable effect to the profit and the performance. They have to start finding better professionals in the future as soon as possible, because to change the educational system needs many time.

Table 2. Importance-performance analysis of the weaknesses  
(Source: own research)

	Production type	Individual		Series		Mass		Average	
		Perf.	Imp.	Perf.	Imp.	Perf.	Imp.	Perf.	Imp.
1	Process controls	1	1	5	5	3	1	3	2,3
2	Location	3	3	3	3	3	3	3	3
3	Market share	2	4	4	4	3	4	3	4
4	Skilled workforce	2	4	5	5	2	4	3	4,3
5	Loyalty of top and middle management	2	2	4	5	2	2	2,7	3
6	Direct selling from the fabric	5	5	1	1	1	1	2,3	2,3
7	Feedback about the quality during the production	1	1	5	5	1	1	2,3	2,3
8	Effectiveness of stockpiling	1	2	5	5	1	1	2,3	2,7
9	Marketing activity	2	1	3	5	2	2	2,3	2,7
10	Application of new technologies	1	2	5	5	1	2	2,3	3
11	Condition of machines	1	2	5	5	1	2	2,3	3
12	Maintenance of capital goods	1	2	5	5	1	2	2,3	3
13	Motivation of the management	1	2	4	5	2	2	2,3	3
14	Loss of time	1	3	5	5	1	2	2,3	3,3
15	Professionally trained staff	1	3	5	5	1	2	2,3	3,3
16	Pollution of the production	2	1	2	5	2	1	2	2,3
17	Interest of the production units in the turnover	1	2	3	3	1	2	1,7	2,3
18	Substitutability of raw materials and components	1	2	1	2	1	2	1	2
19	<b>Distribution network</b>	1	5	1	5	1	5	1	<b>5</b>

The largest number of elements is in the first quadrant where the level of importance and performance is high. This result means that in general the companies of the sectors make well they work and they have to focus their activity to maintain or ameliorate the good performance. The generally good performance of the sector is also shown well on the figure 2, because great number of the factors is in the first and third quadrant and in the second and fourth quadrant are only 10% of all elements. In the fourth quadrant we can see the components of the analysis which are wasting resources. In our examination there is only one example, the recycling. This result could mean that the manufacturers don't have to handle too much with recycling their materials, although this could be later a good marketing argument for social responsibility. And in this case the importance of this element will increase.

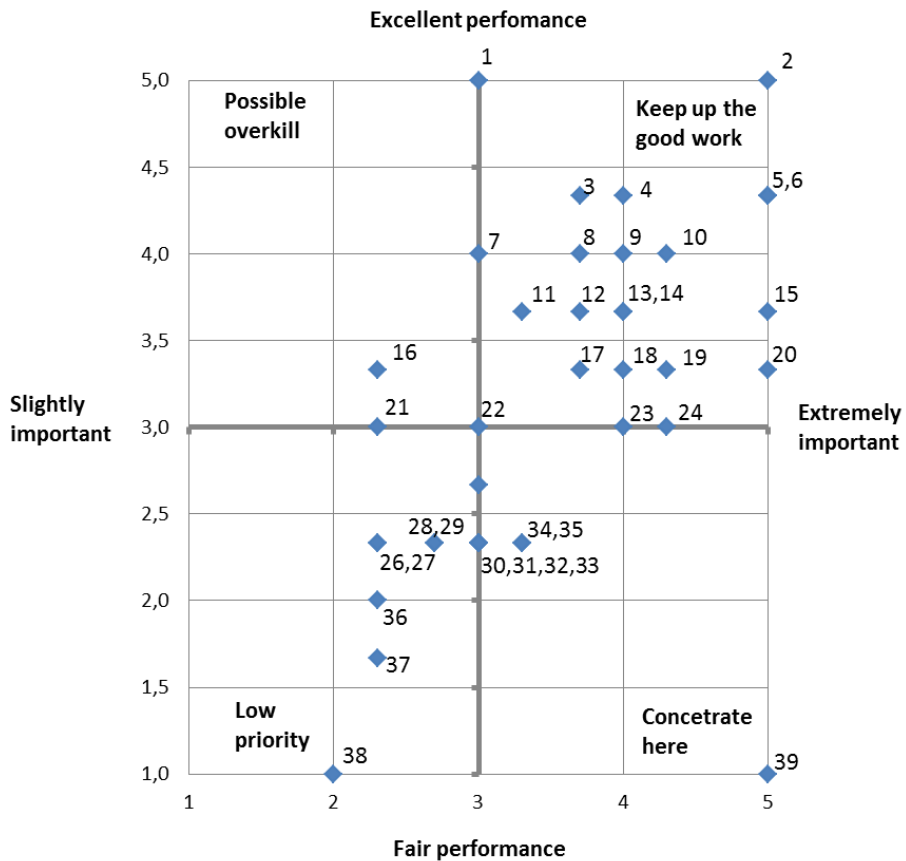


Figure 2. Importance-performance analysis of the Hungarian cob cracker adapter manufacturer sector (Source: own editing based on our research)

The last part of the examination was the analysis of the influence of the external factor to the internal factors. We examined 9 external factors:

1. Increase of consumers' expectation
2. Positive changes in the consumers' opinion
3. Growth of the demand
4. Changes for better situation of agriculture
5. Raise of the competition
6. Change of the technology
7. Severity of the environment protection standards
8. Expansion of the unemployment
9. Continuance of the word's crisis

All external factors were scored between -5 and 5 based on their impact to strengths and weaknesses. The score 5 means a strong positive effect to the internal factor (opportunity). The value 0 means no impression. The point -5

means a strong negative influence (threat). After examining the effects of the external coefficients to the internal ones we averaged the results and we can conclude that mayor part of the external factors are opportunities (see table 3.). Although the partial results show some deviances and in some cases totally different impacts, we can make an order based on the average.

The increase of consumers' expectation has the most positive effect to the internal factors. This result means that the examined manufacturers make high quality products. The continuance of the word's crisis means the most important threat with its -1,28 average value. But as the deviation is the highest in this case comparing to the other external factors that means not always negative effects. For example this factor has positive impact to the certificate of quality, to flexibility for the orders, to suitability of the produced adapters for different combines, price comparing with the substitutes and finally substitutability of raw materials and components. The deviation is also high in the case of the external factor number 2, 3 and 5.

The raise of the competition has also high deviation because it has positive and negative effects. This opportunity has negative impact to the profitability, to the market share, to the ability of growth and the condition of working machines. The growth of demand has also some negative effects like condition of working machines, effectiveness of stockpiling, maintenance of capital goods, skilled workforce and price comparing with the substitutes.

The positive change in the consumers' opinion has also high deviation, but in this case there aren't any negative effects. The expansive deviation is due to the great variability of the power of impact. In this case we can see numbers between 0 and 5. Many cases it has no effects and some cases it has strong impact, like product differentiation, product quality and great number of buyers.

Table 3. Effects of external factors to the internal factors  
(Source: own research)

Statements	1	2	3	4	5	6	7	8	9	Aver.
<b>Average</b>	<b>1,84</b>	<b>1,69</b>	<b>1,11</b>	<b>1,01</b>	<b>0,89</b>	<b>0,54</b>	<b>0,25</b>	<b>-0,42</b>	<b>-1,28</b>	<b>0,62</b>
<b>Deviation</b>	<b>1,0</b>	<b>1,6</b>	<b>1,8</b>	<b>1,3</b>	<b>1,8</b>	<b>0,6</b>	<b>0,7</b>	<b>1,0</b>	<b>2,4</b>	<b>1,3</b>
Certificate of quality	3,0	3,3	2,0	0,0	4,0	0,0	3,0	0,0	3,0	2,0
Product differentiation	3,0	5,0	3,0	2,7	3,0	0,0	0,0	0,0	1,0	2,0
Flexibility for the orders	2,7	1,3	3,0	2,0	3,7	0,0	1,3	0,0	3,0	1,9
Great number of buyers	3,0	4,3	5,0	3,0	1,7	1,3	0,0	-2,0	0,3	1,8
Suitability of the produced adapters for different combines	2,0	2,0	4,3	1,7	2,3	0,0	0,0	0,0	3,0	1,7
Flexibility of order deadlines	1,7	2,0	3,7	3,0	2,7	0,0	0,0	0,0	0,0	1,4
International affairs	3,0	3,3	2,7	0,0	3,0	0,0	1,3	0,0	-1,7	1,3
Product quality	2,3	5,0	0,0	1,0	3,0	1,5	0,0	-2,0	0,0	1,2
Price comparing with the substitutes	2,7	3,0	-0,7	2,0	-1,3	0,8	0,0	0,0	3,7	1,1
Direct selling from the fabric	1,0	1,3	1,7	2,3	1,3	0,0	0,0	0,0	1,7	1,0
Flexibility of production capacity	3,3	3,7	2,0	3,3	0,3	1,3	-0,3	-1,0	-3,3	1,0
satisfying the costumer	2,3	1,3	1,3	0,0	0,7	1,5	2,0	0,0	0,0	1,0
Profitability	3,0	3,7	2,3	3,7	-2,0	1,3	0,0	0,0	-3,0	1,0
Professional experiences	2,7	3,3	2,3	0,0	1,0	1,0	0,0	-2,0	0,0	0,9
Number of suppliers	2,3	1,7	3,0	0,7	3,3	0,0	0,0	0,0	-3,0	0,9
Motivation of the management	1,7	0,0	2,0	1,3	4,0	1,3	0,0	0,0	-2,7	0,8
Reliability of supplier	2,0	3,0	2,0	0,7	3,3	0,0	0,0	0,0	-4,0	0,8
Loyalty of top and middle management	2,0	2,0	1,0	1,7	1,7	0,3	0,0	2,7	-4,3	0,8
Market share	3,0	3,7	2,3	3,7	-2,0	1,3	0,0	-1,3	-5,0	0,6
Loss of time	2,7	0,0	0,0	0,0	1,7	1,0	0,0	0,0	0,0	0,6
Ability of growth	3,0	3,7	2,3	3,7	-2,0	1,3	0,0	-2,0	-5,0	0,5
Professionally trained staff	2,0	3,0	1,7	0,0	1,0	1,5	0,0	-2,0	-2,7	0,5
Application of new technologies	1,7	1,0	0,0	0,7	2,3	1,3	0,7	-1,7	-1,7	0,5
Packing of the final product	2,3	0,3	1,3	0,0	0,0	0,0	-0,7	0,0	0,0	0,4
Raw material supply	2,0	0,7	3,7	0,0	0,0	0,5	0,0	0,0	-4,0	0,3
Substitutability of raw materials and components	0,7	0,0	0,0	0,0	0,0	0,0	0,0	0,0	2,0	0,3
Feedback about the quality during the production	1,7	0,0	0,0	0,0	0,0	0,8	0,7	0,0	-0,7	0,3
Recycling	0,0	0,0	0,0	0,0	0,0	0,8	1,3	0,0	0,0	0,2
Process controls	1,3	0,0	0,0	0,0	1,7	0,5	0,0	0,0	-2,0	0,2
Pollution of the production	0,0	0,0	0,0	0,0	0,0	1,3	1,0	0,0	-1,0	0,1
Effectiveness of stockpiling	2,3	0,3	-2,3	0,7	0,0	0,8	0,0	0,0	-1,7	0,0
Transport distance	0,0	0,0	0,0	0,0	0,0	0,0	0,0	0,0	0,0	0,0
Location	0,0	0,0	0,0	0,0	0,0	0,0	0,0	0,0	0,0	0,0
Marketing activity	1,0	0,0	0,0	0,0	1,7	0,0	0,0	0,0	-3,0	0,0
Maintenance of capital goods	2,0	0,7	-1,3	1,7	0,0	-0,8	0,0	0,0	-3,3	-0,1
Skilled workforce	1,0	3,0	-1,3	0,0	0,0	1,0	0,0	-3,0	-3,7	-0,3
Distribution network	1,3	0,0	0,0	0,0	0,0	0,0	0,0	0,0	-4,7	-0,4
Interest of the production units in the turnover	0,0	0,0	0,0	0,0	0,0	0,0	0,0	0,0	-5,0	-0,6
Condition of machines	1,3	0,7	-3,3	0,0	-3,7	1,3	0,0	-1,0	-2,3	-0,8

## Conclusions

In our examination we made a SWOT analysis and an importance-performance analysis in the Hungarian cob cracker adapter manufacturer's sector. After

evaluating the results we can conclude that although there are differences among the different types of productions according to the application we can rank the internal factors on the basis of importance and performance.

We determined 39 strengths and weaknesses of the sector. The most important internal factors are the certificate of quality, the product quality, the satisfying the customer, the profitability, the packing of the final product and the distribution network. All these elements are strengths except the last one, which is the most important weakness.

Based on the results of the importance-performance analysis we can conclude that in general the companies of the sectors make well they work and they have to focus their activity to maintain or ameliorate the good performance. There is only one factor, the distribution network on which the manufacturers have to focus and which needs the most intervention.

On the basis of the examination about the influence of the external factor to the internal factors we could determine the opportunities and threats. The increase of consumers' expectation has the most positive effect to the internal factors. This result means that the examined manufacturers make high quality products. The continuance of the world's crisis means the most important a threat but the deviation is very high because its effect is not always negative. For example this factor has positive impact to the certificate of quality, to flexibility for the orders, to suitability of the produced adapters for different combines, price comparing with the substitutes and finally substitutability of raw materials and components.

The raise of the competition has also high deviation because it has positive and negative effects. This opportunity has negative impact to the profitability, to the market share, to the ability of growth and the condition of working machines. This high deviation can show us that a threat or a possibility can have different (positive or negative) effects too. From this conclusion we can declare that the success of our strategy and activity is highly depending from the knowledge and the preparation, and not only from the external environment.

Summarizing the results it can be concluded that the sector's performance is sufficient. The most important tasks are to maintain or to develop the efficiency and to improve the distribution network.

## **Acknowledgement**

The research was supported/subsidized by the TÁMOP-4.2.2.B-10/1-2010-0011 „Development of a complex educational assistance/support system for talented students and prospective researchers at the Szent István University” project.

## **References**

- [1] A. Goda, V. Medina, L Zsidai (2011): *Manufacturing process development with 5S at different types of production*, Mechanical Engineering Letters, Szent István University, Gödöllő p. 171-178. HU ISSN 2060-3789

- [2] John A. Martilla, John C. James (1977): *Importance-Performance Analysis*. Journal of Marketing Vol. 41, No. 1. p. 77-79. 353 (American Marketing Association, 1977)
- [3] HR Portal (2012.08.10.): *A HR stratégia - Környezeti elemzés*. <http://www.hrportal.hu/index.phtml?page=feature&id=34227>
- [4] B. Naga Jyoth, G.R. Babu, I.V. Murali Krishna (2008): *Object Oriented and Multi-Scale Image Analysis: Strengths, Weaknesses, Opportunities and Threats-A Review*. Journal of Computer Science, Science Publications, 2008.
- [5] L. Józsa (2000): *Marketingstratégia*. Műszaki Könyvkiadó, 2000. p. 106-112.
- [6] P. Kotler, K. Lane Keller (2006): *Marketingmenedzsment*. Akadémiai Kiadó, Budapest, p. 350-378.

# **IT Development Trends in the Mechanization of Crop Production**

Imre KOVÁCS, István HUSTI  
Institute of Engineering Management  
Szent István University

## **Abstract**

The improvement of mechanization of field work, machinery and equipment is a continuous process. We are witnessing the spread and agricultural use of the more and more modern equipment, which reflects to the technical and technological level of the area. In this process the IT content development has an increasing role, as for the use of modern machines and the tasks of management it is needed such information, which is unavailable or inaccurate on the traditional way. The designers and manufacturers of the agricultural machinery are able to meet the challenges of information needs on a higher and higher level through the IT innovation. In recent decades, we meet a wide range of solutions to have quick and accurate information about the use and characteristics of the machines. The „host” side has also developed a lot; as the gained information is often automatically linked to the business enterprise resource planning systems. In our study we systematize the IT developments of the mechanization of field work, covering the specific features of their utilization too.

## **Keywords**

farm and machinery management, IT, farm management system, global position system

## **1. Introduction**

The mechanization as a costly resource of agricultural enterprises made it necessary to be update in real-time. The enterprise resource planning systems provide for this a high level (IT) support. After the transformation of the ownership structure from the end of the 1990s, the world's leading developers of enterprise resource planning systems have opened sales representatives in Hungary, making their solutions available to the users. Herdon's examinations (2004) have unequivocally proved that the effectiveness of economic activity is increasingly determined by the knowledge, so the workplaces need more and more skills and attainments. In developed countries the key factor of economic growth has got the knowledge based management work. To help and support this activity the establishment of IT systems is required.

The system of instruments and methods of enterprise resource planning (ERP) has developed significantly the past twenty years. This is mainly because of the widespread availability of IT tools, as well as the more rapid access to information for the management professionals working on different levels with well-founded decisions (Bögel, 2003).

In Hungary the IT applications for agricultural purposes was generated mainly by the changes in ownership structure of agricultural workers and in the managerial approach after the change of regime. The resource planning systems for agriculture made necessary the application of a series of specifications which are embodied in farm management information systems (FMIS).

Meanwhile, in the development of the mechanization of crop production new guidelines, global positioning and its information solutions have appeared. Machines moving on the field and performing operations with synchronization of data about the power and working machine relations has been in continuous development, and as a result of positive tests they became available in the practical life. Today, the closed and cooperative synthesis of the two areas (enterprise resource planning - crop production machines IT developments) form a complex data network.

## **2. IT development of crop production machines**

The IT development of power and working machines of crop production can be traced back to the development of precision farming. The wide range of sources of literature demonstrates that the agricultural operations can be made in big and in many cases heterogeneous areas, however, in the relationship between plant and technical device we need an accuracy of a few centimeters. This justified the development of more accurate positioning of the power and farm machinery relations on the field.

The global position system (*GPS*) is based on the measurement of the exactly distances from the satellites. The 24-satellite system has been created by the U.S. Department of Defense and it is operated primarily for military purposes, but the signals provided by the system can be used free of charge for civilian purposes too. The 24 satellites circuit in 6 orbits at an angle 55 degrees from the equator, and on 20 thousand kilometers above. At least 5 and up to 11 satellites are visible above the horizon. The GPS receiver moving on the earth determines its distance from the satellites with help of the signals transmitted by the orbiting satellites. It calculates the exact distance from the three dimensional position. To determine the vertical coordinate it is needed distance the data of a fourth satellite. The absolute accuracy of this system is 10-15 meters on the surface. This accuracy is still unfit to work in the field. (Hajdú, 2008)

The accuracy of GPS data can greatly enhance with differential (DGPS: *Differential Global Positioning System*) correction. The basis of the DGPS is that there are at least two independent data collection at different locations at the same time. First measurement is in a known stable ground station position (so-

called reference stations) and the second one is in the unknown position of the GPS receiver. The errors of the mobile GPS receivers can be decreased by the data from the reference station. When the position error magnitude and direction (differential or correction signal) will be measured in a location with known coordinate points (base station), and this data will be transmitted to the mobile receiver, the positioning of magnitude will be more accurate, and the inaccuracy will be only some centimeters. With free-to-air differential signals of EGNOS satellites operated by Europe the accuracy is 0.4 meters. To have more precise positioning signal we have to pay, or we need to have own base station.

The GreenStar system developed by John Deere consists of four levels ensured precise work: the already mentioned EGNOS correction signal (+ / - 40 cm), Starfire 1 (+ / - 30 cm), Starfire 2 (+ / - 10 cm) and the RTK (*Real Time Kinematic*) (+ / - 2 cm). While at the first three signals the radiation is only between the satellites and the receiver, in the RTK case it is intervening a third, in the factory or on the field, set up base station, which is designed to fix the GPS signal drift and other errors. Thanks to this solution it can be achieved the + / - 2 cm accuracy. (Agro Napló, 2010).

If we know so accurately the machine interface relations, it is possible the so called coordinate driven handling of devices on the field. The machine control can be carried out in two ways. One is the parallel tracking system (Parallel Tracking), and the other is the automatic steering system (AutoTrac).

The parallel tracking systems indicate for the tractor driver the trace which has to follow and the possible difference from it. The navigation-aid tools can be divided into two groups by the display method: one group includes simple designed LED display devices, while the assets in the other group indicate the route to be followed on LCD. In this case the machine operator has to intervene and take the corrective action when there is a deviation from the trace.

In the case of automatic steering systems the interventions can be made by hydraulic or mechanical tools. The most important achievement of the automatic steering is that with the use of the system is possible to have unlimited repeatability, so the machine can go on the same trace even months or years later. But for this it is essential to establish the base station in fix place. The automatic steering is not only useful for the power machines, but also can be extended for working machines too. The control of working machinery can be on a passive or an active way. In the first case it happen the control of the power machine, whereas in the second case the working machine is controlled. (Agro Napló, 2010).

The ISOBUS standard, introduced in 2001 can create the connection in the informatics data flow of power- and farm machines. The world's car manufacturers have agreed to implement the same standards and same communication interfaces among power and working machines, terminals and enterprise resource planning systems. (Figure 1).

The ISOBUS is based on ISO 11783 and makes possible to control with a single monitor in the cab all tools – baler, sprayer, spreader, drill, etc. – and communicate with the tractor and the resource planning system to facilitate the

documentation for all field activities. The transfer of data collected by the different power machines for resource planning systems is realized by the ISO 11787 (ADIS: Agricultural Data Interchange Standards). The standard is precisely determines data flow syntax among the sensors, processors, storages and monitoring units (Stafford, 2000). The figure 2. shows the data flow of the most important field crop operations.



Figure 1. Connection possibilities based on ISO 11783 (Source: TeeJet, 2010.)

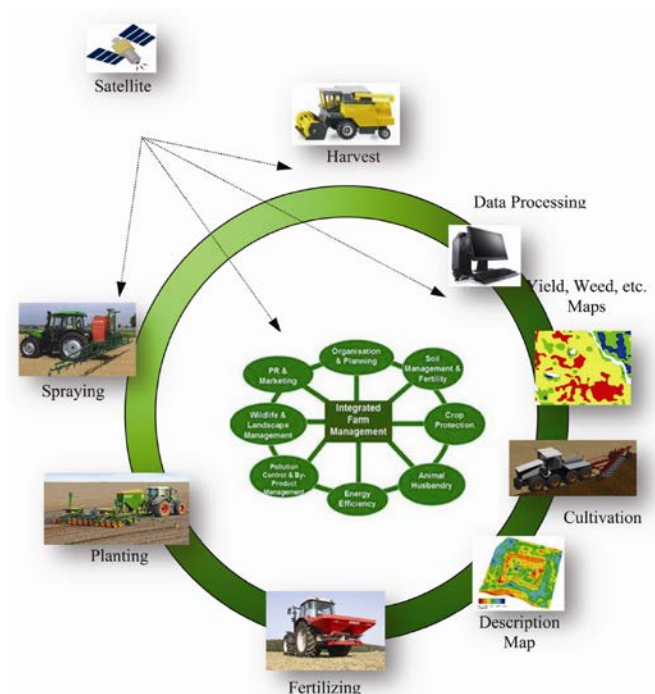


Figure 2. The elements of crop production information channels (Source: Roberson, 2000)

The most important set of data can be determined by constraints of the soil, the organic matter content, the pH and the moisture content values during the cultivation. The sensors based on the 1600-2600 nanometer spectral-band infrared reflection give us a real picture about the physical and chemical parameters of soil up to 3.6 km/h speed too (Shibusawa, 2000).

The continuous rise of fertilizer prices and the environment protection requires a nutrient management streamlining. The production area specific nutrient replacement method adopting the nutrient requirements and based on the test results of the given field can reduce the use of fertilizers, and increase the yield. The production area specific nutrition can be achieved by controlling the application of variable intensity scatter (solid), and the flow of direct injection (liquid) (Swisher, 1999.)

At the seeding thanks to the RTK system is no longer required the previous use of mechanical tracer. The exact following of traces allows even the precise seeding at night, the line-closer unit mounted on precision drills makes possible in the rotating or irregular-shaped fields to avoid the seeding again, and to prevent the negative impact on crop budgets of the double seeding. (Agro Diary, 2010)

The third critical operation is the good plant protection. The spreader frame sections or main valve of the system (iSteer - SideShift) can be automatically closed by the exact position of the sprayer based on the RTK. Watching the field boundaries, the system detects the sprayed and non-sprayed surfaces, so it is possible to spray only a specified area. Since the turning is not double sprayed, pesticide saving depending on the shape and size of field can be up to 5-8%. (Forrest, 2006).

At the harvest the yield sensors provide data about the current yields. The determination of production area specific crop yields may be measured by mass, mass flow, and optical sensors. Based on the data of production units can be made the full yield mapping.

The precision positioning allows to use in additional the so-called fleet tracking. The vehicle monitoring system provides continuous monitoring of vehicles and operators. It allows knowing the actual position of machines, to track movement of tractor and harvester. At vehicle tracking it is fundamental to know the current status of the fuel, to measure the fuel consumption and to monitor it. The vehicle tracking (Assystant) system will automatically create reports about the route and the use of fuel.

## **Conclusion**

In the development of technical elements of crop production the developments of IT played a dominant role in the past few years. The focus of the IT development of power and working machines was on the more precisely determination of the location of machine-relations. The data flow between data collector sensors and the central processing unit is regulated by international

standards during the operations. The- IT developments completed and proven in practice contribute greatly to perform more accurate the mechanical works on the field, and to realize efficiently the expected benefits of mechanization. The provided information gives more favorable basis for the rational decision-making and for the management tasks associated with the mechanization.

All data collected during the operations can be evaluated by using the modular built resource planning systems. Therefore our attention is devoted to this area in the future.

### **Acknowledgement**

The research was supported/subsidized by the TÁMOP-4.2.2.B-10/1-2010-0011 „Development of a complex educational assistance/support system for talented students and prospective researchers at the Szent István University” project.

### **References**

- Agro Napló (2010): Egy nyomon járunk – az RTK rendszer alkalmazásának lehetőségei és előnyei. Agro Napló Országos mezőgazdasági szakfolyóirat, XIV. évfolyam 10. szám, Zsigmond Kft. Pécs, ISSN 2061-5523
- Bögel Gy. (2003): Informatikai beruházás – üzleti megtérülés. Műszaki Könyvkiadó. Budapest, 2003. ISBN 9631619796. p. 82-86.
- Forrest, L (2006): Deere introduces Swath Control Pro for GreenStar 2-equipped sprayers. Southeast Farm Press; 3/15/2006, Vol. 33. p.: 17.
- Hajdú J., Deákvári J., Magó L. (2008) Megéri a GPS? Haszon Agrármagazin, Haszon Lapkiadó Kft., Budapest. p. 7-11.
- Herdon M. (2004): Információtechnológia az agrárgazdaságban. Gazdálkodás XLVIII: (1), Gyöngyös, p.1-13.
- Roberson, G. (2000): Precision agriculture: a comprehensive approach. Cooperative Extension, North Carolina State University. p. 52-61.
- Shibusawa, S., Anom, W.S., Sato, H., Sasao, A., 2000. On-line real-time soil spectrophotometer. Proceedings of Fifth International Conference on Precision Agriculture (CD), July 16-19, 2000. Bloomington, MN, USA.
- Stafford, J. V. (2000): Implementing precision agriculture in the 21st century. Journal of Agricultural Engineering Research 76, p. 267-275.
- Swisher, D.W., Sudduth, K.A., Borgelt, S.C., (1999): Optical measurement of granular fertilizer flow rates for precision agriculture. ASAE Paper No. 99-3111, American Society of Agricultural Engineers, St. Joseph, MI, USA.
- TeeJet: Néhány szó az ISOBUS kapcsán. Web: [www.teejet.com](http://www.teejet.com), 2012.08.16.